ABSTRACT

Title of Document: PACIFIC SEA SURFACE TEMPERATURES IN THE TWENTIETH CENTURY: VARIABILITY, TREND, AND CONNECTIONS TO LONG-TERM HYDROCLIMATE VARIATIONS OVER THE GREAT PLAINS

Bin Guan, Doctor of Philosophy, 2008

Directed By: Professor Sumant Nigam
Department of Atmospheric and Oceanic Science

Pacific sea surface temperatures (SSTs) exhibit variability on interannual to centennial time scales. This dissertation addresses the challenge to separate SST natural variability from the nonstationary (largely anthropogenic) warming trend; and, based on the clarified variability/trend patterns, evaluate SST forcing of long-term hydroclimate variations over the Great Plains.

First, a consistent analysis of natural variability and secular trend in the twentieth century Pacific SSTs is presented. By focusing on spatial and temporal recurrence, but without imposition of periodicity constraints, this single analysis discriminates between biennial, ENSO and decadal variabilities, leading to refined evolutionary descriptions; and between these natural variability modes and secular trend. Specifically, canonical ENSO variability is encapsulated in two modes that depict the growth and decay phases. Another interannual mode, energetic in recent decades, is shown linked to the west-to-east SST development seen in post–climate

shift ENSOs: the non-canonical ESNO mode. Pacific decadal variability (PDV) is characterized by two modes: the Pan-Pacific mode has a horse-shoe structure with the closed end skirting the North American coast, and a quiescent eastern equatorial Pacific. The second decadal mode—the North Pacific mode—captures the 1976/77 climate shift and is closer to Mantua's Pacific Decadal Oscillation. Implicit accommodation of natural variability leads to a nonstationary SST trend, including midcentury cooling.

These Pacific—and residual Atlantic—SST modes are then investigated for their connections to long-term hydroclimate variations over the Great Plains. During the Dust Bowl, dry anomalies in summer are found primarily linked to cool SSTs in the central tropical Pacific associated with non-canonical ENSO, as well as warm SSTs in the eastern tropical Atlantic associated with Atlantic Niño; in spring, however, dry anomalies are overwhelmed by connections to extratropical basins, when the cool phase of the SST trend coincided with a warm phase of the Atlantic Multidecadal Oscillation (AMO). Dry (wet) anomalies during the 1950s (1980s) are shown linked to the warm (cool) phase of the North Pacific decadal mode, as well as a warm (cool) AMO. The analysis suggests comparable importance of the Pacific and Atlantic Oceans in drought forcing, and highlights the role of the extratropical basins.

PACIFIC SEA SURFACE TEMPERATURES IN THE TWENTIETH CENTURY: VARIABILITY, TREND, AND CONNECTIONS TO LONG-TERM HYDROCLIMATE VARIATIONS OVER THE GREAT PLAINS

By

Bin Guan

Dissertation submitted to the Faculty of the Graduate School of the
University of Maryland, College Park, in partial fulfillment
of the requirements for the degree of
Doctor of Philosophy
2008

Advisory Committee:
Professor Sumant Nigam, Chair
Professor James Carton
Professor Karen Prestegaard
Dr. Phillip Arkin
Dr. Alfredo Ruiz-Barradas

Dedication

To
my parents,

who always support me in every step of my life,
for their patience and encouragements when their child is far away from them.

And also to
the memory of my grandparents,

who instilled in me the value of education and hard work.

Acknowledgements

I thank Professor Sumant Nigam, my advisor, for his support and guidance throughout the course of my study. This dissertation would not have been possible without his constant encouragements and the plenty of time he spent with me on mentoring and discussions. It has been a true pleasure working with him. Thanks go to Dr. Alfredo Ruiz-Barradas for expert help with data sets and analysis issues, and many helpful suggestions. I am also grateful to other members of the dissertation committee, Professor James Carton, Professor Karen Prestegaard, and Dr. Phillip Arkin, for careful reading of my dissertation.

The assistance of the AOSC staff during my study is gratefully acknowledged. Thanks are due to the entire AOSC family who made my five-year stay enjoyable and rewarding.

Table of Contents

List of Tables

List of Figures

Chapter 1 Introduction

1.1 Background

The Pacific Ocean exhibits large-scale coherent variability on interannual to centennial time scales. Such variability is well tracked by quantities at the air-sea interface, such as sea surface temperatures (SSTs). Meanwhile, the global ocean, especially near the surface, has undergone a warming trend in the twentieth century, associated with increased atmospheric concentration of greenhouse gases. Distribution of the total warming is however nonuniform in both time and space, suggesting a potential overlap of natural and forced changes.

Through atmospheric/oceanic teleconnections, variations in SST affect weather and climate far beyond the source region. A well known example is the El Niño–Southern Oscillation (ENSO), which dominates the tropical interannual SST variability and leads to anomalous weather conditions worldwide every few years. The Pacific decadal variability (PDV) has recently been recognized as another important component of the Pacific low-frequency climate variability. While its origins and mechanisms remain to be fully explored, decadal SST variations in the Pacific have been shown linked to climate anomalies over the neighboring continents, including warm season hydroclimate variations (especially long-term droughts) over North America (e.g., Nigam et al. 1999; Barlow et al. 2001; Schubert et al. 2004; Seager et al. 2005).

Compared to ENSO, the spatiotemporal structure of the PDV remains to be robustly characterized, given the shortness of the observed records (e.g., Deser and

Blackmon 1995; Zhang et al. 1997; Nakamura et al. 1997; Mantua et al. 1997; Barlow et al. 2001) and the difficulties in simulating low-frequency variability even on ENSO time scales in state-of-the-art climate models (e.g., Wu et al. 2003; Joseph and Nigam 2006). A related challenge concerns PDV mechanisms, especially where/how it is originated. Clearly, an improved characterization of the PDV structure will help to better understand its origins and impacts.

Much interest has been generated in separation of natural and anthropogenic variability, given the recent signs of climate change. Such separation is much needed for SST, which is among the most influential climate variables, and often used in validating coupled models. However, current characterization of SST natural variability and secular trend leaves room for aliasing one into another, due to potential overlap of the PDV and global warming/secular trend patterns. The overarching scientific challenge is to improve characterization of the secular trend and natural variability (PDV in particular) in the context of one another.

1.2 Motivation

The first part of the work is motivated by the somewhat ambiguous PDV characterization in literature, and the potential to improve using advanced techniques. Previous analyses have shown the existence of one or more decadal modes in the Pacific. The modal structures and their interpretations however exhibit considerable diversity among different analyses. One dominant method for modal decomposition has been the empirical orthogonal function (EOF), which is most efficient in explaining the total variance of a data set using a few leading modes. Conventional EOF, however, due to its sensitivity to sampling variations, requires assumptions on

the physical domain. A typical selection has been either a Pan-Pacific domain or a North Pacific domain. Given the dominance of ENSO, low-pass filtering of the physical fields is not uncommon (and often required by the specific methodology) in PDV extraction, but the frequency bands used for filtering are somewhat arbitrary. These analysis issues can in principal be avoided by using spatial *and* temporal model characterization, i.e., the extended EOF technique.

Observations and model simulations have demonstrated links between seasonal to decadal SST variations in the Pacific and hydroclimate variations over the Great Plains. Of special interest has been the cause of long-term droughts. It has been argued, based on atmospheric GCM experiments, that the Dust Bowl, a decade-long dry period in the 1930s, is mainly caused by cool SST anomalies in the *tropical Pacific*. The results, however, are not unquestionable. For example, the model that reasonably simulated the Dust Bowl drought almost failed to simulate another major drought in the 1950s when tropical Pacific SSTs were actually much cooler than during the Dust Bowl (see Schubert et al. 2004). On the other hand, the model produced a fictitious drought in the 1970s when the Great Plains was fairly wet (see also Seager at al. 2005, with a different model); the tropical Pacific was indeed cool during this period. It is hence fair to ask whether decadal SST-drought linkages are robustly represented in GCMs, currently. This motivated the clarifying analysis of such linkages on an observational basis, which forms the second part of the work.

1.3 Objectives

The work aims to

- improve PDV characterization in the context of other natural variability modes as well as the secular trend, and
- clarify the connections between Pacific/Atlantic SSTs and long-term hydroclimate variations over the Great Plains.

1.4 Outline of chapters

A consistent analysis of natural variability and secular trend in Pacific SSTs in the twentieth century is presented in Chapter 2. In Chapter 3, the Pacific and residual Atlantic SST modes are investigated for their links to long-term hydroclimate variations over the Great Plains. Chapters 2 and 3 are self-contained, each having its own introductory and summarizing sections, and reflecting two individual submissions. A general summary is given in Chapter 4, with discussions of results and future work. Appendix A gives the formulation of the rotated extended EOF, the primary methodology used in Chapter 2.

Chapter 2 Pacific Sea Surface Temperatures: Variability and Trend[1]

2.1 Introduction

Sea surface temperature (SST) plays a critical role in our planet's climate. Its seasonal distribution as well as departures from the seasonal cycle influence weather and climate in both near and faraway regions. Coherent, large-scale SST departures, or anomalies, are manifest on interannual, decadal, and multi-decadal to century long timescales in the Pacific basin (and other oceans). A particularly well known and relatively well understood anomaly pattern is the El Niño–Southern Oscillation (ENSO), with robust SST variability on interannual timescales in the central and eastern tropical basin, and with ocean-atmosphere interaction as the driving mechanism for the oscillation.

The significance of variability on decadal timescales—commonly referred to as Pacific decadal variability (PDV)—was recognized following the nearly decade-long persistence of anomalous conditions in the extratropical basin since winter of 1976/77 (Nitta and Yamada 1989; Trenberth 1990). The decadal variability of Pacific climate has sometimes been referred to as "shift" of regime, or just climate-shift perhaps, because similar low-frequency changes (including oppositely signed ones) in the earlier twentieth century record had not been fully appreciated at that time. The climate-shift around 1976/77 has been recognized with a wide array of evidence in the North Pacific ocean-atmosphere system (e.g., Trenberth 1990; Ebbesmeyer et al.

[1] This chapter has been published (Guan and Nigam 2008).

1991; Graham 1994; Miller et al. 1994), which is likely not unique as found by more recent studies (Mantua et al. 1997; Minobe 1997; Hare and Mantua 2000). Pacific decadal variability has received considerable attention since the mid-1990s when ocean climate and fisheries were linked in the North Pacific (Mantua et al. 1997) and when PDV was linked to North American hydroclimate. The warm-season links are apparently important for both seasonal hydroclimate anomalies (e.g., Ting and Wang 1997) and multi-year droughts over the North American continent (e.g., Nigam et al. 1999; Barlow et al. 2001; Schubert et al. 2004; Seager et al. 2005).

The recent signs of climate change have generated substantial interest in separation of natural and anthropogenic variability, necessitating a discriminating analysis of low-frequency variations in the Pacific (and Indian Ocean) basin. The present study addresses this challenge by characterizing the secular trend in Pacific SSTs from an analysis that simultaneously extracts the recurrent spatiotemporal patterns of natural variability. The mutual consistency between natural variability and secular trend characterizations and among the natural variability modes themselves is a defining attribute of this analysis.

The problem is challenging, in part, because high-quality observational records are not of long enough duration for stable characterization of decadal variability and long-term trends in Pacific climate. Besides, some key variables such as subsurface ocean temperature (or heat content), which can effectively track coherent, low-frequency ocean variations remain inadequately defined. The data challenges not withstanding, the study describes an innovative analysis of the observations in hand, driven by the premise that a robust, improved characterization

of secular trend and natural variability patterns, including PDV structure, is possible with current datasets.

The study presents a *single* analysis for characterization of *all* the non-seasonal modes of Pacific ocean-atmosphere variability, including secular trend. One reason for the lack, hitherto, of a unified analysis concerns the analysis method employed in most previous studies [empirical orthogonal functions (EOFs)], and more specifically, its limitations in discriminating between spatially overlapping patterns having distinct variability timescales. The Pacific, interestingly, is home to at least two such patterns, ENSO and the PDV (e.g., Graham 1994).

The study describes findings on spatiotemporal structure of Pacific SST variability from an analysis that uses spatial *and* temporal recurrence in pattern recognition, all without imposing any periodicity constraints on data—the extended EOF (EEOF) analysis (Weare and Nasstrom 1982). As shown later, rotated EEOF analysis can effectively characterize variability evolution, including nascent phase structure; in contrast, canonical EOF analysis identifies the mature phase, whose large amplitudes contribute most to the explained variance. The present analysis shows how consideration of spatiotemporal recurrence can effectively discriminate between biennial, ENSO, and PDV variability patterns, and between secular trend and natural variability, all without any advance filtering (and potential aliasing) of data.

The primary analysis involving computation of rotated EEOFs of seasonally resolved, unfiltered SST anomalies in the Pan-Pacific domain during the twentieth century (1900–2002) is described in sections 2.3 and 2.4, while datasets and the analysis method are briefly discussed in section 2.2. The stability (robustness) and

physicality of variability patterns is ascertained from an extensive suite of sensitivity analysis, reported in sections 2.4 and 2.5. A synopsis and concluding remarks follow in section 2.6.

2.2 Dataset and analysis method

2.2.1 Dataset

The primary data analyzed in this chapter are the Met Office's (UKMO) Hadley Centre sea Ice and Sea Surface Temperature dataset (HadISST) 1.1 SST, which is globally available on a 1° × 1° grid for the period from 1870 onward. The SSTs were constructed using a reduced-space optimal interpolation and subsequent insertion of quality-controlled gridded observations onto the reconstruction (Rayner et al. 2003). Because of the relatively long record, data continuity, and statistical homogeneity, HadISST is the dataset of choice for analysis of Pacific low-frequency variability. The National Centers for Environmental Prediction–National Center for Atmospheric Research (NCEP–NCAR) reanalysis (Kalnay et al. 1996) provided the 1000-hPa winds for aspects of the analysis.

Seasonal means are computed from the monthly values, and the seasonal cycle, determined by the long-term mean of each season, is removed. The SST anomalies are interpolated to a 5° × 2.5° longitude–latitude grid in the interest of computational efficiency. To ensure each grid-cell's influence in the analysis is commensurate with its area, gridded SSTs were weighted by the square root of the cosine of the latitude (e.g., Chung and Nigam 1999). The SST data were not subjected to additional normalization, in particular, by the local standard deviation. The

undertaken EOF analysis is thus covariance rather than correlation based, giving regions with greater variance more influence in determining the outcome. The SSTs were also not filtered, as in some previous studies (e.g., Zhang et al. 1997).

The analysis is conducted in the Pan-Pacific domain (120°E–60°W, 20°S–60°N), which spans the Tropics of both hemispheres and the northern extratropics in the Pacific longitudes. A large domain analysis should yield more accurate characterization of the variability patterns from the full- and not just core-region sampling of their patterns. For instance, PDV and ENSO variability can be better defined from sampling of both their tropical and extratropical footprints.

2.2.2 Rotated extended EOF

A variant of regular EOF is the so-called extended EOF (EEOF), which, instead of providing a single spatial pattern (a "snapshot" of the mature phase), gives an l-member contiguous sequence of spatial patterns Δt apart in time (Weare and Nasstrom 1982). The parameters l and Δt are chosen so that the focus period ($l\Delta t$) covers a significant portion of variability evolution. The technique is equivalent to multi-channel singular spectrum analysis (von Storch and Zwiers 1999) when the chosen pattern interval (Δt) is the same as the sampling interval of the data record. A five-member anomaly sequence at seasonal intervals is used in the primary analysis, and sensitivity to these choices is discussed in section 2.5. The computations are conducted in MATLAB.

In canonical EOF analysis, modal structures are selected on the basis of their ability to successively explain maximal variance in the *entire* analysis domain, which can be both an advantage and a drawback. It would be a drawback if one or more

physical modes were dominant only in an analysis subdomain, for their limited contribution to domain variance could then reduce the chances of their correct identification. Not only that, emphasis on maximal accounting of the full domain variance can also make canonical analysis sensitive to domain size. Some of these deficiencies can be remedied by rotation of EOFs (Richman 1986), which yields more stable, physical results. Among the various rotation techniques, VARIMAX is a most common choice in climate studies. The technique maximizes the variance of the squared spatial loadings, leading to highly clustered structures that facilitate physical interpretation (Horel 1981).

The number of modes rotated in primary analysis is determined by the scree test (Cattell 1966). A "Rule N" test (Overland and Priesendorfer 1982) was first run, which showed the 29 leading EEOFs to be above the noise level. The scree test was conducted by plotting the unrotated eigenvalues against their root numbers, and finding the point where the curve becomes flat. The statistically significant modes to be rotated are those with "large" eigenvalues (i.e., ones easily separable from others in visual inspection of the distribution). For the primary analysis, seven modes are rotated (cf. Fig. 2.1; figures are placed at the end of each chapter), and the analysis's sensitivity to the number of rotated modes is discussed in section 2.5.

The leading variability modes identified by the primary analysis are described in the next two sections. Seasonal-mean anomalies of all four calendar seasons are analyzed together in the interest of tracking and identifying variability patterns on the basis of recurrent spatiotemporal evolution. The names and labels attached to the

modes and the percentage variance they explain are given in Table 2.1. The corresponding principal components (PCs) are shown in Fig. 2.2.

Table 2.1. Leading modes identified by the rotated EEOF analysis of unfiltered, seasonal SST anomalies during 1900–2002 in the Pan-Pacific domain of 120°E–60°W, 20°S–60°N.

No.	*Variance Explained (%)*	*Name*	*Label*
1	17.7	$ENSO^{+}$	$ENSO^{+}$
2	13.6	$ENSO^{-}$	$ENSO^{-}$
3	10.2	Trend	Trend
4	5.3	PDV Pan-Pacific	PDV^{PP}
5	4.3	Non-canonical ENSO	$ENSO^{NC}$
6	4.3	PDV North Pacific	PDV^{NP}
7	3.5	Biennial	Biennial

2.3 ENSO evolution

2.3.1 Canonical evolution

The current analysis, emphasizing evolution, describes ENSO using two modes, one depicting the growing phase while the other its decaying phase; together they describe the canonical ENSO (cf. Rasmusson and Carpenter 1982), as shown in Fig. 2.3. The season labels attached to the SST maps in Fig. 2.3 are obtained from additional analysis,[2] since the primary analysis is an all-season one. Note, ENSO is characterized by its mature phase (northern winter) pattern in regular EOF analysis.

During the growth phase of ENSO[3] (hereafter $ENSO^{-}$, "–" for peak minus; Fig. 2.3, left column), positive SST anomalies first appear in the eastern equatorial Pacific, and then extend westward across the dateline—the classic evolution. Unlike the growth phase, the decay phase (hereafter $ENSO^{+}$, "+" for peak plus; Fig. 2.3, right

[2] Lead/lag regressions are computed for ENSO PCs, with all but one calendar season's PC zeroed out. Four sets of maps are thus obtained for each ENSO PC. The season labels in Fig. 2.3 are then determined by finding which of the four maps is closest to the displayed modal evolution.
[3] ENSO discussion in this chapter is mostly in the context of El Niño evolution, but it is equally applicable to the cold La Niña phase.

column) is characterized by near-simultaneous loss of amplitude across the basin; the loss being especially steep during spring and summer. The rapid summer-to-winter build-up and the slow winter-to-summer demise of the midlatitude basin anomalies are also noteworthy. Although not investigated here, there is indication of SST development in the tropical North Atlantic and western Pacific (and Indian Ocean, not shown) with ENSO maturity and decay; consistent with earlier findings [e.g., Carton and Huang (1994) on the Atlantic and Nigam and Shen (1993) on Indian Ocean links].

The relation between ENSO PCs and the Nino3.4 SST index (a widely used marker of ENSO variability) is shown in Fig. 2.4. The $ENSO^{-}$ ($ENSO^{+}$) PC leads (lags) the Nino3.4 index by two (one) seasons, consistent with the spatial patterns in Fig. 2.3, in that simultaneous regressions of the $ENSO^{-}$ ($ENSO^{+}$) PC represent the summer (spring) season pattern. The PCs themselves have a three-season shift in time.

2.3.2 Non-canonical evolution

Of special interest is the fifth-leading mode, the most notable feature of which is *eastward* development of positive SST anomalies along the equator, beginning with the central Pacific ones (Fig. 2.5). As this development is opposite of that in canonical ENSO, the mode is referred to as the non-canonical ENSO mode (labeled $ENSO^{NC}$). A striking feature of the mode is also its connection to the North American continent, which intensifies with equatorial SST development. The northeastward sloping SST structure is reminiscent of the northeast trade wind distribution, and not inconsistent with diminished trade winds and latent heat flux.

The ENSO^{NC} PC exhibits stronger amplitude and longer time scales in the post–climate shift (1977 onward) period (cf. Fig. 2.2). Correlations with Nino3.4 index are strongest at 5-season lead in the recent period (see Fig. 2.6, open circles), and contemporaneously in the earlier period (not shown). The mode thus opposes canonical ENSO evolution in the 1977–2002 period. Given that El Niño SST anomalies exhibit west-to-east development in this period (Wang 1995), the ENSO^{NC} mode must not only oppose but overwhelm the canonical mode contributions, at least in this feature. Equatorial SST development can be surmised from the Fig. 2.6 cross-correlations.[4]

The ENSO^{NC} mode captures recent changes in ENSO evolution. The progressively increasing variance and period manifest in this mode's PC in recent decades are consistent with previous findings on increased ENSO energy and persistence in the post–climate shift period (e.g., Gu and Philander 1994; Zhang and Busalacchi 2005). Using nonlinear, neural network based EOF analysis, Monahan (2001) found a non-canonical ENSO mode that also characterized temporal nonstationarity relatable to the 1976/77 climate-shift; spatial evolution of this mode however differs from the one described herein. ENSO-unrelated interannual SST variability was also investigated by Mestas-Nuñez and Enfield (2001), and their 0–8-yr mode could well represent aspects of non-canonical ENSO (and biennial, discussed later) variability. Departures from canonical El Niño development have been also characterized using the Trans-Niño index (Trenberth and Stepaniak 2001),

[4] The negative correlation (−0.54) between ENSO^{NC} and ENSO^{+} modes at −1 seasons indicates that the former lags the negative phase of the latter (i.e., the ENSO^{NC} follows La Niña decay). The positive correlation (0.36) between the non-canonical and ENSO^{-} modes at +4 seasons, on the other hand, indicates that coastal warming follows the ENSO^{NC} mode (or central Pacific SST development), by almost a year.

which is defined as the difference between the normalized SST anomalies in the Nino1+2 and Nino4 regions. This index is correlated with $ENSO^{NC}$ PC at −0.65.

2.3.3 Evolution timescale

The inherent time-scale of canonical and non-canonical ENSO modes is estimated from lead/lag autocorrelations of their PCs (Fig. 2.7). Also shown are autocorrelations of the original and synthetic Nino3.4 SST indices. The original index is the standard one (i.e., from "raw" SST anomalies) while synthetic ones are from reconstructed SST anomalies. Anomalies are reconstructed from canonical and non-canonical PCs by adding products of PCs and their zero-lag regressions. Synthetic Nino3.4 indices are then generated in the usual manner, by averaging SST anomalies in the 170°W–120°W and 5°S–5°N equatorial strip.

The lead/lag autocorrelation statistic is a simple, straightforward way to analyze event longevity and identify oscillatory timescales. The width of the autocorrelation curve provides an estimate of event duration in any one phase, or the approximate half-period. Inspection of Fig. 2.7 shows the canonical modes ($ENSO^{-}$, $ENSO^{+}$) and the standard Nino3.4 index to have similar distributions, with first zero-crossings at ±1 yr, i.e., about 2 yr apart. In contrast, autocorrelations of the $ENSO^{NC}$ PC fall off more slowly, leading to first zero-crossings that are 5–6 yr apart. Interestingly, these longer timescales are not prominently manifest in the synthetic Nino3.4 index ($ENSO^{-}$ +$ENSO^{+}$ +$ENSO^{NC}$); reflecting dominance of the canonical contributions. The addition of $ENSO^{NC}$ mode to canonical variability does however reduce autocorrelations of the derived index at ±2 yr, from −0.34 to −0.17; leading to reduced oscillatory tendency. Given that $ENSO^{NC}$ mode is notably flexed in recent

decades, one would expect ENSO phase transitions in the earlier period to be more regular, assuming other modes are, energetically, quasi-stationary. Perusal of PCs in Fig. 2.2 indicates this is not the case, perhaps, because of significant variations in the energy of the canonical modes themselves.[5]

The difference in autocorrelation distribution of the standard and synthetic Nino3.4 indices, especially, in zero-crossing times is also noteworthy in Fig. 2.7. Zero-crossings of both synthetic indices are further apart by ~0.5 yr, pointing to a somewhat longer ENSO period than indicated by the standard index. As the three-mode synthetic index is based on all ENSO-related modes in the EEOF analysis, the period discrepancy is a bit perplexing, leading one to question the suitability of the standard Nino3.4 SST index as marker of true ENSO variability (defined by the three-mode synthetic index, in context of this analysis).

Alternatively, one could ask if this difference in ENSO-period can be accounted for by inclusion of the only other, and hitherto unconsidered, interannual mode—biennial variability (shown and discussed later)—in the synthetic index definition. The expanded four-mode definition, indeed, eliminates the above-noted difference in autocorrelation functions. While this is reassuring, it does emphasize the implicit inclusion of biennial variability in the standard Nino3.4 index. For reference, seasonal correlations of the standard Nino3.4 SST index with synthetic indices in the 1900–2002 period are 0.84 with the two-mode (canonical modes) index, 0.92 with the three-mode (additional $ENSO^{NC}$) index, and 0.95 with the four-mode (additional biennial) index.

[5] Increased energy of the canonical modes in the post–climate shift period is reflected in greater negative autocorrelations of the related synthetic Nino3.4 index at 2-yr lead/lag: −0.52 versus −0.29 in the earlier period and −0.34 in the full record.

2.3.4 SST evolution at the equator

ENSO evolution is commonly described by displaying SST development at the equator. The Hovmöller display is helpful in tracking the longitudinal propagation of SST anomalies and in monitoring ENSO period. Evolution is examined through lead/lag index regressions in the entire record and in the pre– and post–climate shift periods. Figure 2.8 shows equatorial SST evolution over a nine-season span centered on the ENSO warm phase. Regressions of the standard Nino3.4 SST index based on the full twentieth-century record are shown in the top-left panel, while those for the pre– and post–climate shift periods are in the top-middle and right panels. Immediately apparent is the very different evolution of equatorial SST anomalies: from east-to-west in the earlier record (canonical picture) and west-to-east in recent decades (non-canonical development), with the full-period regressions being a weighted average.

The contribution of canonical modes ($ENSO^{-}$ and $ENSO^{+}$) in equatorial SST development, from regressions of the related synthetic Nino3.4 index, is displayed in the second from top row. There is evidently little change in evolution structure across periods other than an amplitude increase in recent decades. The canonical contribution is thus quite stationary with respect to climate-shift, and at odds with the recent evolution, not surprisingly. The combined contribution of the canonical and non-canonical modes is plotted in the second from bottom row for all three periods, again from regressions of a synthetic index but one based on three modes. It is apparent that only when $ENSO^{NC}$ is included in the reconstruction can the change in SST evolution across the climate shift be reproduced. The century-based pattern is

also in better accord, with maximum amplitudes being more away from the South American coast.

Consideration of canonical and non-canonical modes has led to credible reconstruction of ENSO SST evolution at the equator, but not in one aspect—the duration of warm anomalies, which is shorter in regressions of the standard Nino3.4 index (top row). The implicit inclusion of biennial variability in the standard index must lead to this discrepancy, for reasons noted earlier (cf. Fig. 2.7). This is verified from yet another construction of SST evolution (bottom row), this time from regressions of the four mode-based Nino3.4 index; the fourth mode being biennial variability. The new reconstruction is in remarkable agreement with that displayed in the top row, confirming the significant but implicit contribution of biennial variability in the standard Nino3.4 SST index.

The earlier posed question on which ENSO index—standard or the three mode-based synthetic Nino3.4 SST index—better marks ENSO variability is now weightier, especially, in context of theoretical and modeling analysis of ENSO dynamics and thermodynamics.

2.3.5 ENSO^{NC} and the Pacific meridional mode

Recently, Chiang and Vimont (2004) have argued for the existence of a meridional mode in the Pacific basin, similar to the one posited for the Atlantic where the mode represents interannual-to-decadal variability in the tropical basin. Both meridional modes are envisioned to be similarly driven, through SST-wind coupling in the deep Tropics and wind-driven SST anomalies in the northern Tropics. The meridional mode is the leading mode in Chiang and Vimont's maximum covariance

analysis of Pacific SST and 10-m wind, but after the local linear trend and ENSO variability is removed from data. ENSO variability is filtered by subtracting regressions of the Pacific cold-tongue index[6] (CTI; Deser and Wallace 1990).

Our interest in investigating links between the meridional and ENSO^{NC} modes stems from their common characterization as being independent of ENSO variability: in a linear sense in case of the meridional mode, and in a modal context in case of ENSO^{NC}. Despite linear/modal independence, these modes remain connected to aspects of ENSO variability: ENSO nonlinearity in case of meridional mode, and non-canonical evolution in case of the ENSO^{NC} mode. Such common attributes motivate the present examination of sameness of these modes.

The SST and 1000-hPa wind regressions of the ENSO^{NC} PC are plotted in Figs. 2.9a,b in a domain and format similar to Chiang and Vimont's (2004) Fig. 1a, and with their analysis period (second half of the twentieth century); ENSO^{NC} PC is still from the earlier, full-period analysis. The SST pattern, especially the one at two-season lead (Fig. 2.9a) is similar to Chiang and Vimont's in the Tropics and subtropics, but wind features along the equator are less similar. The simultaneous pattern (Fig. 2.9b) exhibits even less similarity in view of SST development at the equator in the intervening season. The lack of correspondence likely results from how data is filtered in the two analyses. Chiang and Vimont prefilter the data, as described above, and while there is no explicit filtering here, temporally orthogonal PCs in EOF (and EEOF) analysis effectively filter the record for unrelated variability.[7] But there

[6] The SST cold-tongue index, defined as the average SST anomaly in the 6°S–6°N and 180–90°W equatorial box, is also commonly used to mark ENSO variability. Its seasonal correlation with the Nino3.4 SST index is 0.99 in the 1900–2002 record.
[7] PC orthogonality remains intact under EOF rotation.

is no assurance that the same signal is getting filtered in both analyses, especially, since the standard Nino3.4 SST (or cold tongue) index also represents aspects of $ENSO^{NC}$ and biennial variability, as shown earlier in this section.

The $ENSO^{NC}$ structure is thus reexamined in Figs. 2.9c,d, this time from PC regressions on explicitly filtered SST, with the filtering exactly as in Chiang and Vimont (2004). The PC is from the primary (full twentieth century) analysis, as before, given our interest in robust characterization of the secular trend in context of natural variability. The regressions, especially, the simultaneous one (Fig. 2.9d) now exhibits striking correspondence with the Chiang and Vimont SST and wind patterns. Further and more conclusive support for the sameness of the meridional and $ENSO^{NC}$ modes comes from rotated EEOF analysis of the detrended 1945–2002 SSTs. Regressions of the $ENSO^{NC}$ PC from this analysis,[8] shown in Figs. 2.9e,f, are almost indistinguishable from patterns in Figs. 9c,d and also from Chiang and Vimont's Fig. 1a.

The above analysis shows that the $ENSO^{NC}$ mode is closely related to the meridional mode of Chiang and Vimont (2004). It moreover suggests that the largely tropical $ENSO^{NC}$ mode, while not involved in canonical ENSO evolution, encapsulates lower frequency changes in ENSO variability, as shown in Figs. 6–8. Its seasonal structure and evolution must therefore be characterized in context of *all* non-seasonal modes of variability with tropical footprints (canonical ENSO, biennial, decadal variability, and climate trend); much as in this study. The analysis also

[8] The new $ENSO^{NC}$ PC in correlated at 0.95 with the original one (cf. Fig. 2.2) in the overlapping period.

highlights the pitfalls of using the standard Nino3.4 (or cold tongue) SST index to represent (filter) canonical ENSO variability.

2.3.6 Biennial variability

Biennial variability is captured by the seventh (last) mode; see structure of PC7 in Fig. 2.2. Biennial variability in the tropical Pacific was noted in context of ENSO variability by Rasmusson et al. (1990), who argued for its importance in the ENSO cycle on the basis of the near 2-yr timescale of individual warm and cold events and their phase-locking with the annual cycle. Rasmusson et al. viewed ENSO as a superposition of biennial and lower-frequency variability—a view strongly supported by our analysis of SST evolution, especially Figs. 2.7 and 2.8.

The biennial mode (Fig. 2.10) shows SST anomalies emerging from the eastern equatorial Pacific and extending westward over time, towards the dateline. At the beginning of the displayed cycle, SSTs resemble the cold ENSO phase. However, in just about three seasons ($t-3$ to t), SSTs switch sign and become tightly focused around the equator in the central/eastern basin. The amplitude ($\lesssim 0.4$ K) and meridional extent are also smaller than in canonical ENSO. This biennial variability structure is somewhat different from earlier descriptions: the asymmetry in cold and warm phase evolutions and westward propagation of SSTs in the cold tongue sector were, perhaps, not recognized earlier. Pacific biennial variability also had links to the Indian Ocean in Rasmusson et al. (1990) and Barnett (1991), but none are evident here (not shown).

2.4 Pacific decadal variability and secular trend

Decadal variability is captured by two modes in this analysis: the fourth (Pan-Pacific) and the sixth (North Pacific) leading modes. The related PCs (Fig. 2.2) exhibit variations on long timescales (longer than ENSO's), capturing the climate shifts in the twentieth century: PC4 has the 1920s shift, while the 1940s and mid-1970s shifts are manifest in PC6. These shifts have been noted in context of Pacific SST variability by Mantua et al. (1997) and Minobe (1997).

2.4.1 Pan-Pacific mode

The Pan-Pacific (hereafter PDV^{PP}) evolution is shown in Fig. 2.11, with panels now a year apart; regressions in the analysis-domain are in the left column, while global SST correlations are in the right one. The PDV^{PP} mature phase (second panel from the bottom) contains negative SST anomalies in a limited region of the central North Pacific, surrounded by stronger positive anomalies extending eastward from the Bering Sea and then downward until Baja California; and then sweeping back southwestward towards the tropical Pacific (a horse-shoe shaped structure). Noteworthy is the lack of SST anomalies in the central/eastern equatorial Pacific and hints of clockwise development along the North American west coast, with SSTs becoming as large as 0.4 K before decaying.

A Pan-Pacific mode equivalent has been identified in some previous studies, but with somewhat different structure and names. Our PDV^{PP} is similar to Barlow et al.'s (2001) where data was not prefiltered and rotation applied, as here, but where regular rather than EEOF analysis was executed. Barlow et al.'s mode (their Fig. 2b) exhibits a far greater equatorial reach than ours though. Our PDV^{PP} structure differs

from Zhang et al. (1997), Nakamura et al. (1997) and Wu et al. (2003) notably in the quiescence of the central/eastern equatorial Pacific in all phases, and in the near insignificance of SST anomalies in the central North Pacific. This mode has been referred to as "ENSO-like" (e.g., Zhang et al. 1997), a somewhat misleading name in our opinion, given the very different spatiotemporal structure of ENSO (Fig. 2.3) and PDV^{PP} (Fig. 2.11). [For reference, the Pan-Pacific mode and Mantua et al.'s Pacific Decadal Oscillation (PDO) are correlated at 0.23; not surprising, given the PDO's North Pacific focus.]

The origin of Pacific decadal variability remains intriguing, but global SST correlations of the PDV^{PP} mode provide some insights; correlations are contoured at 0.1 intervals, beginning with 0.2 in the right panels of Fig. 2.11. Immediately apparent is the strong connection to the northern Atlantic, especially the western tropical/subtropical basin, a weak link to the equatorial Pacific, particularly in the pre-mature phase, little connection to the central North Pacific sector; and development of an Indian Ocean connection, albeit modest, during modal evolution.

The PDV^{PP} links with the Atlantic, especially the Caribbean where correlations are ~0.4–0.5, indicate Pacific–Atlantic basin connectivity on decadal timescales. While such connections have not been explicitly analyzed, they are to an extent manifest in analysis of Mestas-Nuñez and Enfield (1999, their rotated EOF 1 and 2), and in the related Atlantic Multidecadal Oscillation (AMO) SST footprint (Enfield et al. 2001, their Fig. 1b). An intercomparison shows considerable similarity between the PDV^{PP} mature phase footprint in the Atlantic and the AMO structure. The modes are also temporally linked: seasonal correlation is 0.42, and 0.48 with the

PDV^{PP} leading AMO by 5 seasons. To be sure, there are differences between these modes as well, in part, due to differences in the underlying analyses (e.g., Mestas-Nuñez and Enfield detrended and prefiltered SSTs prior to analysis, based on complex EOFs; their analysis period was also different).

2.4.2 North Pacific mode

The second decadal mode (North Pacific, hereafter PDV^{NP}; Fig. 2.12, left panels) is characterized by a zonally elongated band of positive SST anomalies centered along the sub-Arctic front and the dateline. Modal evolution apparently involves tropical SSTs as well: cold SST development in the eastern basin in tandem with the growth of positive anomalies in the central North Pacific. A causal role for eastern Pacific SSTs is, however, unlikely given their modest amplitude ($\lesssim 0.2$ K) and location (atop the climatological SST cold tongue). SST anomalies are even weaker in the Indian Ocean and the western tropical Pacific but potentially more significant (see right panels of Fig. 2.12), given the smaller SST interannual variability there, and more influential given the much warmer climatological state on which they reside. Note, the tropical Indian Ocean was recently shown to be a sensitive forcing region for the North Pacific climate (Deser and Phillips 2006).

A distinct North Pacific mode of decadal variability, similar to PDV^{NP}, was noted in earlier studies (e.g., Deser and Blackmon 1995; Nakamura et al. 1997; Mantua et al. 1997; Nigam et al. 1999; Barlow et al. 2001; Wu et al. 2003). Because of the North Pacific focus, Mantua's PDO and our PDV^{NP} resemble each other in the midlatitude basin (the two are correlated at -0.57); both capture the recent 1976/77

climate shift as well. Not all previous extractions of the North Pacific mode share this attribute though (e.g., Deser and Blackmon 1995).

The origin of North Pacific decadal variability remains to be elucidated. The shortness of the observational record has stymied progress, as also the finding of weak connections to the tropical Pacific in context of a mindset (based on two decades of ENSO research) reflecting the primacy of the Tropics.

The right panels of Fig. 2.12 display global SST correlations of the PDV^{NP} PC, and show, perhaps for the first time, rather striking links of the North Pacific decadal mode to the western tropical Pacific and Indian Ocean SSTs—links not evident in the regression patterns for reasons noted earlier. The western Pacific/Indian Ocean correlations develop in tandem with the opposite signed ones in the North Pacific: being ~0.3 at $t-8$, ~0.4 at $t-4$, and up to 0.5 in the PDV^{NP} mature phase (t); note the focusing of correlations over Micronesia and the Philippine Sea in the mature phase.[9] Correlations build up in the southeastern equatorial Pacific as well, exceeding 0.4 at $t-4$ but dissipating prior to the attainment of peak North Pacific amplitudes. Also noteworthy and potentially interesting are the leading correlations (~0.4) southeastward of Greenland.

A more in-depth analysis, including modeling, will be necessary to establish causal significance of the correlated regions in Fig. 2.12. The Indian Ocean and western tropical Pacific SST links of the PDV^{NP} mode revealed by this analysis are, however, not inconsistent with the recently highlighted role of the Indian ocean basin

[9] Connections between the tropical/subtropical Indian Ocean and North Pacific SSTs were noted by Kawamura (1994), but Zhang et al. (1996) found the regions weakly connected in the ENSO filtered fields.

(SST, aerosols) in global climate variability: NAO trend (Hoerling et al. 2004), droughts (Lau et al. 2006), monsoon changes/trend (Chung and Ramanathan 2006), and—the one most closely related to this study—Aleutian sector climate variability/shift (Deser and Phillips 2006).

2.4.3 Mode physicality

The physicality of the extracted modes is a concern in most statistical analysis, including this one. Could the identified modes be statistical artifacts, for instance? While there is no well-defined strategy to ascertain mode physicality, decadal variations in SST and related physical variables (e.g., precipitation, salinity) can have reflections in the climate-sensitive marine (and terrestrial) ecosystems, including fish recruitment records (Mantua et al. 1997; Chavez et al. 2003);[10] which can be advantageously used to gauge the physicality of the decadal modes.

Mode physicality is assessed here from correlations of the PDV PCs and the North Pacific and Bering Sea biological time series assembled by Hare and Mantua (2000) for the 1965–1997 period. Correlations of the PDO index and biological time series provide a reference point in this assessment. Table 2.2 lists the three most correlated biological records for each mode: PDV^{PP}, PDV^{NP} and PDO. The PDO correlations are noted in each case, for reference. The highest annual correlation of the PDV^{PP} mode (0.54) is with the Eastern Pacific zooplankton biomass record and then with the British Columbia salmon catches (−0.42)—not surprising, given the coastal focus of the Pan-Pacific mode. The PDV^{NP} mode is most correlated with the Gulf of Alaska halibut record (−0.74), marginally exceeding the highest PDO

[10] The ecosystem changes can feedback to the physical climate (e.g., Miller et al. 2003).

correlation (0.73) also with the same recruitment record. The extracted decadal modes, PDV^{PP} and PDV^{NP}, thus appear to be reasonably physical, at least, by this measure. Characterization of variability mechanisms and modeling analysis is, however, needed to rigorously assess the physicality of these modes.

Table 2.2. Correlations of the two PDV principal components with selected biological time series in the data available period (1965–1997). Time series 1–3, 4–6, and 7–9, in the Hare and Mantua (2000) dataset, are most correlated with the PDV^{PP}, PDV^{NP}, and the PDO index, respectively. All time series are annually resolved. The numbers following the time series name are the original dataset tags, listed for reference here. Note, time series 4 and 7 are identical.

No.	*Biological time series*	*PDV^{PP}*	*PDV^{NP}*	*PDO*
1	Eastern Pacific zooplankton biomass (40)	0.54		0.10
2	British Columbia coho salmon catch (67)	−0.42		−0.17
3	British Columbia pink salmon catch (68)	−0.42		−0.13
4	Gulf of Alaska halibut recruitment (43)		−0.74	0.73
5	West Coast mackerel recruitment (81)		−0.73	0.66
6	Central Alaska Chinook catch (51)		−0.68	0.59
7	Gulf of Alaska halibut recruitment (43)	−0.13	−0.74	0.73
8	Eastern Bering Sea rock sole recruitment (20)	0.24	−0.61	0.67
9	Central Alaska pink catch (54)	0.29	−0.62	0.67

2.4.4 Twentieth century SST trend

The third-leading mode captures the secular trend in the Pacific SST record, as apparent from its PC (Fig. 2.2), which is strikingly similar to both the global surface air temperature trend [e.g, National Aeronautics and Space Administration Goddard Institute for Space Studies (NASA GISS)] and the ocean heat content trend (Levitus et al. 2005). Modal structure (Fig. 2.13) shows pervasive SST-warming except for two small regions of cooling in the Northern Hemisphere: an equatorial sliver in the central Pacific and another off the southern tip of Greenland. The

warming is evidently largest along the eastern coasts of Asia and North America, where the twentieth-century SST change is as much as 1.5 K. A similar SST pattern emerges from the least squares fitting of the SST trend at each grid point. The displayed EEOF-based extraction and the fitted trend are spatially correlated at 0.9.

The EEOF-based extraction is preferred, as the secular trend is not constrained to be stationary in time here (which is the case in least squares fitting). It is, moreover, desirable, as noted in the introduction, to extract secular trend in the context of natural variability. The modest fluctuations in PC3 (Fig. 2.2) as it shifts from negative values in the early-century to positive ones in recent decades reflects the accommodation of natural variability.

It is interesting to compare our secular trend with that found in earlier studies. An additional cooling center in the North Pacific is present in Cane et al.'s (1997, their Fig. 3) analysis of linear trend in the 1900–91 Kaplan SSTs (Kaplan et al. 1998). A longer period (1854–1992) analysis by Kaplan et al. (2000) also finds much the same. [The additional cooling center must be due to dataset differences as least squares fitting of the Hadley SST record does not contain this feature.]

2.5 Sensitivity analysis

Robustness of the spatiotemporal variability modes is ascertained in this section from perturbation of the primary analysis. Table 2.3 summarizes the sensitivity tests. Each test focuses on an aspect of the primary analysis (T0): analysis domain (T1), climatology base period (T2), analysis period (T3 and T4), number of rotated modes (T5), and sampling window length (T6–T8). Tests T1–T5 closely follow the primary analysis (T0), except for the indicated changes. Tests T6–T8 are

devised to assess if the five-season-long sampling window is of sufficient duration to sample decadal variability, and these are, of necessity, implemented somewhat differently. In these, SST is first residually reconstructed from the primary analysis PCs and EOFs [i.e., by excluding ENSO ($ENSO^{-}$, $ENSO^{+}$, $ENSO^{NC}$) and the biennial modes from the raw anomalies]. The reconstructed SSTs are then analyzed with longer sampling windows (14–20-season duration), but with rotation of three modes in the interest of comparison with the primary analysis.

Table 2.3. Sensitivity tests: T0 is the primary analysis. The Pacific analysis domain is 120°E–60°W, 20°S–60°N, while the Indo-Pacific one extends it further westward to 30°E.

Name	*Domain*	*Period*	*Climatology*	*Rotated*	*Time Window*
T0	Pacific	1900–2002	1900–2002	7	1 season × 5
T1	Indo-Pacific	1900–2002	1900–2002	7	1 season × 5
T2	Pacific	1900–2002	1945–2002	7	1 season × 5
T3	Pacific	1945–2002	1945–2002	7	1 season × 5
T4	Pacific	1900–1976	1900–1976	7	1 season × 5
T5	Pacific	1900–2002	1900–2002	9	1 season × 5
T6	Pacific	1900–2002	1900–2002	3	2 season × 5
T7	Pacific	1900–2002	1900–2002	3	2 season × 7
T8	Pacific	1900–2002	1900–2002	3	4 season × 5

Table 2.4 summarizes the test findings by tabulating the mode order, percentage of explained variance, and correlation between the T0 and test case PCs. Of these, correlations is perhaps most indicative of analysis stability. Table 2.4 suggests

- robust stability of the $ENSO^{-}$, $ENSO^{+}$, biennial, and trend modes; correlations in the 0.92–1.0 range;
- that analysis period differences (T3, T4) impact the low-frequency modes, not surprisingly. $ENSO^{NC}$ is impacted most (0.69–0.97) because of its uneven energy

in the record, more in the second half (cf. Fig. 2.2), consistent with its accounting of more variance in T3 than in T0 or T4;

- lack of separation between the trend and PDV^{NP} mode in the pre–climate shift period, for the third mode in T4 is correlated to both the trend (0.92) and PDV^{NP} (0.77) modes of T0. This lack of separation is also suggested by their similar PC structure in this period in Fig. 2.2;
- insensitivity of the PDV modes to sampling window variations (T6–T8), indicating sufficiency of the 5-season sampling window of the primary analysis for detection and separation of biennial, ENSO, and decadal variabilities, and secular trend, all in one step.

Table 2.4. Sensitivity test results: column 1 shows the leading modes identified in the primary analysis (T0); numbers following the name indicate the percentage variance explained by the mode and its rank, respectively. Columns 2–9 list attributes of the leading modes in the eight sensitivity tests (T1–T8), with the three slash-delimited numbers indicating correlation between the test case and primary analysis PCs, the percentage variance explained by that mode, and its rank in the test analysis. Column 10 is identical to column 1. Asterisks indicate "not applicable".

T0	*T1*	*T2*	*T3*	*T4*	*T5*
$ENSO^{PP}$ /17.7/1	1.00/16.6/1	1.00/16.6/1	1.00/18.4/1	0.99/18.7/1	0.99/17.2/1
$ENSO^{PM}$ /13.6/2	1.00/12.8/2	1.00/12.8/3	1.00/14.3/2	0.99/14.7/2	1.00/13.8/2
Trend /10.2/3	0.99/11.4/3	0.99/15.1/2	0.95/ 6.1/3	0.92/ 8.3/3	0.98/ 9.8/3
PDV^{PP} / 5.3/4	0.99/ 5.0/4	0.99/ 4.9/4	0.82/ 4.1/6	0.96/ 7.8/4	0.77/ 6.1/4
$ENSO^{NC}$ / 4.3/5	0.98/ 3.8/6	1.00/ 4.1/5	0.97/ 6.0/4	0.69/ 2.8/7	0.84/ 3.5/6
PDV^{NP} / 4.3/6	0.98/ 4.4/5	0.99/ 4.0/6	0.79/ 4.7/5	0.77/ 8.3/3	0.68/ 3.2/7
Biennial / 3.5/7	0.98/ 3.4/7	1.00/ 3.3/7	0.98/ 3.8/7	0.92/ 3.4/5	0.95/ 3.5/5

T6	*T7*	*T8*	*T0*
*	*	*	$ENSO^{PP}$ /17.7/1
*	*	*	$ENSO^{PM}$ /13.6/2
0.97/16.3/1	0.96/15.9/1	0.90/15.3/1	Trend /10.2/3
0.92/ 6.7/2	0.87/ 5.8/2	0.78/ 5.7/3	PDV^{PP} / 5.3/4
*	*	*	$ENSO^{NC}$ / 4.3/5
0.92/ 5.9/3	0.87/ 5.6/3	0.78/ 5.9/2	PDV^{NP} / 4.3/6
*	*	*	Biennial / 3.5/7

A lingering concern in EOF analysis pertains to rotation—not just the number of modes rotated (investigated above) but to rotation itself: Does rotation of EOFs yield more "physical" modes of variability? A physical realization of the extracted modes would, surely, be the ultimate proof of physicality, but it is seldom that variations from climatology are comprised of just one mode of variability in nature (i.e., with all other modes suppressed at the same time). Of course, when this happens, an observational "analog" of that mode is encountered. The number of observational analogs of an extracted set of modes in the record can be one objective measure of the "physicality" of that extraction, and this strategy is used here.

An observed anomaly will be deemed a modal analog in context of an extraction, should any one PC be larger than all others in that analysis by at least one unit of magnitude; note, PCs are orthonormal, with/without rotation. The identification is objective and easily implemented, and Table 2.5 presents the number of analogs found in five analyses. The number is expectedly small, as analogs are rare; ~10% in Table 2.5 as 408 anomalies (five-season span) are analyzed in each case. A significant increase (~20%) in the number of analogs in the corresponding rotated analysis (regular or extended) is noted. Interestingly, rotating 9 modes reduces the number of analogs, further justifying our choice of rotating 7 modes in the primary EEOF analysis.

Table 2.5. Number of "analogs" in five EOF analyses of 1900–2002 Pacific SST variability. See text for details, including analog definition.

EOF	*Rotated EOF*	*EEOF*	*Rotated EEOF (7 rotated)*	*Rotated EEOF (9 rotated)*
46	56	37	46	37

2.6 Summary

The twentieth century SSTs in the Pacific basin are analyzed for consistent characterization of natural variability and secular trend; motivated by the need to apportion oceanic warming, both temporally and regionally. The evolution-centric analysis is conducted using the extended EOF technique which was introduced to climate sciences by Weare and Nasstrom (1982) almost a quarter-century ago, and interestingly, demonstrated on Pacific SSTs!

The technique is effective in separating variability modes having similar spatial patterns but different temporal evolution and/or time scales. Pacific decadal variability, which is reckoned to include an "ENSO-like" structure, would thus be a choice test problem. But for reasons unknown, PDV characterization has hitherto been undertaken with temporally filtered data sets, when filtering can inadvertently alias the target structures; data detrending can, likewise, be problematic. Many of these concerns become moot with extended EOF analysis. The method is particularly effective in characterizing both the nascent and mature phases of variability.

Findings from a *single* analysis that effectively discriminates between biennial, ENSO, and decadal variabilities, and between these natural variability modes and secular trend, are reported in this chapter. The principal findings are:

- *canonical ENSO variability*: encapsulated in two modes that depict the growth (east to west along the equator; $ENSO^{-}$) and decay (near-simultaneous amplitude loss across the basin; $ENSO^{+}$) phases; $ENSO^{+}$ lags $ENSO^{-}$ by 3 seasons, and the Nino3.4 SST index by one season;

- *non-canonical ENSO variability*: represented by an interannual mode of comparatively lower frequency that has been energetic in recent decades; shown linked to the west-to-east SST development seen in post–climate shift ENSOs; the $ENSO^{NC}$ mode. It leads the Nino3.4 index by five seasons in the recent record. The $ENSO^{NC}$ mode is closely related to Chiang and Vimont's (2004) meridional mode which represents interannual-to-decadal variability in the tropical basin, much as in here;
- *ENSO time scale*: autocorrelation of synthetic Nino3.4 SST indices shows that the $ENSO^{NC}$ mode leads to some reduction in canonical ENSO's oscillatory tendency, while addition of the biennial mode reduces the duration of canonical episodes, by ~0.5 yr;
- *Nino3.4 SST index*: comprised of canonical, non-canonical and biennial variability. Original index correlated with the synthetic one based on canonical modes at 0.84, with the canonical plus non-canonical based synthetic index at 0.93 and with the index that additionally includes the biennial mode at 0.95;
- *Pacific decadal SST variability*: characterized by two modes:
    - the *Pan-Pacific* mode (PDV^{PP}) has a horse-shoe shaped structure with the closed end skirting the North American coast; and a quiescent central/eastern equatorial Pacific. Surprising connections to the tropical/subtropical Atlantic (Caribbean correlations 0.4–0.5), with structure resembling the Atlantic Multidecadal Oscillation; AMO and PDV^{PP} are correlated at 0.42, and at 0.48 at five-season PDV^{PP} lead. Reference to this mode as "ENSO-like" is misleading in our opinion.

- the *North Pacific* mode (PDV^{NP}) has a zonal band of SST anomalies extending eastward from Japan as its principal feature. The mode captures the 1976/77 climate shift and exhibits some correspondence to Mantua's Pacific Decadal Oscillation (correlation 0.57). The present analysis shows, perhaps for the first time, the striking links of the North Pacific mode to the western tropical Pacific and Indian Ocean SSTs. Links to the region southeast of Greenland are also noteworthy.
- *mode physicality*: physicality of decadal modes (whose long time scales potentially permit marine population adjustments) is assessed from correlations with biological time series in the North Pacific (from Hare and Mantua 2000). The reported extractions evidently fare at least as well as the PDO index (cf. Table 2.2).

- *twentieth-century secular trend*: implicit accommodation of natural variability leads to a nonstationary SST trend, including mid-century cooling. The SST-trend is remarkably similar to the global surface air temperature and ocean heat content trends. Geographically, a sliver of cooling in the central equatorial Pacific is seen in the midst of widespread but nonuniform warming. Intercomparison shows that linear trend overestimates warming near the Aleutians and along the North American coast, and also in the tropical Indian and Atlantic basins.

The analysis provides a basis for

- investigation of the origin and mechanisms of Pacific decadal variability. The finding of connections with the adjoining tropical basins provides interesting leads, as does analysis of the subsurface structure, upper-ocean heat content in

particular (e.g., Xie et al. 2000, Schneider and Cornuelle 2005). An Estimating the Circulation and Climate of the Ocean (ECCO; Koehl et al. 2006)-based analysis is planned;

- assessment of climate system models, from analysis of SST variability in Intergovernmental Panel on Climate Change (IPCC) simulations of the twentieth-century climate; where greenhouse gas loadings have the same trend as in nature;
- refining estimates of regional climate/hydroclimate change, from analysis of the non-stationary secular trend and linear trend regressions, especially their differences;
- advancing understanding of the mediating role of oceans in climate change: similarity of the SST (ocean heat content) and surface air temperature trends must imply oceanic control. But why then is the mid-century cooling attributed to aerosols present in near–real time in the ocean surface and subsurface records (Hegerl et al. 2007)? What about ocean thermal inertia?

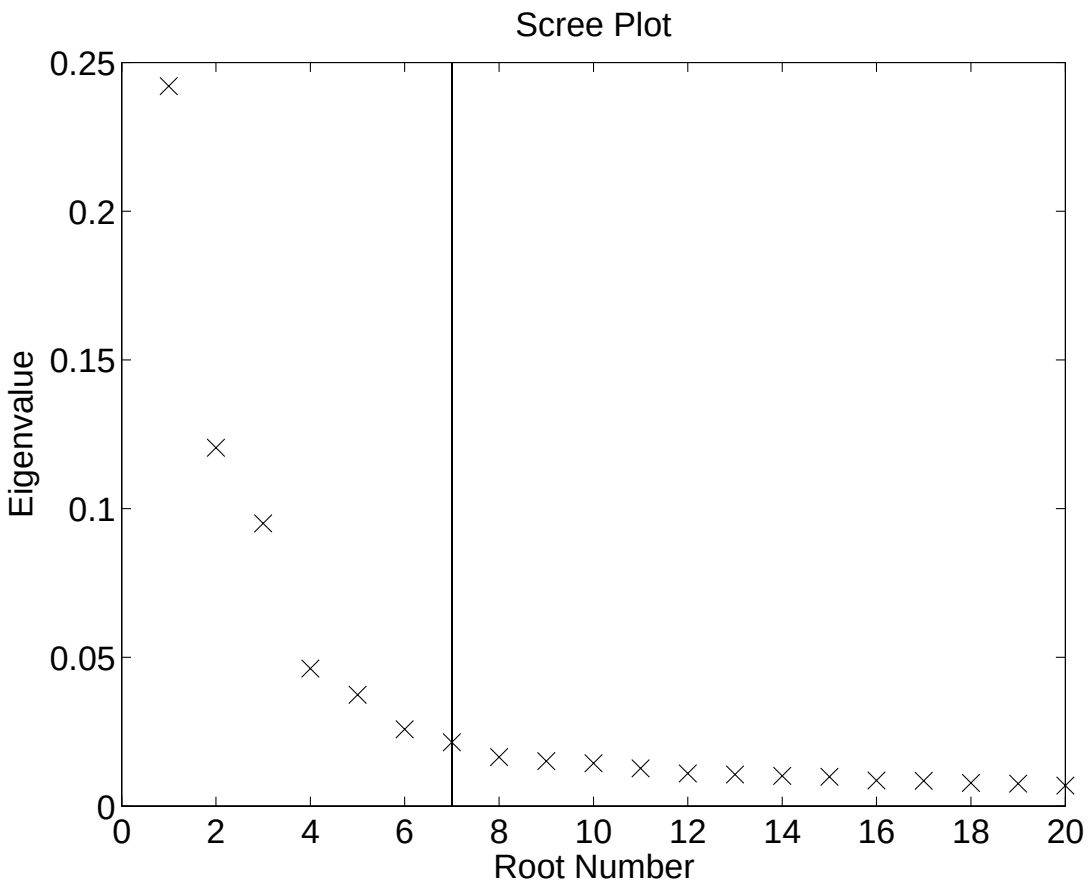

Fig. 2.1. Scree plot from the rotated extended EOF analysis of Pacific SST variability. The eigenvalues shown are before rotation. The cutoff number for rotation was chosen to be 7, marked by the vertical line.

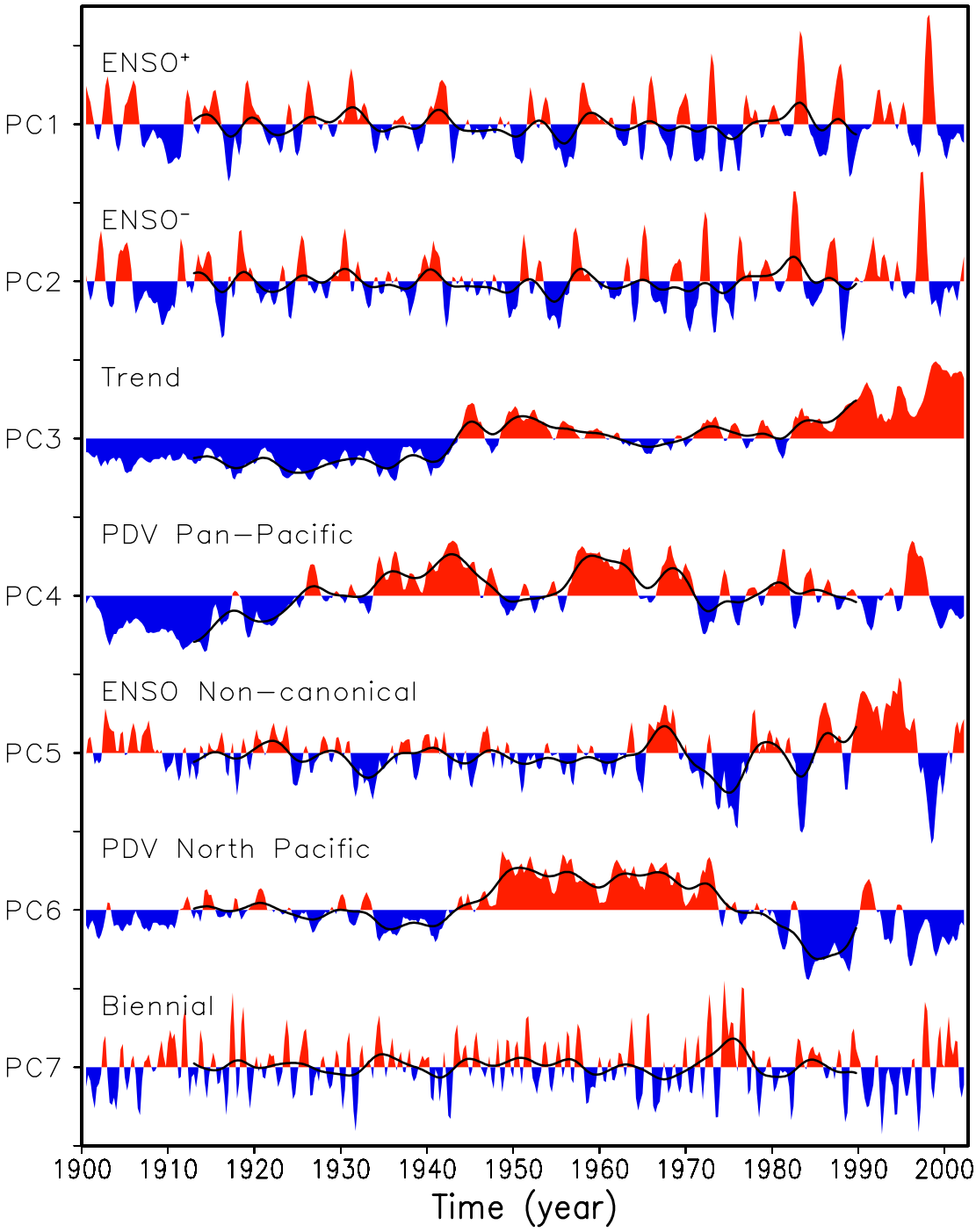

Fig. 2.2. Leading principal components (PCs) of Pacific SST variability in the twentieth century (1900–2002). Tick marks on the vertical axis are drawn every three units. The original PCs are shaded, while heavily-smoothed versions (from 50 applications of a 1-2-1 smoother) are shown using solid black lines.

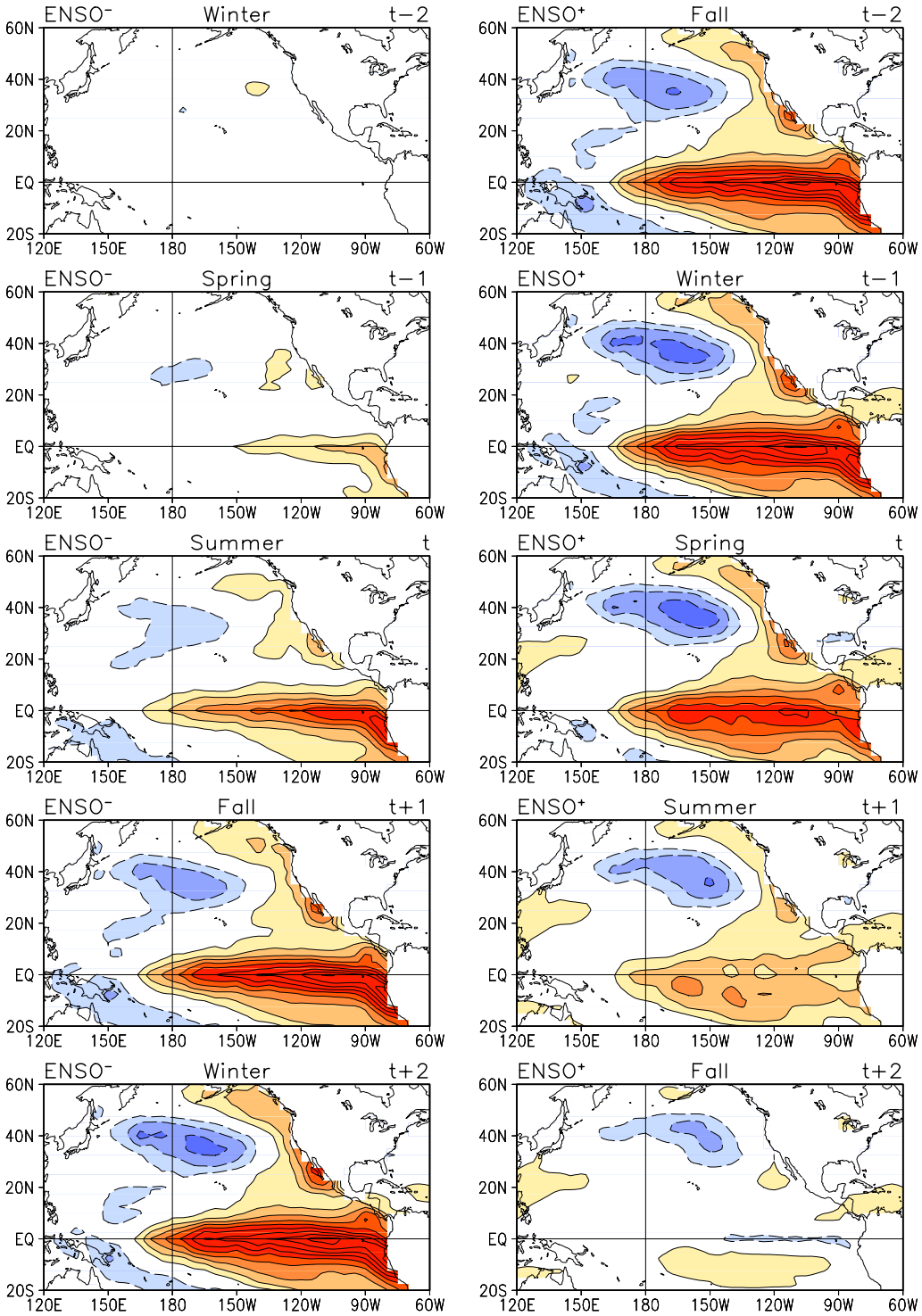

Fig. 2.3. Canonical ENSO evolution: (left) ENSO$^-$ (buildup phase); (right) ENSO$^+$ (decay phase). A five-season SST sequence is displayed with time running downward. Maps are assigned calendar seasons based on additional analysis; see text for details. Solid (dashed) contours denote positive (negative) values and the zero-contour is suppressed. Contour interval is 0.1 K.

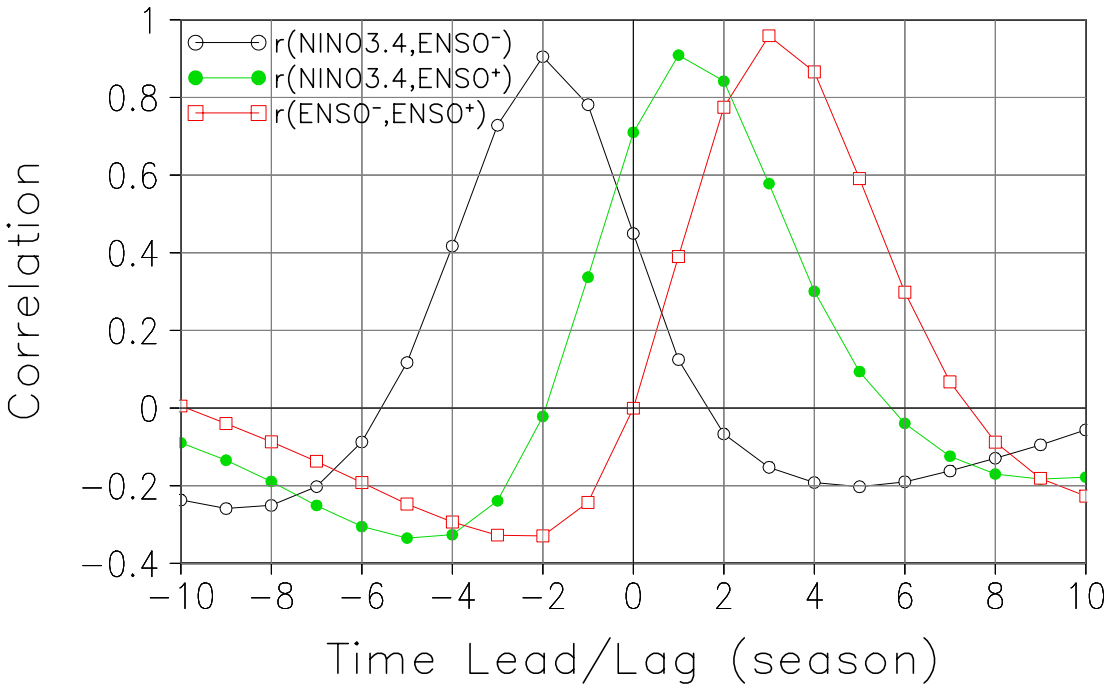

Fig. 2.4. Cross-correlations of $ENSO^-$ and $ENSO^+$ PCs, and of each with the Nino3.4 SST index, at various seasonal lead/lags. The curve key is in the upper left corner, with the following plotting convention: when r(A,B)>0 for t<0 , B leads A; if r>0 for t>0, B lags A. Cross-correlations show that $ENSO^-$ ($ENSO^+$) PC leads (lags) the Nino3.4 index by two (one) seasons, and consistently, $ENSO^+$ lags $ENSO^-$ by three seasons.

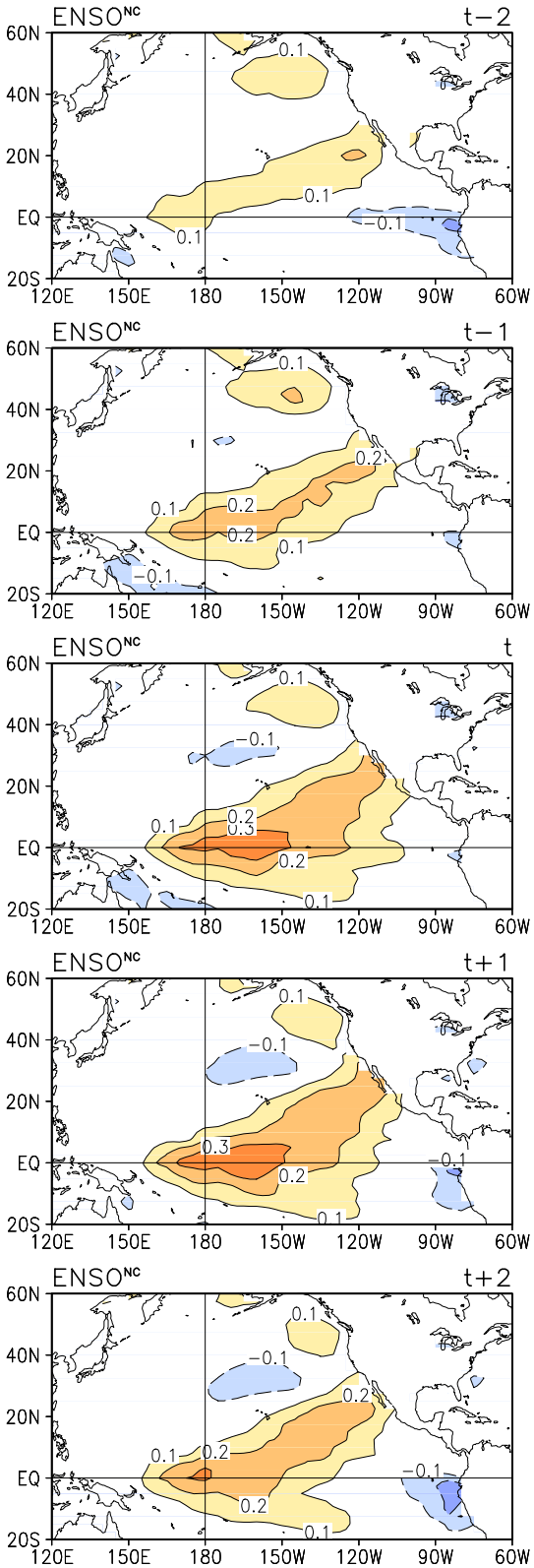

Fig. 2.5. Non-canonical ENSO evolution over a five-season span, with time running downward. Contour/shading convention is as in Fig. 2.3.

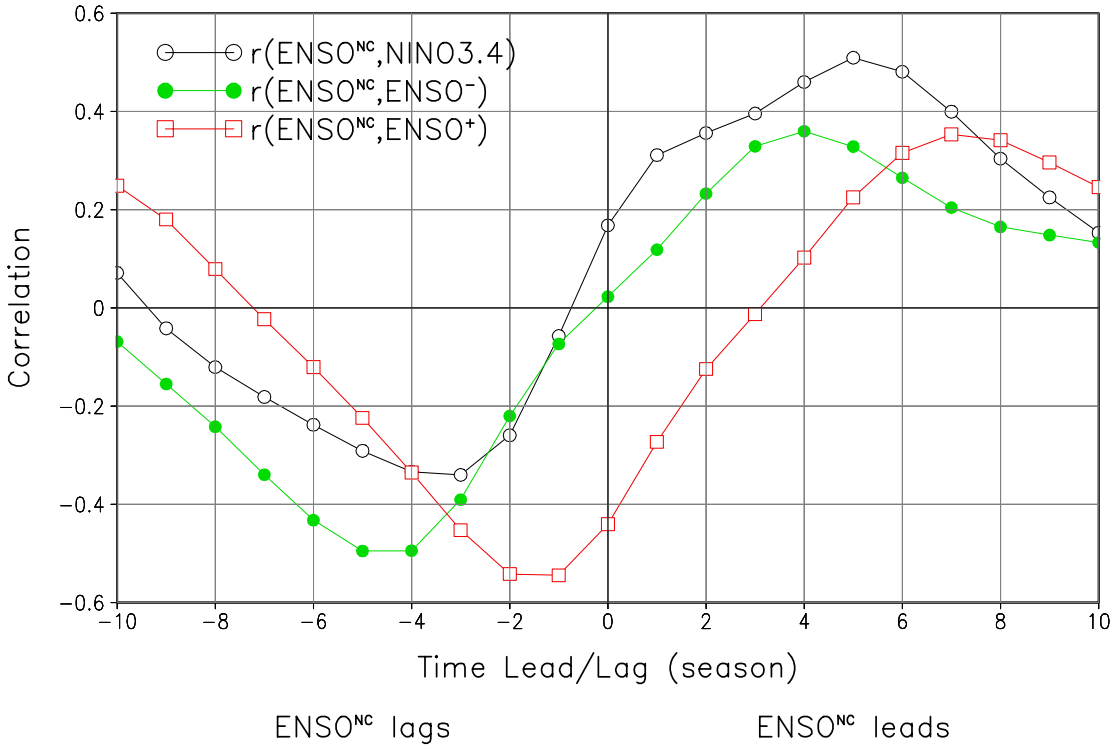

Fig. 2.6. Cross-correlations of the non-canonical ENSO mode ($ENSO^{NC}$) with $ENSO^{-}$ and $ENSO^{+}$ PCs and the Nino3.4 SST index; all in the 1977–2002 subperiod when $ENSO^{NC}$ is particularly energetic. The curve key is in the upper left corner and the plotting convention is the same as in Fig. 2.4; also indicated along the *x* axis here. The cross-correlations show $ENSO^{-}$/Nino3.4/$ENSO^{+}$ to lag $ENSO^{NC}$ by 4/5/7 seasons.

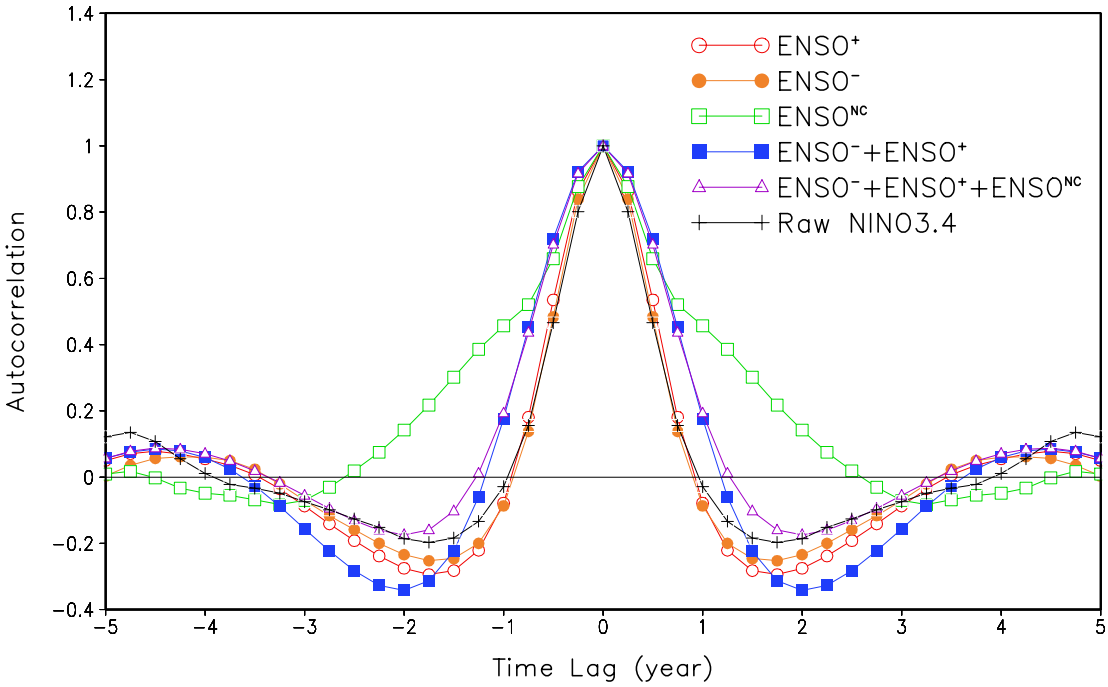

Fig. 2.7. Autocorrelation of the ENSO^{-}, ENSO^{+}, and ENSO^{NC} PCs, and the original and synthetic Nino3.4 SST indices. Synthetic indices are from SST reconstruction using various combinations of ENSO modes; the curve key is in the upper right corner.

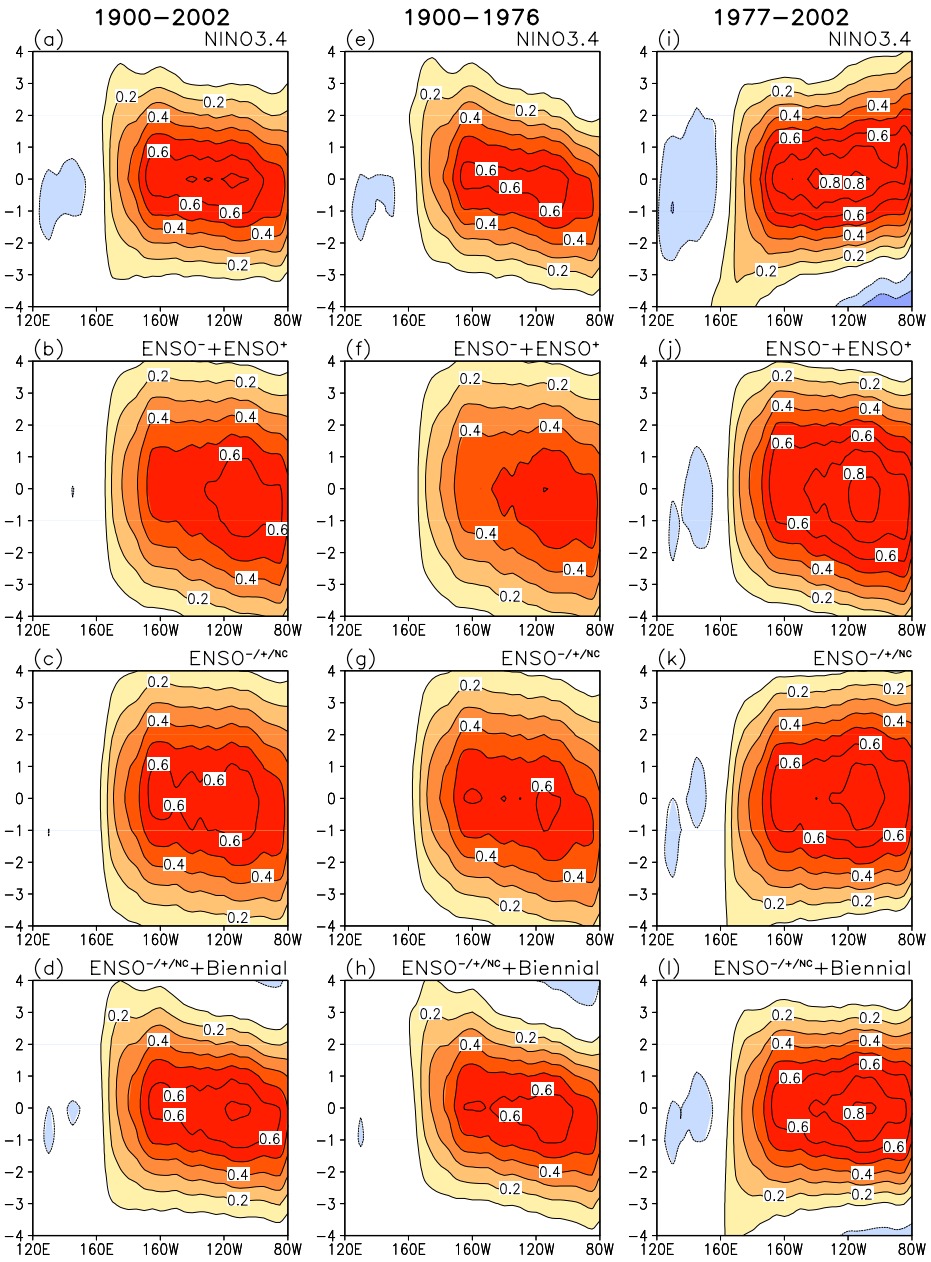

Fig. 2.8. ENSO SST evolution at the equator: lead/lag regressions of the Nino3.4 SST index, with time running upward. The 5°S–5°N averaged SSTs are displayed over a nine-season span. Regressions of original (top row) and synthetic indices (rows 2–4) are shown. Synthetic index is from the two canonical modes (second from top row), canonical + non-canonical (second from bottom), and canonical + non-canonical + biennial modes (bottom row); as also indicated in the title line of each panel. Three time periods are examined: (left) 1900–2002 (full period), (middle) 1900–1976 (pre–climate shift), and (right) 1977–2002 (post–climate shift). Contour/shading convention is as in Fig. 2.3.

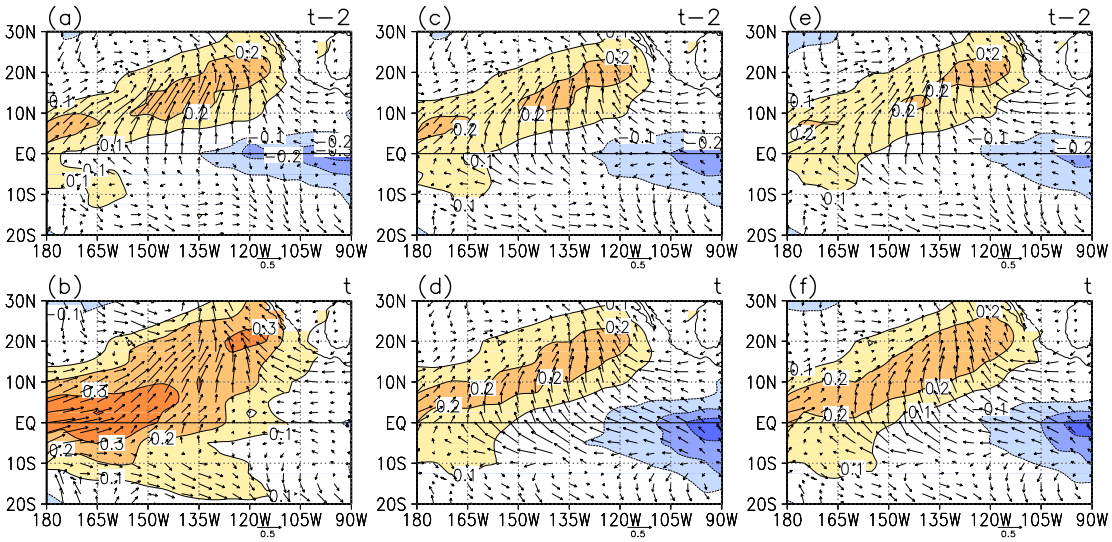

Fig. 2.9. SST and 1000-hPa wind regressions of the ENSO^{NC} mode in the 1949–2002 period: the (top) two-season lead and (bottom) simultaneous regressions are displayed. The ENSO^{NC} PC is from the primary 1900–2002 period analysis in (a)–(d), and from the rotated EEOF analysis of detrended 1945–2002 SSTs in (e), (f) [to facilitate comparison with Chiang and Vimont (2004)]. Regressions in (c)–(f) are on detrended and ENSO-filtered fields; see text for more details. Contour/shading convention is as in Fig. 2.3.

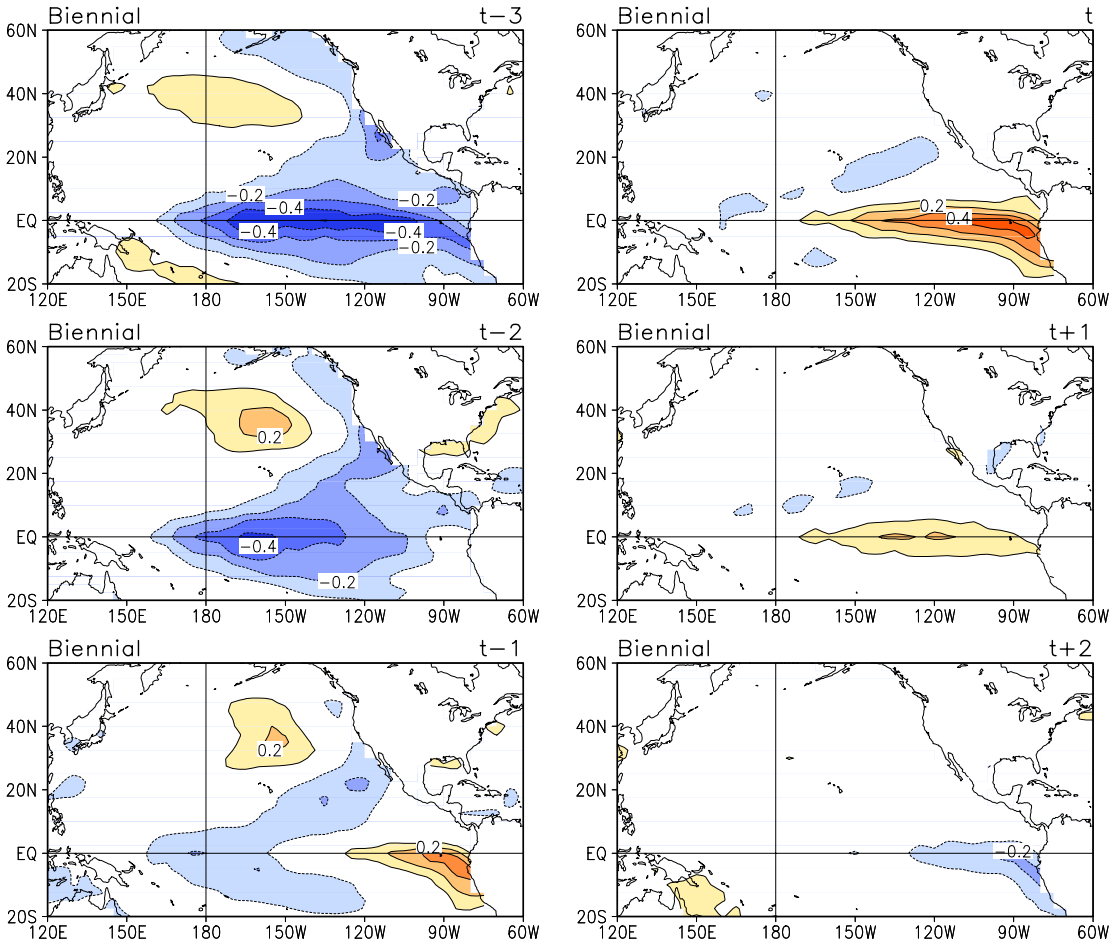

Fig. 2.10. Biennial variability evolution over a six-season span, with time running downward in both columns. Contour/shading convention is as in Fig. 2.3.

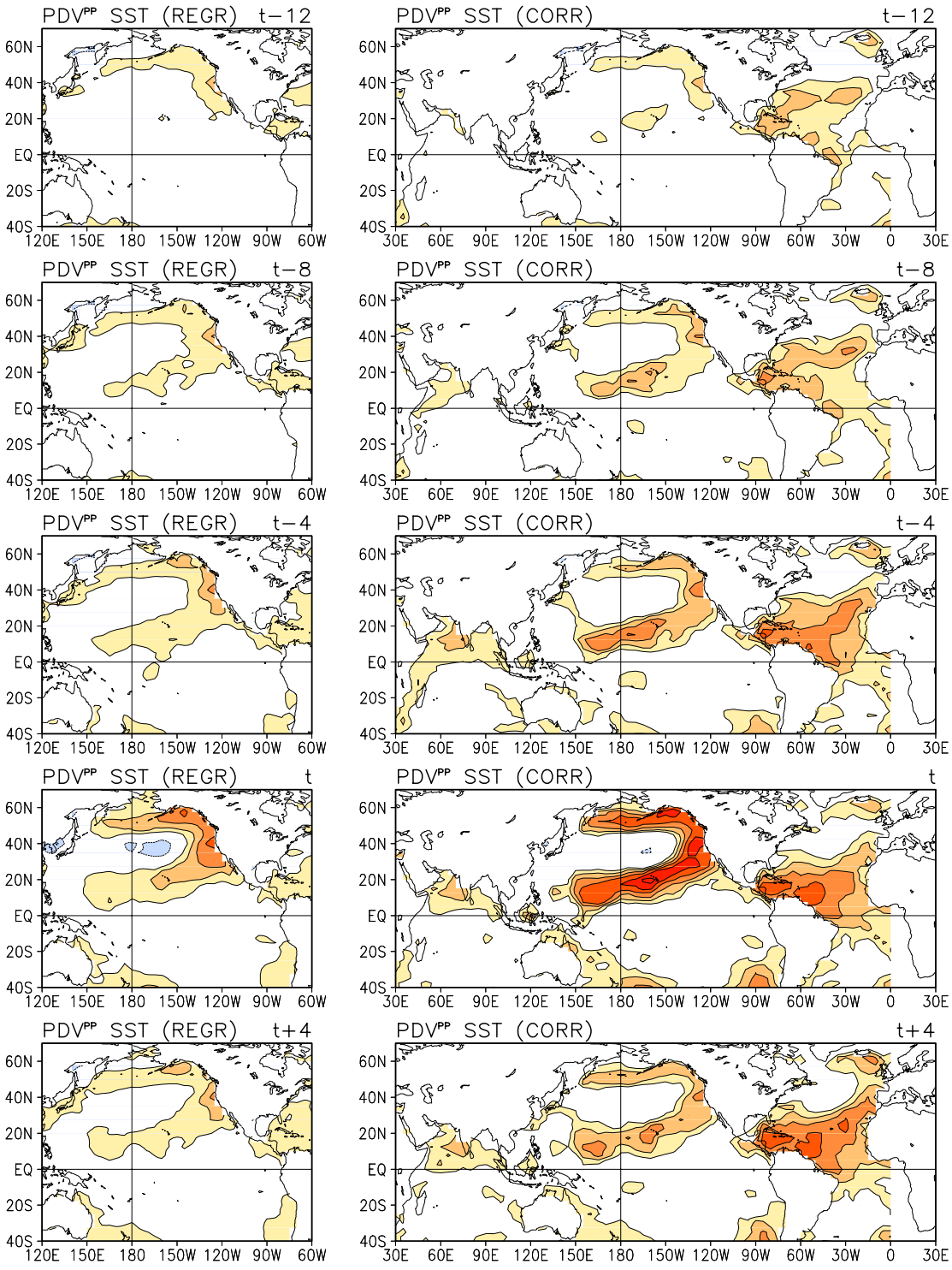

Fig. 2.11. Evolution of Pan-Pacific decadal SST variability (PDV^{PP}): (left) Pacific basin regressions and (right) global correlations are shown over a 5-yr span, at yearly intervals. Contour interval and shading threshold is 0.1 K in left panels. Correlations are also contoured at 0.1 intervals, but the contouring and shading threshold is 0.2. Rest is as in Fig. 2.3.

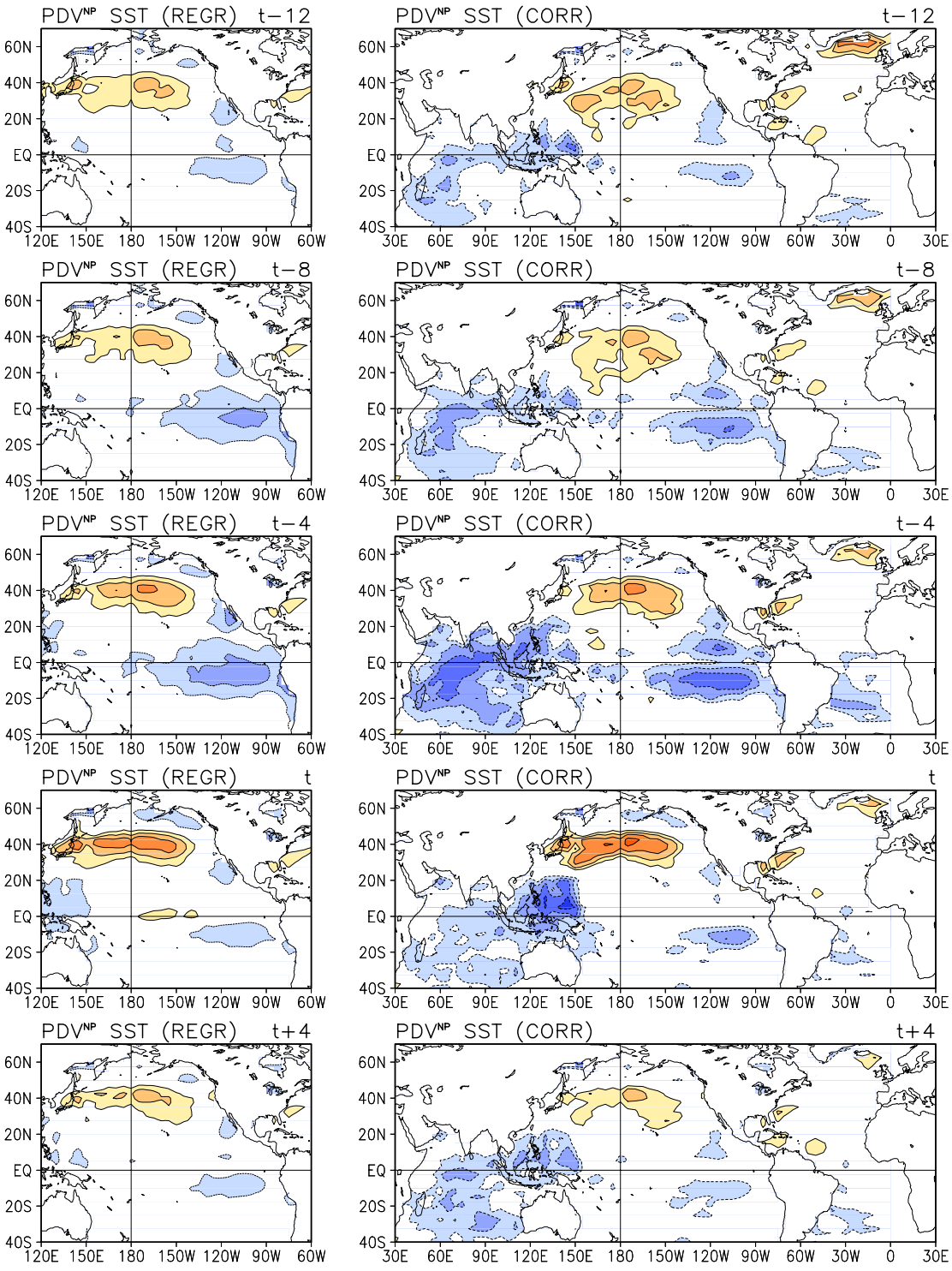

Fig. 2.12. Evolution of North Pacific decadal SST variability (PDV^{NP}) over a 5-yr span; rest as in Fig. 2.11.

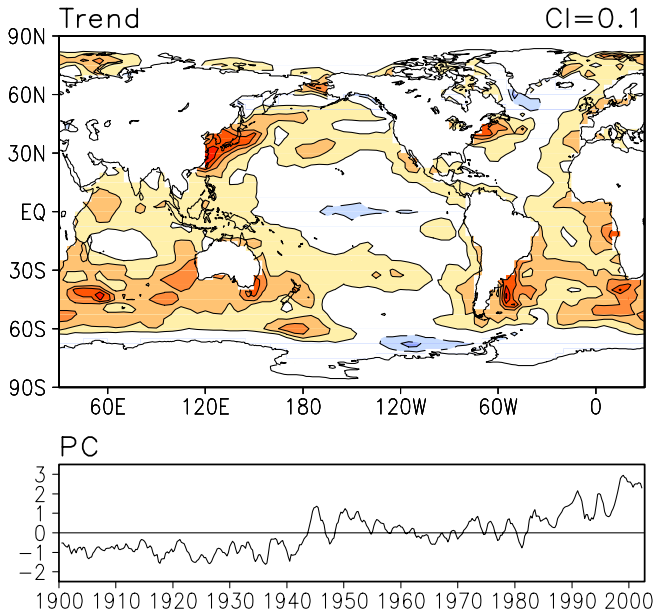

Fig. 2.13. Secular trend in twentieth century SSTs based on Pacific basin analysis and consistent with natural SST variability in the same period. Map is generated from SST regressions on the third-leading PC of the primary analysis (the trend mode, in earlier discussion). Solid (dashed) contours denote positive (negative) values and the zero-contour is suppressed. Contour interval is 0.1 K.

Chapter 3 Long-term Hydroclimate Variations Over the Great Plains: Pacific and Residual Atlantic Linkages[11]

In Chapter 2, Pacific SST variability and trend during the twentieth century is discussed with seven EEOF modes. These modes will now be investigated for their hydroclimate connections over the Great Plains. Of interest is to identify and contrast the SST modes important to the major dry/wet episodes in the last century. Relative importance of the Atlantic Ocean will also be investigated.

3.1 Introduction

The U.S. hydroclimate of the twentieth century is marked by two prolonged dry periods: one in the 1930s, and the other in the 1950s. The decade-long drought in the 1930s was so severe that turned much of the Great Plains, the U.S. breadbasket, into a "Dust Bowl". The 1950s drought, while relatively short (lasted 4–5 years), sustained precipitation anomalies that were as low as during the Dust Bowl.

Seasonal precipitation anomalies in the U.S. are related to the location and strength of the jet stream and associated storm activities (Trenberth and Guillemot 1996). Feedbacks between the atmosphere and soil moisture are also important, which tend to reinforce and perpetuate the original dry/wet conditions (Koster et al. 2000). It is less known as how dry/wet conditions can be maintained on decadal time scales; possible mechanisms include external forcing from the adjoining ocean basins (e.g., Schubert et al. 2004; Seager et al. 2005) and memory of the deep soil (Schubert et al. 2004).

[11] In preparation for publication (Guan et al.).

Observational studies have linked warm season precipitation anomalies/droughts in the U.S. to sea surface temperature (SST) variations in tropical and North Pacific (e.g., Ting and Wang 1997; Barlow et al. 2001). The role of North Atlantic is emphasized by McCabe et al. (2004) in multidecadal droughts. Drought experiments conducted by Schubert et al. (2004) have linked the Dust Bowl drought to decadal Pacific and Atlantic SST anomalies: the drought, in terms of precipitation deficits, can be well simulated with observed SST forcing, i.e., cooler-than-normal tropical/extratropical Pacific SSTs and warmer-than-normal North Atlantic SSTs. Similar results have been obtained by Seager et al. (2005) who also examined other persistent dry/wet episodes during the twentieth century. It is further argued that the driving SST forcing comes from the tropical Pacific.

The detailed processes remain to be fully explored and understood as how low-frequency variations in Pacific/Atlantic SSTs help to maintain long-term U.S. droughts. Meanwhile, spatiotemporal structure of these SST variations remains to be robustly characterized on decadal/multidecadal time scales. In Chapter 2, a new, evolution-centric analysis is conducted on the Pan-Pacific SSTs during the twentieth century, where seven modes, including two on decadal time scales, are extracted with reasonable robustness. In this chapter, the impacts of these modes on the U.S. hydroclimate will be evaluated; specifically, their relative contributions to three prolonged dry/wet episodes over the Great Plains during the twentieth century. The analysis also includes the effects of the Atlantic Ocean, based on an EEOF analysis (similar to that described in Chapter 2) of the Atlantic SSTs residual to the leading seven Pacific modes.

A brief description of the data sets and analysis procedures is given in section 3.2. The analysis begins in section 3.3 with an investigation of the Great Plains precipitation index, including definition of three prolonged dry/wet episodes. SST-based reconstruction of seasonal rainfall anomalies during these periods, including individual contributions from the Pacific and residual Atlantic modes, as well as seasonal evolution of the SST-drought linkages, is described in sections 3.4 ad 3.5. A summary is given in section 3.6.

3.2 Data and methodology

3.2.1 Data

The principal variable to be investigated is precipitation. The high-resolution CRU TS 2.1 precipitation will be used in constructing the Great Plains precipitation index as well as developing reconstruction equations. The data come from land station observations that are checked for inhomogeneities using improved technique, providing a best estimate of the month-to-month variations for the twentieth century record (Mitchell and Jones 2005). Monthly values are available for the period of 1901–2002 on a 0.5° × 0.5° grid.

Given the high-frequency nature of precipitation and our interest in lower-frequency variations, a reference variable will be used here, the Palmer Drought Severity Index (PDSI), which is slowly-varying due to the memory terms in its definition. The PDSI is a nondimensional number that measures the severity of meteorological drought, the calculation of which is based on the (im)balance between the actual water supply (i.e., precipitation) and that required to maintain a normal soil

moisture level for a particular location and calendar month (Palmer 1965). The PDSI takes both precipitation and surface air temperature as inputs. Five levels of drought are predefined (values of PDSI indicated in brackets), i.e., incipient drought (−0.5 to −0.99), mild drought (−1.0 to −1.99), moderate drought (−2.00 to −2.99), severe drought (−3.00 to −3.99) and extreme drought (less than or equal to −4.00). Five wet levels are similarly defined. The PDSI data set (Dai et al. 2004) to be used contains monthly values over the global land areas (on a 2.5 × 2.5 grid) during the 1870–2003 period.

Evaporation and total (i.e., stationary plus transient) moisture flux convergence, another two terms in the atmospheric water balance, will be used in aspects of this analysis. Evaporation estimates are produced at NOAA/CPC using a one-layer hydrological model (Huang et al. 1996; van den Dool et al. 2003). The model, based on the water budget in the soil, takes observed precipitation (and surface air temperature), and gives the partitioning in soil moisture, evaporation and runoff. The model parameters are tuned by runoff observations in Oklahoma and applied to the entire United States. Gridded evaporation data are available for the period of 1931–2002, at monthly interval. The horizontal resolution is 2.5° × 2.5°. Moisture flux and convergence are derived from the ERA-40 reanalysis (Uppala et al. 2005), available for the 1958–2001 period.

Residual SSTs are formed by linearly removing the leading seven Pacific EEOF modes from the raw data (HadISST 1.1 SST; the same were used in Chapter 2).

Seasonal means are formed for each of the above variables before subsequent analysis; no further smoothing/filtering is applied unless noted otherwise. For each

variable, climatology is defined over the respective data availability period, or 1900–2002, whichever is shorter.

3.2.2 Methodology

A Great Plains precipitation index will be constructed, with which the surface and upper-level fields associated with dry/wet anomalies will be characterized via index regressions. However, precipitation variations may be caused by more than one physical process, which may be compounded in the index regressions. For example, tropical and extratropical Pacific SSTs may affect the U.S. precipitation in different ways, and become important in different seasons (to be shown later). As such, it is useful to adopt an oceanic viewpoint and track the connections of individual Pacific/Atlantic modes to the Great Plains separately. This is achieved by regressing the Pacific and residual Atlantic mode PCs on the Great Plains precipitation. Relative contributions of these modes to three long-term dry/wet episodes are quantified by contrasting the synthetic (i.e., SST-reconstructed) and raw precipitation anomalies.

3.3 The Great Plains hydroclimate variability

3.3.1 Index definition

Indices (i.e., areal averages) of seasonal Great Plains (90–100°W, 35–45°N; see the small box in Fig. 3.3a) PDSI, precipitation and evaporation anomalies are shown in Fig. 3.1, with the raw time series in color shading, while heavily-smoothed versions (from 50 applications of a 1-2-1 smoother) in black curves. Note that the smoothed precipitation and evaporation indices are shown on a finer scale (on the right hand side) than the unsmoothed ones. The Great Plains domain is defined as in

Ruiz-Barradas and Nigam (2005), which encompasses the local maximum in the standard deviation of observed summertime precipitation.[12] We will see later how this domain matches the core region of the Dust Bowl. The precipitation index is moderately correlated with the PDSI index at 0.54, but correlation is increased to 0.91 when the indices are smoothed to retain decadal and longer scale variations[13]. This suggests that the low-frequency portion of precipitation anomaly can be an effective drought indicator, as is used here.

All indices show the 1930s is the most prolonged dry period during the twentieth century (Fig. 3.1). The 1950s drought is also notable: while drought lasted for a shorter time period, precipitation anomalies were no weaker than during the Dust Bowl. The three indices agree well in their low-frequency part, as indicated by the smoothed indices. Unlike PDSI, which is rather persistent, precipitation and evaporation display significant seasonal and year-to-year fluctuations. Evaporation anomalies are in general about one third as large as precipitation anomalies, indicating the other term in the atmospheric water balance, i.e., moisture flux convergence, is more important in generating interannual precipitation variations in the Great Plains.

We define three prolonged dry/wet episodes based on the smoothed[14] Great Plains precipitation index: 1931–1939 (Dust Bowl), 1953–1956 and 1982–1986. These are the periods when the smoothed index goes above or below its standard

[12] Other definitions of the Great Plains domain have been used in previous studies (e.g., Ting and Wang 1997; Schubert et al. 2004). Sensitivity tests show that the indices calculated here are stable to reasonable perturbations to the selected domain, and consistent with previous studies.
[13] We note that common data sources [GHCN2 rain gauges; Peterson et al. 1998] were incorporated in the construction of the precipitation and PDSI used here, which may have contributed to part of the high correlation.
[14] The defined time periods are not unduly sensitive to the times of smoothing.

deviation. Note that the unsmoothed precipitation index will be used in all subsequent calculations unless otherwise stated.

3.3.2 Seasonality

Standard deviations of the Great Plains precipitation index are shown in Fig. 3.2 (upper-left panel, green) as a function of the seasonal cycle. The same is also shown for the PDSI (white) and evaporation (black) indices, for comparison. It is seen that precipitation exhibits larger interannual variability in spring, summer and fall. The value in winter is only about one half of those in the other seasons. Seasonality is obvious in evaporation variability, too, which is largest in summer, smallest in winter, and moderate in spring and fall. Unlike precipitation and evaporation, the PDSI has nearly equal interannual variability over all four seasons.

Mean anomalies of Great Plains precipitation, evaporation and PDSI, averaged for the three long-term dry/wet episodes defined above, are shown in Fig. 3.2 (upper-right and lower panels). It is seen that the driest season, in terms of precipitation deficits, is summer for the Dust Bowl, while fall for the 1950s drought. Fall is also the wettest season for the 1980s wet episode. This seasonal preference is also tracked by the PDSI for the two droughts, but not for the 1980s wet period (when fall PDSI is only as large as the winter and spring values). Evaporation anomalies are largest in summer for all three episodes. Considering the peak season, about 40% of the precipitation anomalies can be explained by evaporation anomalies during the Dust Bowl; the percentage is marginal during the 1950s/80s. The above results suggest that moisture flux convergence contributes importantly to the Great Plains

water budget, especially in fall when evaporation is much decreased compared to summer.

3.3.3 Index regressions: moisture balance and circulation patterns

Simultaneous regressions on the summertime Great Plains precipitation index are shown in Fig. 3.3 for several fields. The index, which contains only summer values, has been smoothed by repeating a 1-2-1 smoother for six times. The smoothing is to retain low-frequency variations, which are of interest here. Regressions for other seasons also show the dominance of (total) moisture flux convergence, although with different spatial patterns and associated circulation structures (not shown). The precipitation regression (Fig. 3.3a) is marked by wet anomalies centered over the defined Great Plains domain. Evaporation (Fig. 3.3b) is too weak to be shown at the current contour interval (0.1 mm/day). On the other hand, moisture flux convergence (Fig. 3.3c) well matches precipitation in terms of magnitudes and the location of maximum wetness. A moisture pathway can be identified extending from a divergent area in northern Mexico into the Great Plains. There is no indication of direct moisture transport from the Pacific, suggesting the impacts of the Pacific Ocean on low-frequency variations of the Great Plains rainfall is via modulation of the atmospheric circulation, instead of moisture flux anomalies transported from the Pacific.

An examination of the upper-level circulation patterns do reveal interesting features associated with Great Plains rainfall anomalies, shown in Fig. 3.3d. Wet anomalies in the Great Plains can be seen associated with wave-like structures in the 200-hPa height field. Specifically, a height center is located to the southeast of the

Great Plains, while a low center to the northwest. Wave structures are better appreciated when the precipitation index is not smoothed (Fig. 3.3e). Similar patterns in association with Great Plains precipitation variations have been found by Ting and Wang (1997) and Ruiz-Barradas and Nigam (2005) in the middle-level atmosphere.

3.4 Drought linkages: Pacific SST

3.4.1 Pacific modes

A detailed discussion of the Pacific modes has been given in Chapter 2. Here, the modes will be investigated for their drought linkages. We will see later that such linkages do vary over the seasonal cycle, and it is needed to look at each season separately. Principal components (Fig. 3.4) and spatial patterns (Fig. 3.5) of the seven Pacific modes are shown here for the summer season (when the Great Plains was driest during the Dust Bowl). Examination of the seasonal SST distributions associated with these modes shows that only the ENSO-related modes, i.e., $ENSO^{-}$, $ENSO^{+}$, non-canonical ENSO and biennial variability, exhibit significant seasonal evolution; the PDV and trend modes vary only slightly from one season to another. For seasonal evolution of $ENSO^{-}$, $ENSO^{+}$, non-canonical ENSO and biennial modes, the reader is referred to Figs. 2.3, 2.5 and 2.10.

3.4.2 Reconstruction of dry/wet episodes

a. Dust Bowl (1931–1939)

Observed and reconstructed summer precipitation anomalies, averaged for the Dust Bowl period, are shown in Fig. 3.6. Reconstruction is obtained as multiplication

of the SST PCs to their precipitation regressions. All seven modes described in Chapter 2 are included in the reconstruction. The reconstruction reproduces major dry/wet centers reasonably well, with about half the observed magnitudes (cf. Figs. 3.6a,b). This is consistent with Fig. 3.2 (upper-right panel) in that more than one half of the precipitation deficits during Dust Bowl summers cannot be explained by the reduction in evaporation. Reconstruction skill is even better when the SST PCs are smoothed (Fig. 3.6c). Contribution of individual modes is quantified by the ratio between synthetic and observed Great Plains precipitation index averaged for the Dust Bowl period, shown in Table 3.1. The mean observed index is −0.51 mm/day for the nine-year period. The largest contribution is from the non-canonical ENSO mode (16.3%), while the second and third from the trend mode (9.7%) and PDV North Pacific (5.2%); they together contribute 31.2% to the observed anomalies. Contributions from the other four modes are relatively small. The seven modes altogether contribute 29.1% to the observed anomalies; slightly lower than does the three-mode combination due to cancellations from the negatively-contributing modes, mostly PDV Pan-Pacific.

Table 3.1. Percentage contributions of the seven Pacific modes (columns 3–9 for individual contributions and column 10 for the seven-mode total) to observed precipitation anomalies (column 2; mm/day) over the Great Plains (90–100°W, 35–45°N) for four cases (column 1).

Case	Obs.	$ENSO^{+}$	$ENSO^{-}$	Trend	PDV^{PP}	$ENSO^{NC}$	PDV^{NP}	Biennial	*Total*
1931–39 Sum	−0.51	−0.2	1.3	9.7	−3.1	16.3	5.2	−0.1	29.1
1931–39 Spr	−0.35	−1.9	0.6	37.0	2.8	−0.4	−2.2	3.6	39.5
1953–56 Fal	−0.78	14.3	4.8	0.4	−0.6	0.8	30.0	−0.4	49.3
1982–86 Fal	0.82	5.7	5.0	−0.6	0.6	−0.2	27.9	−1.7	36.7

Geographically, precipitation anomalies are largely associated with non-canonical ENSO over the central/southern Great Plains (Fig. 3.6d), while with the trend mode (Fig. 3.6e) in the northern Plains. A limited contribution is from PDV North Pacific in the lower-left corner of the Great Plains domain (Fig. 3.6f). The signs of the summertime connections are such that cold phases of non-canonical ENSO (cold central equatorial Pacific SSTs), PDV North Pacific (cold midlatitude North Pacific SSTs) and the trend mode (cold SSTs in the North Pacific, mostly midlatitudes) are accompanied by concurrent dry anomalies in the Great Plains.[15] For non-canonical ENSO, the associated anomalies virtually have a single sign over the U.S. continent, maximizing over the Great Plains. The trend mode, on the other hand, shows opposing connections over the northern Plains and the east coast[16]. The results above suggest that the Dust Bowl drought owes its severity, to at least a fair extent, to the combined effects from three Pacific modes that involve cold SSTs in the tropical and extratropical basins; all contributing to dry anomalies in the Great Plains. Observed and synthetic SST forcing patterns for this and other long-term dry/wet periods will be discussed shortly.

The Dust Bowl drought has been reconstructed by McCabe et al. (2004) based on a different drought variable: the 20-yr moving drought frequency; as well as a different set of predictors: PDO, AMO (Atlantic Multidecadal Oscillation; Enfield et al. 2001), and the warming trend (represented by mean Northern Hemisphere surface temperature). Our analysis compliments their results by showing the importance of

[15] We will see later that the signs (and patterns) of SST-drought connections may change dramatically over the seasonal cycle. For example, the warm phase of PDV North Pacific links to wet anomalies in summer but dry anomalies in fall over the Great Plains.
[16] Similar out-of-phase structure can also be found in the least-square-fitted summer precipitation trend.

non-canonical ENSO to the Dust Bowl, a mode that so far has not been systematically explored in the context of long-term droughts.

Dry anomalies are also relatively large in spring during the Dust Bowl period, as has been suggested by Fig. 3.2 (upper-right panel). Average precipitation is −0.35 mm/day in spring, about 70% of the summer value. Considering the much smaller evaporation anomalies than in summer, this suggests a more important role of moisture flux convergence in the springtime water balance. The reconstruction shows reasonable skill for this season as well (cf. Figs. 3.7a,b), but with the trend mode being overwhelming: the trend mode alone contributes 37% to observed precipitation anomalies in spring, only slightly lower than the total contribution of 39.5% from all seven modes.

b. 1950s drought (1953–1956)

Dry anomalies are largest in fall during this period in the Great Plains: mean anomaly is −0.78 mm/day over the four-year period, even lower than during the Dust Bowl summers. In fact, negative anomalies span almost the entire U.S. continent, with maximum values extending southeastward from the Great Plains to the Gulf Coast (Fig. 3.7c). The overall pattern is well reproduced in the reconstruction (Fig. 3.7d). The reconstruction is dominated by PDV North Pacific (in its warm phase), which contributes 30.0% to the observed anomaly. Cold ENSO contributes another 19.1%: 4.8% from the growing phase, and 14.3% from the decaying phase.

The 1950s drought has also been reconstructed by Barlow et al. (2001) from the leading three Pacific modes (extracted by regular EOF with rotation), but for the summer season. The PDSI-based drought pattern therein is in broad consistence with

the precipitation pattern shown here. However, SST-drought linkages suggested by the two analyses are significantly different. We find that summer precipitation anomalies during this period is difficult to be reconstructed from the seven Pacific modes, due, primarily, to the canceling effects from ENSO (canonical and non-canonical; both positively contributing) and PDV North Pacific (negatively contributing). In fall, however, PDV North Pacific's drought linkage switches sign, and meanwhile becomes much stronger than ENSO (canonical evolution; non-canonical ENSO's drought linkage is nearly neutral in fall if averaged over the Great Plains). The fall reconstruction, as a result, is dominated by PDV North Pacific, with reasonable skill in terms of structure and magnitudes. The inefficiency of the seven Pacific modes in reproducing the 1950s summer precipitation anomalies suggests that other forcing/feedback mechanisms need to be considered. Fig. 3.2 (lower-right panel) shows that more than one half of the summer precipitation anomalies during this period can be explained by reduced evaporation. Whether the latter contains a lagged response to prior SST forcing remains to be explored. This, together with the interest of seasonal prediction, motivates an ongoing investigation of the lagged SST-drought connections (such as winter SST forcing of summer droughts). The fair reconstruction in Barlow et al. (2001) is likely due to the different choice of drought variable: the PDSI, which is defined with both current and previous conditions. Possible effects from the Atlantic were noted in their discussion. The AMO, for example, has been shown by McCabe et al. (2004) to be a major contributing mode, along with PDO and the warming trend, in their long-term (20 yr) drought frequency reconstructions, including for the 1950s/60s dry period. However, we find that the inclusion of the

Atlantic Ocean does not help the reconstruction of concurrent 1950s summer dry anomalies, suggesting the importance of local processes in generating these anomalies, and a possible lagged response to prior SST forcing.

c. 1980s wet period (1982–1986)

This period is marked by peak wet anomalies in fall; mean anomaly is 0.82 mm/day over the five-year period in the Great Plains. Anomalies are relatively small in spring, and slightly negative in summer (see Fig. 3.2, low-left panel). The broad-scale pattern bares some resemblance to the 1950s drought, with flipped signs (cf. Figs. 3.7c,e). Reconstruction shows reasonable skill over the Great Plains (Fig. 3.7f). The dominant mode, as in the 1950s drought, is PDV North Pacific (in its cold phase), which contributes 27.9% to the observed anomaly. Warm ENSO contributes another 10.7%: 5.0% from the growing phase, and 5.7% from the decaying phase.

3.4.3 Seasonal dependence

SST-drought linkages, realized via the atmospheric circulation, may vary over the annual cycle since the mean state of the atmosphere exhibit distinct patterns in different seasons. In that case, a same SST mode may possibly force rather different drought patterns in, say, summer and fall, even if the associated SST anomaly pattern may be relatively stationary. This appears to be the case in the above analysis. For example, non-canonical ENSO is a major contributing mode in Dust Bowl summers, but of little influence in spring during the same years; the trend mode, on the other hand, is much more influential in spring than in summer during the Dust Bowl (see Table 3.1). Implied is a seasonal dependence of the SST-drought linkages,

investigated here for three Pacific modes, i.e., non-canonical ENSO, trend and PDV North Pacific, which have been shown important in the reconstruction of long-term dry/wet episodes over the Great Plains. Spring, summer and fall precipitation regressions for each mode are shown in Fig. 3.8. The signs there correspond to the warm phases of the various modes (see Fig. 3.5). Winter regressions are rather weak over the Great Plains (interannual winter precipitation variability is about one half of the other seasons in this region; see Fig. 3.2, upper-left panel) and not shown.

Non-canonical ENSO is associated with little anomalies in the Great Plains in spring and fall (Fig. 3.8a,c). The interesting season is summer, when warm central equatorial Pacific SSTs are related to wet anomalies over the Great Plains (Fig. 3.8b); consistent with the dominance of non-canonical ENSO during the Dust Bowl summers. The change of precipitation patterns are relatively quick over the seasons, which can hardly be attributed to the relatively slowly-varying modal SSTs. This is especially true for the other two modes that have rather persistent SSTs, to be discussed below.

The trend mode is the most slowly-varying mode among all seven leading Pacific modes, with virtually identical SST structures over the annual cycle. Even so, associated precipitation patterns are different among seasons. The association is strongest in spring, when warming Pacific SSTs are associated with moister Great Plains (Fig. 3.8d). This is consistent with the dominance of the trend mode during the Dust Bowl springs. In summer, the Great Plains is in general wet, but with most anomalies in the northern part (Fig. 3.8e). In fall, the strongest anomalies are outside of the Great Plains domain, mostly to the south/southeast (Fig. 3.8f).

PDV North Pacific has been the most important mode to the 1950s drought and the 1980s wet period, both with peaks in fall. Consistently, precipitation association is the strongest in fall for this mode, when warm midlatitude North Pacific SSTs are associated with dry anomalies in the Great Plains and neighboring regions (Fig. 3.8i). In spring, the mode is associated with some dry anomalies in the southwest corner of the Great Plains domain (Fig. 3.8g), which are then replaced by wet anomalies in summer (Fig. 3.8h).

Mental averaging suggests that, annually, the warm phase of non-canonical ENSO/trend (PDV North Pacific) is associated with wet (dry) anomalies in the Great Plains. For trend and PDV North Pacific, this means that coherent North Pacific SSTs, when arising from different modes/mechanisms, may lead to dramatically different/opposing responses in the Great Plains precipitation.

3.4.4 SST forcing patterns

Observed SST anomaly patterns during the three major dry/wet episodes are examined here and compared to reconstructions. The comparison is particularly to identify the part of the SST forcing that is not represented by the seven Pacific modes so far discussed. Observed and reconstructed SSTs are shown in Fig. 3.9 for four cases. Reconstructions are based on all seven Pacific modes. The Atlantic domain is also shown, for reasons becoming clear below.

The Dust Bowl summers are characterized by cool SSTs in equatorial central/eastern Pacific and midlatitude North Pacific, as well as warm SSTs in the North Atlantic (Fig. 3.9a). Similar pattern has been reported by Schubert et al. (2004), and used in their GCM experiments that reproduced the Dust Bowl drought. The

central equatorial and North Pacific anomalies are reproduced in the seven-mode reconstruction (Fig. 3.9b), but the eastern equatorial Pacific anomalies not, which might be contributed from other Pacific/Atlantic modes. A likely importance of the midlatitudes is suggested by the observation, and reproduced in the reconstruction. Further examination showed that these midlatitude SSTs can largely be reproduced by the three modes of non-canonical ENSO, trend, and PDV North Pacific alone, consistent with their dominance in the precipitation reconstruction.

The SST pattern is somewhat different in spring (Fig. 3.9c). Pacific SSTs are even stronger than in summer in the midlatitudes, while suppressed in the eastern equatorial region. This is well reproduced in the reconstruction (Fig. 3.9d). Again, possible importance of midlatitude SSTs is suggested.

ENSO-like SSTs are observed in both 1950s (Fig. 3.9e) and 1980s (Fig. 3.9g), with opposite phases. In either case the pattern is reproduced in the seven-mode reconstruction (Figs. 3.9f,h), essentially from canonical ENSO and PDV North Pacific. Compared to ENSO, PDV North Pacific contributed more precipitation anomalies in both periods (see Table 3.1), highlighting the role of midlatitude SSTs.

Meanwhile, these dry/wet episodes are consistently accompanied by large SST anomalies in the North Atlantic, such that warm (cold) SSTs are associated with a dry (wet) Great Plains. Only a small fraction of these Atlantic SST variations are representable by the leading Pacific modes. It is therefore of keen interest to see how the inclusion of the Atlantic Ocean (specifically, the part of the Atlantic SST variability that is linearly independent of the Pacific) would help improve the above precipitation reconstructions. This is explored in the following section.

3.5 Drought linkages: Residual Atlantic SST

3.5.1 Residual Atlantic modes

To characterize the Atlantic SST variability, a rotated EEOF analysis is conducted, not on raw SST anomalies, but on residual ones that are linearly independent of the leading seven Pacific modes as described in Chapter 2. The latitudinal band between 20°S and 60°N, as in the case of Pacific, is analyzed. A seven-season time window (seven lags at seasonal interval) is used in the standard EEOF analysis, with the leading four modes VARIMAX-rotated. Sensitivity experiments attest to the stability (robustness) of these modes. Specifically, the modes are reasonably stable to the length of the time window and number of modes rotated. All of these modes can be tracked in similar analysis of total Atlantic SSTs, assuring they are not statistical artifacts due to the residual analysis procedure. The names and labels of these modes and the percentage variance they explain (in the residual SST data) are listed in Table 3.2.

Table 3.2. Leading modes identified by the rotated EEOF analysis of seasonal SST anomalies—after linearly removing the leading seven Pacific modes—during 1901–2001 in the Pan-Atlantic domain of 80°W–20°E, 20°S–60°N.

No.	*Variance Explained (%)*	*Name*	*Label*
1	9.0	Atlantic Multidecadal Oscillation	AMO
2	6.1	Decaying phase of Atlantic Niño	AtlNino^{+}
3	6.1	Growing phase of Atlantic Niño	AtlNino^{-}
4	4.1	Tripole	Tripole

Principal components (PCs) and spatial patterns for the four residual Atlantic modes are shown in Fig. 3.10. Mode 1 is characterized by multidecadal North

Atlantic SST anomalies centered at about 50°N. The mode is temporally correlated with the AMO: correlation is 0.65 between PC1 and the AMO index constructed from residual Atlantic SSTs (i.e., averaged anomalies between 0 and 70°N); the correlation becomes 0.92 when both time series are subjected to 50 applications of a 1-2-1 smoother. Mode 3 and 2 are associated with seasonal growth and decay of SST anomalies in the eastern tropical Atlantic (mostly south of the equator). Mode 3 leads mode 2 by one year, suggesting a recurrent period of about four years for the underlying oscillation. The spatial patterns and temporal evolution bares a close resemblance to the Atlantic Niño mode characterized by Ruiz-Barradas et al. (2000), with some reasonable difference attributable to the filtering of the Pacific linkages. Mode 4 is marked by decadal variations of a north-south SST tripole in the North Atlantic, with the middle/strongest polarity centered near the separation of the Gulf Stream. The mature phase structure closely resembles the winter NAO SST footprint (e.g., Visbeck et al. 2001). A detailed accounting of these residual Atlantic modes will be reported elsewhere (Guan and Nigam).

3.5.2 Hydroclimate connections

It has been shown that hydroclimate connections of the Pacific modes have strong seasonal dependence. A similar analysis is done here for the four residual Atlantic modes. Spring, summer and fall precipitation regressions are shown in Fig. 3.11. The signs shown here correspond to the warm phases of the various modes. Discussions are focused on the Great Plains domain, which for brevity will not be mentioned repeatedly.

For mode 1 (the "AMO" mode), the strongest connection is in fall, when warm midlatitude North Atlantic SSTs are associated with dry anomalies over the Great Plains (Fig. 3.11c). The connection is weaker in spring (Fig. 3.11a), and nearly neutral in summer (Fig. 3.11b). Mode 2, when in its warm phase (decaying "Atlantic Niño"), is associated with strong dry anomalies in summer (Fig. 3.11e) and some weaker ones in spring (Fig. 3.11d). Connection is nearly muted in fall (Fig. 3.11f). Mode 3 (growing "Atlantic Niño"), on the other hand, is associated with dry (wet) anomalies in summer (fall) when in its warm phase (Figs. 3.11h,i). Little is found in spring (Fig. 3.11g). Mode 4 (the tripole mode), when in its warm phase (warm SSTs near the separation of the Gulf Stream and cold ones on both sides), is connected to wet anomalies over the Great Plains in spring (Fig. 3.11j) and fall (Fig. 3.11l), while of little influence in summer (Fig. 3.11k).

3.5.3 Reconstructions from Pacific + Atlantic SSTs

New precipitation reconstructions, shown in Fig. 3.12 (second column), are formed by adding the contributions from the four residual Atlantic modes (Fig. 3.12, left column) to the Pacific SST–based reconstructions (see Figs. 3.6 and 3.7). Observed precipitation is also shown (Fig. 3.12, right column), for comparison.

Reconstruction is improved in each of the four cases by inclusion of the Atlantic Ocean, bringing the magnitudes to as large as 90% of the observation (Dust Bowl spring; cf. Figs. 3.12e,f). Contributions from the two ocean basins are actually on the same order of magnitudes, suggesting that the Atlantic is of comparable importance to these long-term dry/wet episodes over the Great Plains. This is quantified by calculating the total percentage contributions of the four Atlantic modes

to the observed Great Plains precipitation index, shown in Table 3.3. Contributions from individual modes vary among different episodes or during different seasons. Mode 2 and 3, associated with decay and growth of warm SSTs in the eastern tropical Atlantic, contributed 29.6% to the observed precipitation anomaly during Dust Bowl summers. Springtime anomaly during this period is mostly contributed from mode 1 (52.5%), which is associated with warm SSTs in the midlatitude North Atlantic. Mode 1 is the only dominating Atlantic mode during the 1950s and 1980s episodes, which contributed 26.2% and 37.3% to the observed fall precipitation anomaly. The relatively successful reconstructions based on combined Pacific and Atlantic contributions is consistent with the ability of the eleven SST modes in realistically reproducing SST anomaly patterns during the three long-term dry/wet episodes, shown in Fig. 3.13.

Table 3.3. Percentage contributions of the four Atlantic modes (columns 3–6) to observed precipitation anomalies (column 2; mm/day) over the Great Plains (90–100°W, 35–45°N) for four cases (column 1). Total percentage contributions are also calculated for the four Atlantic modes (column 7), the seven Pacific modes (column 8), and all eleven modes together (column 9).

Case	Obs.	Mode 1	Mode 2	Mode 3	Mode 4	*Sub Total*		*Total*
						Atl.	Pac.	
1931–39 Sum	−0.51	−3.0	20.2	9.4	1.7	28.3	29.1	57.4
1931–39 Spr	−0.35	52.5	13.6	0.0	−15.5	50.6	39.5	90.1
1953–56 Fal	−0.78	26.2	0.6	6.6	1.1	34.5	49.3	83.8
1982–86 Fal	0.82	37.3	−0.1	1.1	0.2	38.5	36.7	75.2

3.6 Summary

Pacific and later residual Atlantic SSTs are investigated for their linkages to hydroclimate variations over the Great Plains. Focus has been on the reconstruction

of major dry/wet episodes in the twentieth century, i.e., the Dust Bowl drought (1931–1939), the 1950s drought (1953–1956), and the 1980s wet period (1982–1986), from leading Pacific and residual Atlantic modes.

The beginning Pacific-centric analysis shows that

- dry anomalies during the Dust Bowl summers are associated with three Pacific modes: non-canonical ENSO, trend, and (to a lesser extent) PDV North Pacific, all in their cold phases. Contributions largely come from non-canonical ENSO in the central/southern Plains, while from the trend mode in the northern Plains. The three modes together contribute 31.2% to the observed anomalies over the Great Plains domain (defined as 90–100°W, 35–45°N, corresponding to the core region of the Dust Bowl drought), one half of which being from non-canonical ENSO. The springtime dry anomaly, on the other hand, is associated with the trend mode (cold SSTs in the midlatitude North Pacific), which alone contributes 37.0% to the observed anomalies. SST forcing during this period includes cold anomalies in both the equatorial central/eastern Pacific and the midlatitude North Pacific, with the latter basin contributing more of the dry anomalies;
- the 1950s fall drought is linked to two Pacific modes: PDV North Pacific, in its warm phase, contributed 30.0% to the observed anomaly, while ENSO, in its cold phase, contributed another 19.1% (mostly from the decaying phase). SST forcing during this period features a La Niña-like pattern, which is a combination of PDV North Pacific and ENSO. The 1980s wet episode, also peaking in fall, structurally mirrors the 1950s drought in a broad sense; so does the SST forcing. PDV North Pacific, in its cold phase, is again the most important mode, contributing 27.9% to

the observed anomaly. The warm phase ENSO contributed another 10.7%;

- connection (i.e., covariance) patterns vary over the seasonal cycle between SSTs and dry/wet anomalies over the Great Plains. For non-canonical ENSO, the most affected season is summer, when warm central equatorial Pacific SSTs are linked to wet anomalies throughout the Great Plains domain. For trend, the drought linkage is strongest in spring, when warming Pacific SSTs are associated with a moister Great Plains. The association becomes much weaker in summer over much of the central/southern Plains, while maintaining strength in the northern part. For PDV North Pacific, the most influential season is fall, when warm midlatitude North Pacific SSTs are associated with dry anomalies in the Great Plains. Dry anomalies are also found in spring but limited to the southwest corner of the Great Plains domain, which are replaced by wet anomalies in summer.

It is further shown that

- compared to the Pacific Ocean, the Atlantic Ocean has been comparably important to the major dry/wet episodes over the Great Plains in the twentieth century. Of the leading four residual Atlantic modes, mode 2 and 3 ("Atlantic Niño"), associated with decay and growth of warm SSTs in the eastern tropical Atlantic, contributed 29.6% to the observed precipitation anomaly during the Dust Bowl summers. Springtime anomaly during this period was mostly contributed from mode 1 (52.5%), the "AMO" mode associated with warm SSTs in the North Atlantic. The "AMO" mode dominated the Atlantic contributions during the 1950s (warm SSTs/dry anomaly) and 1980s (cold SSTs/wet anomaly) episodes, amounting to 26.2% and 37.3% of the observed fall precipitation anomalies,

respectively; contributions from the other three modes were virtually negligible during these two periods;

- hydroclimate connections are also seasonally dependent for Atlantic SSTs over the Great Plains. For mode 1 (the "AMO" mode), the strongest connection is in fall, when warm North Atlantic SSTs are associated with dry anomalies over the Great Plains. Mode 2 and 3 (decaying and growing phases of "Atlantic Niño") are both associated with strongest dry anomalies in summer when in the warm phase. For mode 4 (the tripole mode), the strongest connection is in spring and fall, when wet anomalies over the Great Plains are associated with the positive index phase of the SST tripole (warm Gulf Stream SSTs with cold ones on both sides).

SST forcing of long-term droughts cannot be fully understood without taking into account the changes in the global mean surface temperature associated with increased concentrations of atmospheric CO_2. Changes in ENSO behaviors may also lead to variations in the teleconnected climate. Via two Pacific SST modes, i.e., the non-canonical ENSO mode and the trend mode, we explored such issues to some extent. The two modes, as found, are among the most important modes in association with the Dust Bowl drought.

The current analysis provides a basis for drought experiments with atmospheric GCMs, where synthetic SSTs, derived from the EEOF modes and their combinations, are used as external forcing. Such experiments are urgently needed to substantiate the SST-drought linkages discussed above, and are being planned for the NCAR CAM3.5 model.

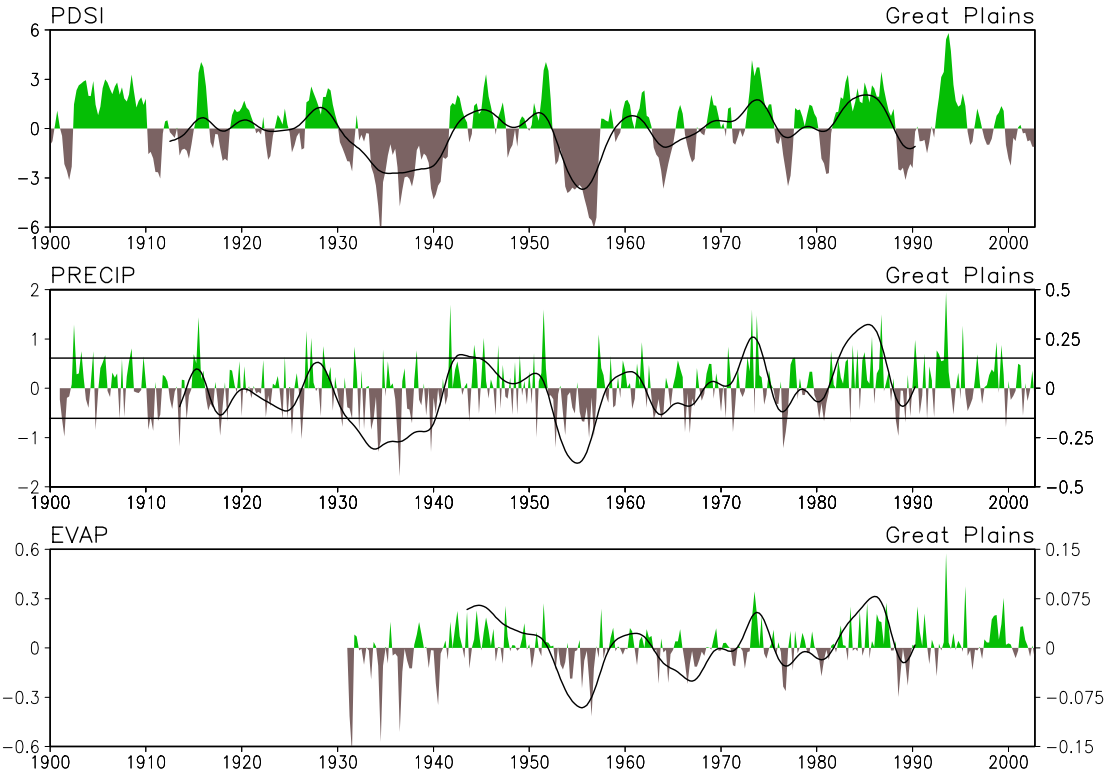

Fig. 3.1. PDSI, precipitation (mm day^{-1}) and evaporation (mm day^{-1}) anomalies averaged over the Great Plains (90–100°W, 35–45°N). The original values are shaded, while heavily-smoothed versions (from 50 applications of a 1-2-1 smoother) are shown using solid black lines. Note that smoothed precipitation and evaporation are shown using the right (finer) scale. The two horizontal lines in the middle panel indicate ± one standard deviation of the *smoothed* precipitation index.

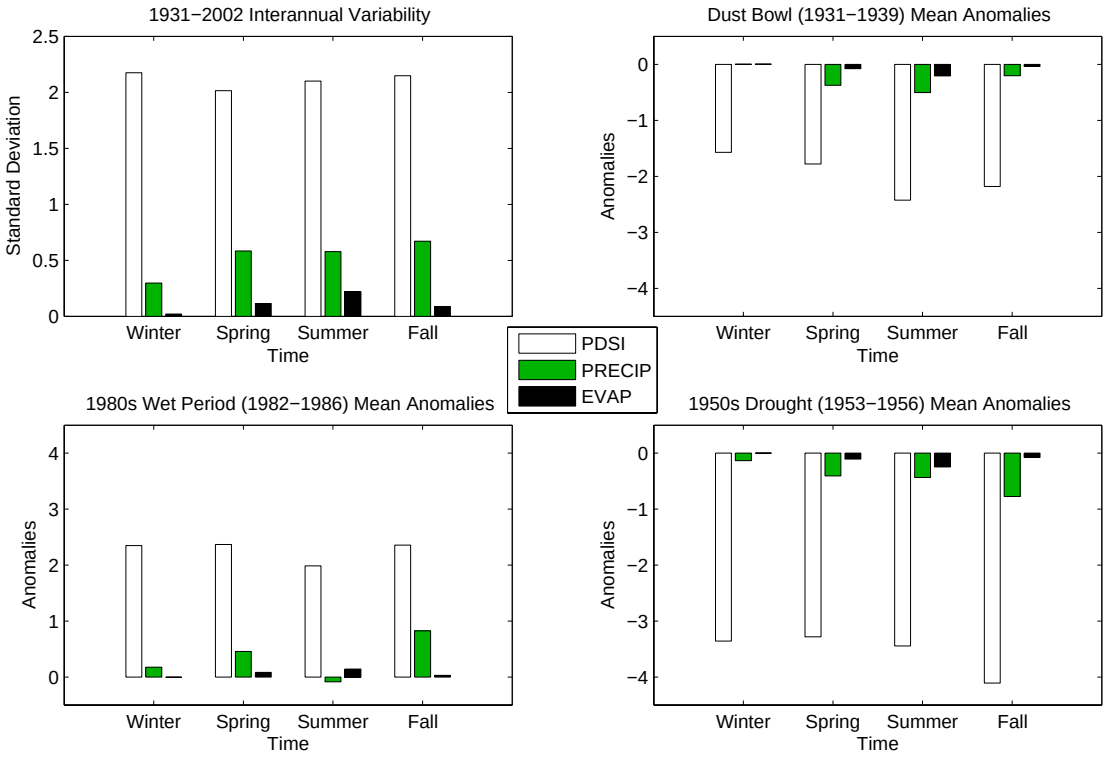

Fig. 3.2. (upper-left) Seasonal standard deviations of PDSI, precipitation (mm day^{-1}) and evaporation (mm day^{-1}) anomalies during 1931–2002, the overlapping data set availability period. (others) Mean anomalies of PDSI, precipitation and evaporation averaged for each season during (upper-right) 1931–1939, (lower-right) 1953–1956 and (lower-left) 1982–1986. All anomalies are with respect to the 1931–2002 seasonal climatology.

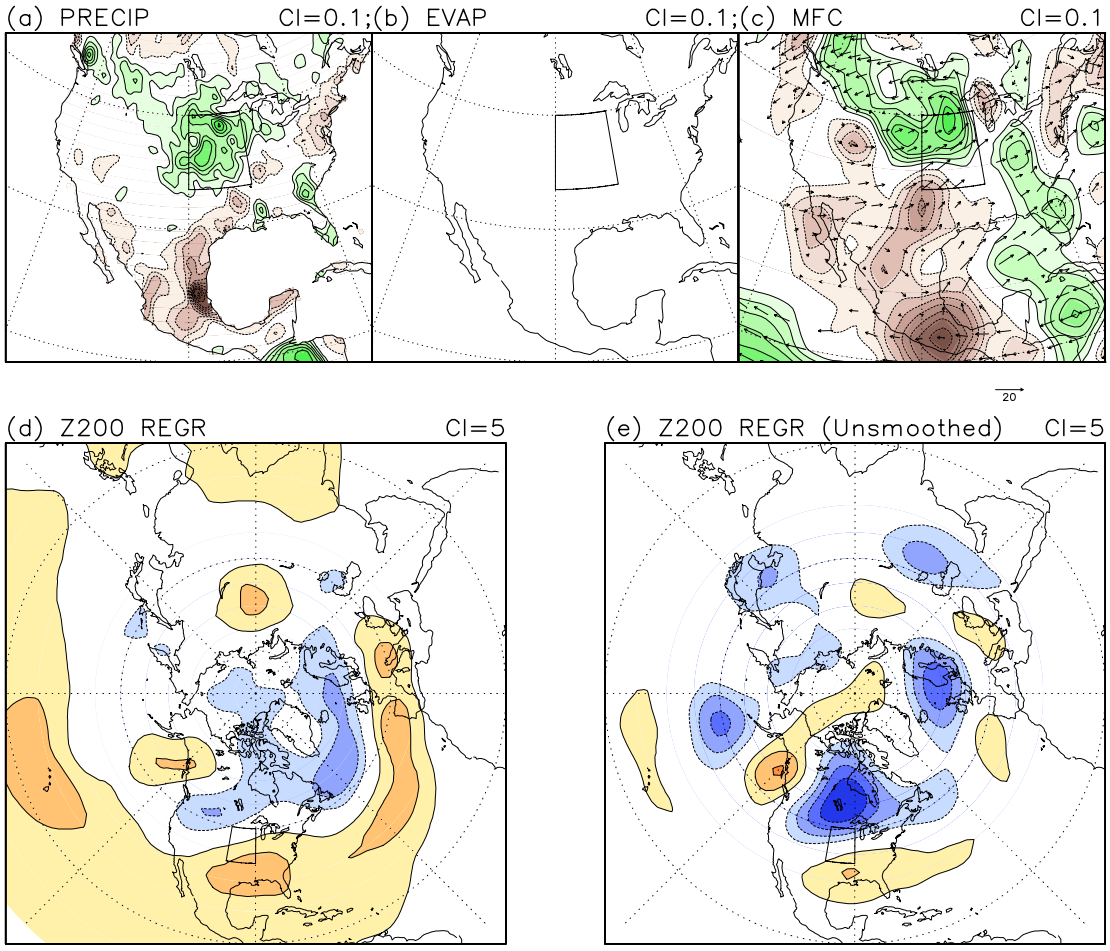

Fig. 3.3. (a)–(c) Regressions of (a) precipitation (mm day^{-1}), (b) evaporation (mm day^{-1}), (c) moisture flux (kg m^{-1} s^{-1}) and convergence (mm day^{-1}) on the summertime Great Plains precipitation index; the latter has been smoothed by six applications of a 1-2-1 smoother and normalized. (d), (e) Regressions of 200-hPa height (m) on (d) smoothed and (e) unsmoothed Great Plains precipitation index. Solid (dashed) contours denote positive (negative) values and the zero-contour is suppressed. Contour interval is 0.1 mm day^{-1} for precipitation, evaporation and moisture flux convergence, and 5 m for height regressions. The small box in each panel (and in subsequent figures) indicates the Great Plains domain. Moisture flux and 200-hPa height are calculated/extracted from the ERA-40 reanalysis. Regression calculations are based on the overlapping data set availability period, i.e., 1958–2001.

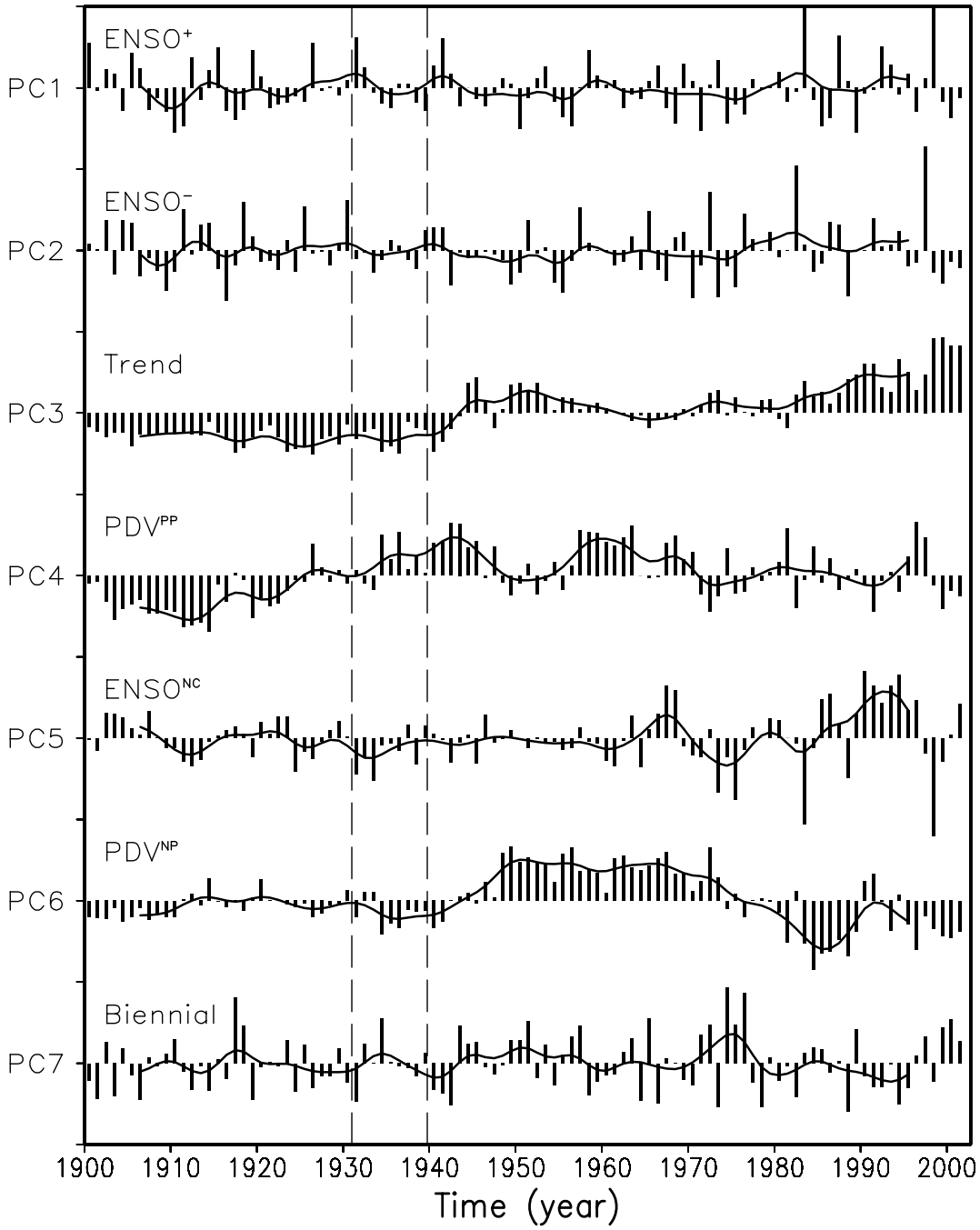

Fig. 3.4. Principal components (PCs) of the leading seven modes of all-season Pacific sea surface temperatures (SSTs) during 1900–2002. Only summer values are shown, which have been renormalized to have zero-mean and unit variance. Tick marks are drawn every three units on the vertical axis. Bars are for the original PCs, while solid lines are for smoothed versions (from six applications of a 1-2-1 smoother). The vertical dashed lines indicate the Dust Bowl period (1931–1939) as defined in section 3.3.

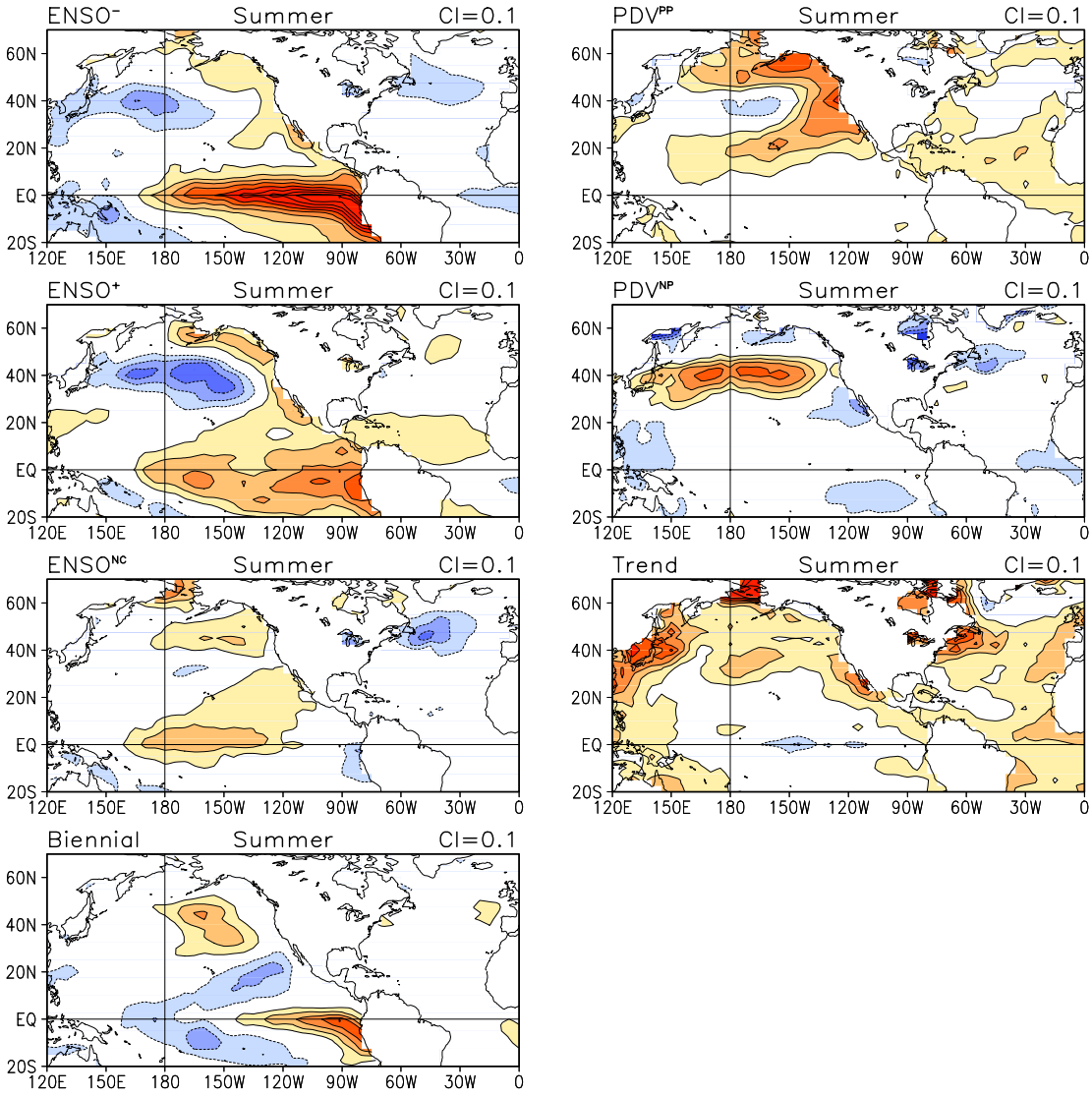

Fig. 3.5. Summer patterns of the leading seven Pacific modes during 1900–2002, obtained by regressing SST (K) anomalies onto the (unsmoothed) PCs as shown in Fig. 3.4. Note that they are not shown in the order of variance explained (ENSO-related modes on the left, while lower frequency modes on the right). Contour interval is 0.1 K.

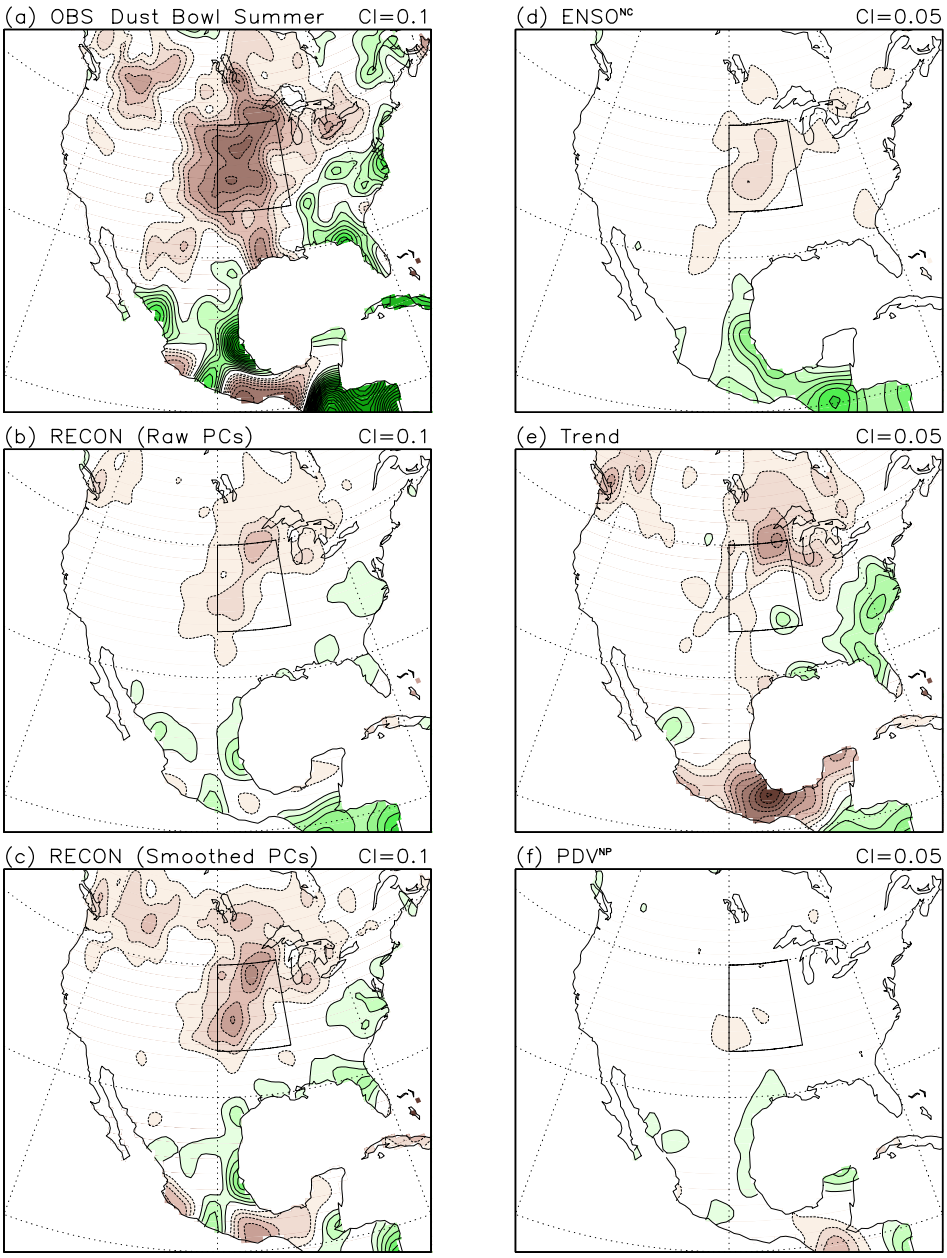

Fig. 3.6. (a)–(c) Precipitation (mm day^{-1}) anomalies averaged for the Dust Bowl (1931–1939) summers: (a) observed; (b) reconstructed from unsmoothed Pacific PCs; (c) reconstructed from smoothed Pacific PCs (as shown in Fig. 3.4). Reconstructions are obtained by multiplying simultaneous summer precipitation regressions with average PCs and taking a summation over the seven modes. (d)–(f) Contribution of (d) non-canonical ENSO, (e) the trend mode and (f) PDV North Pacific to the precipitation reconstruction in (b). All maps have been subjected to five applications of a nine-point smoother (*smth9* in GrADS) before being displayed. Contour interval is 0.1 (0.05) mm day^{-1} in left (right) panels.

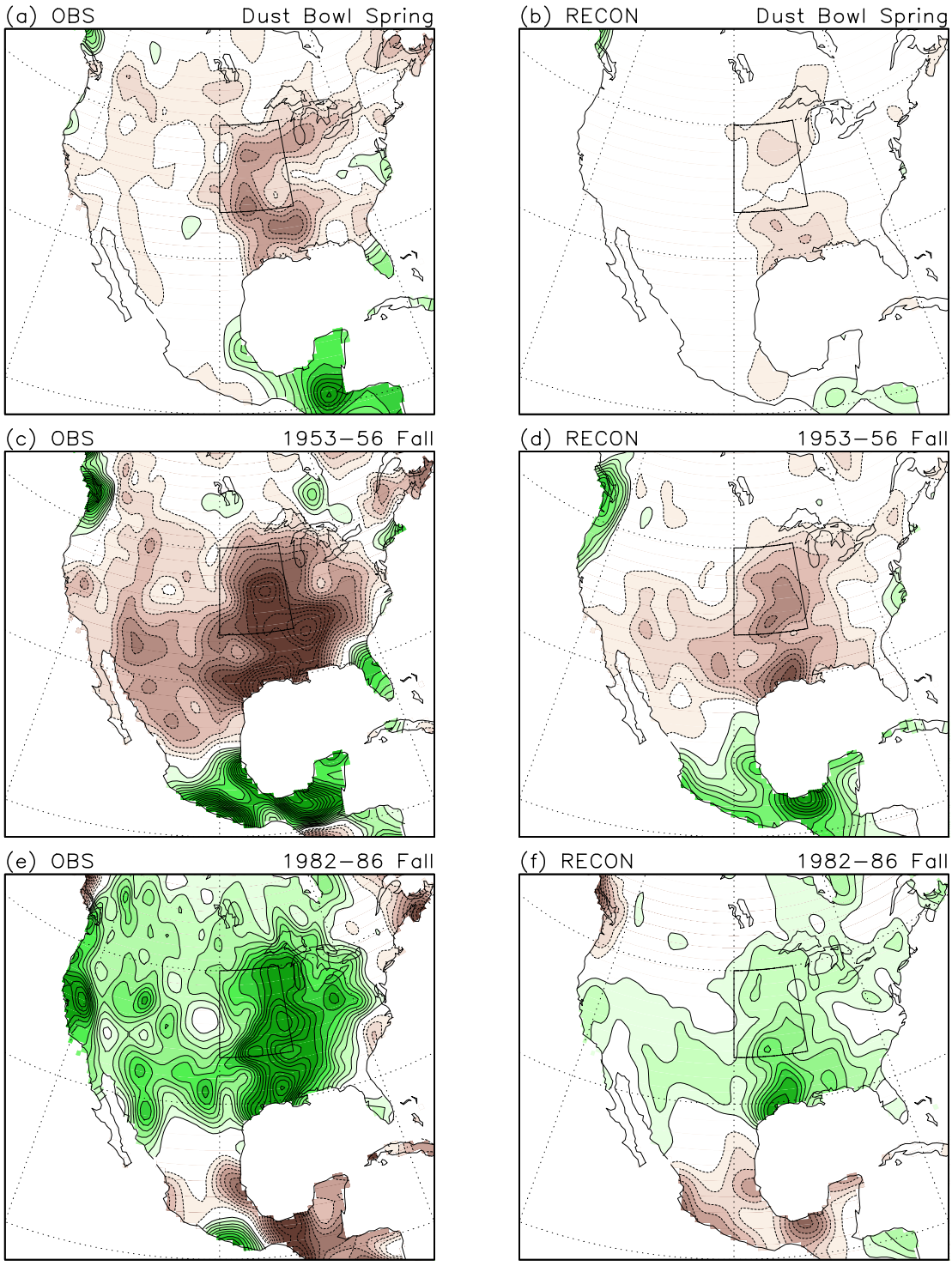

Fig. 3.7. (left) Observed and (right) reconstructed precipitation anomalies for (a), (b) the Dust Bowl (1931–1939) spring, (c), (d) the 1950s (1953–1956) fall drought and (e), (f) the 1980s (1982–1986) fall wet period. Reconstructions are based on simultaneous regressions on unsmoothed Pacific PCs for respective seasons, obtained as in Fig. 3.6. Contour interval is 0.1 mm day^{-1}.

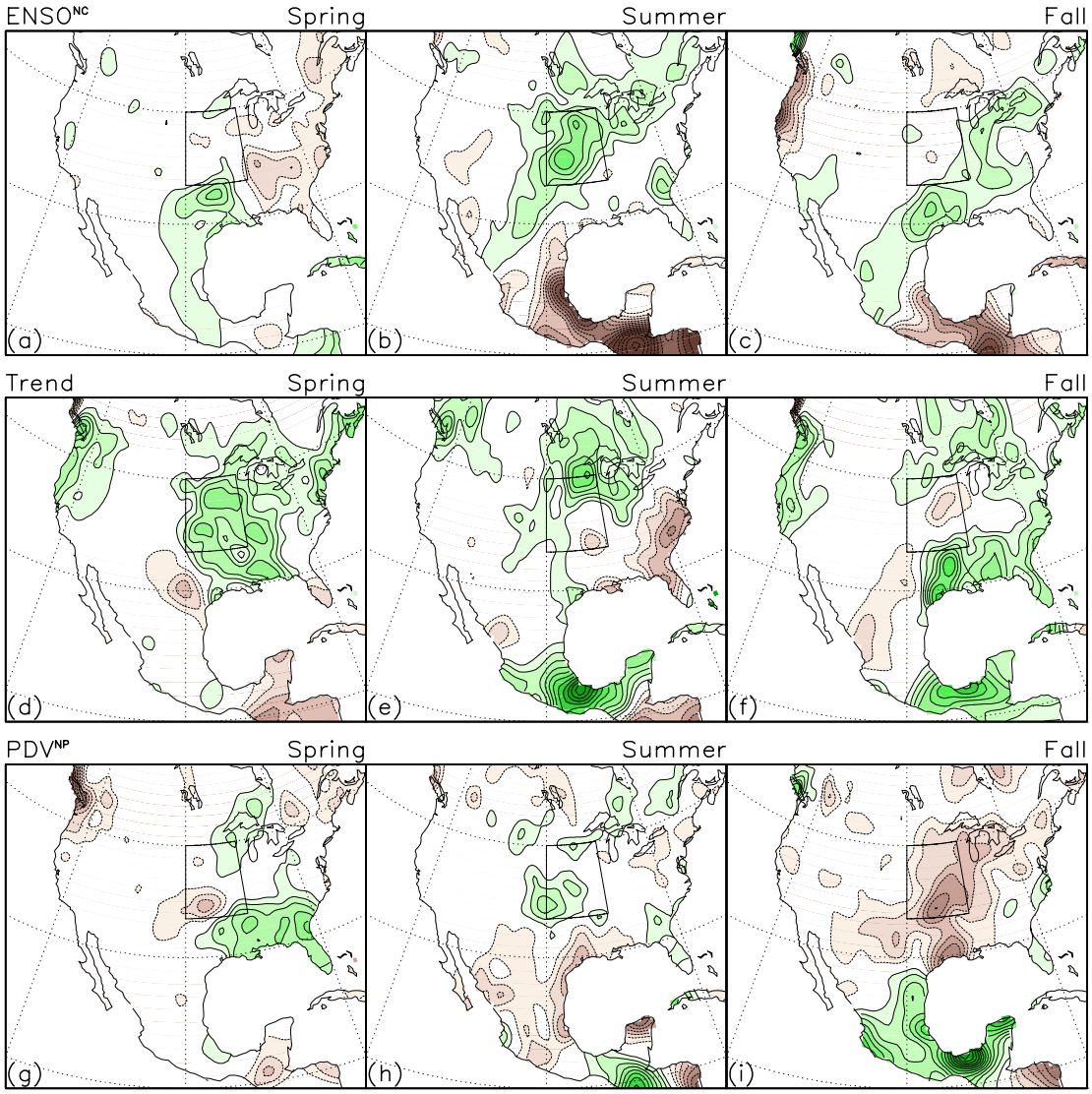

Fig. 3.8. Seasonal evolution of the SST-drought linkages for (top) non-canonical ENSO, (middle) the trend mode and (bottom) PDV North Pacific. Time runs from left to right, with the first (last) column being spring (fall). The maps are obtained from simultaneous regressions of precipitation anomalies on unsmoothed Pacific PCs. Contour interval is 0.05 mm day^{-1}.

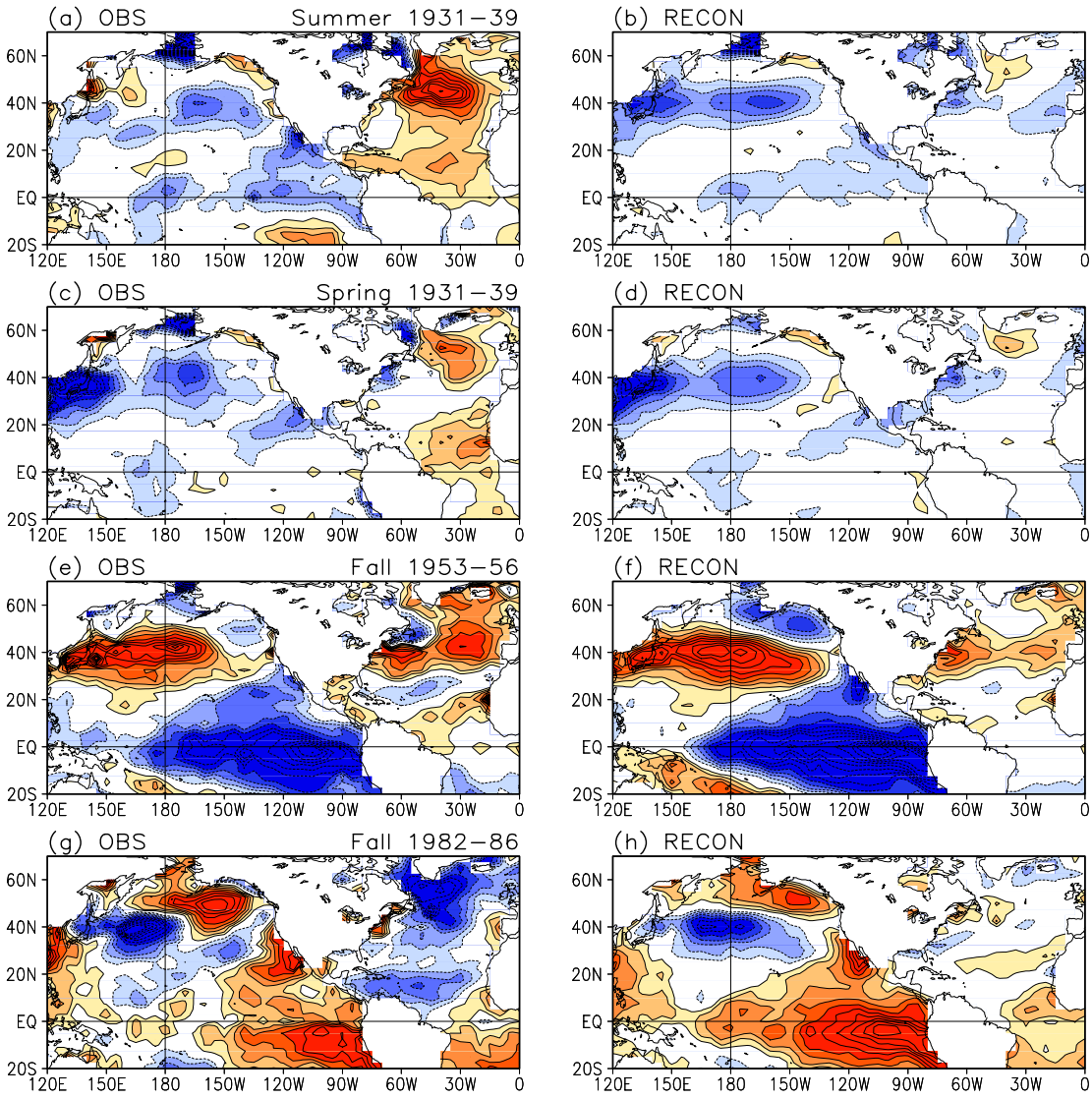

Fig. 3.9. (left) Observed and (right) reconstructed SST anomalies for (a), (b) the Dust Bowl (1931–1939) summer, (c), (d) the Dust Bowl spring, (e), (f) the 1950s (1953–1956) fall drought and (g), (h) the 1980s (1982–1986) fall wet period. Reconstructions are based on the seven Pacific modes. Contour interval is 0.1 K.

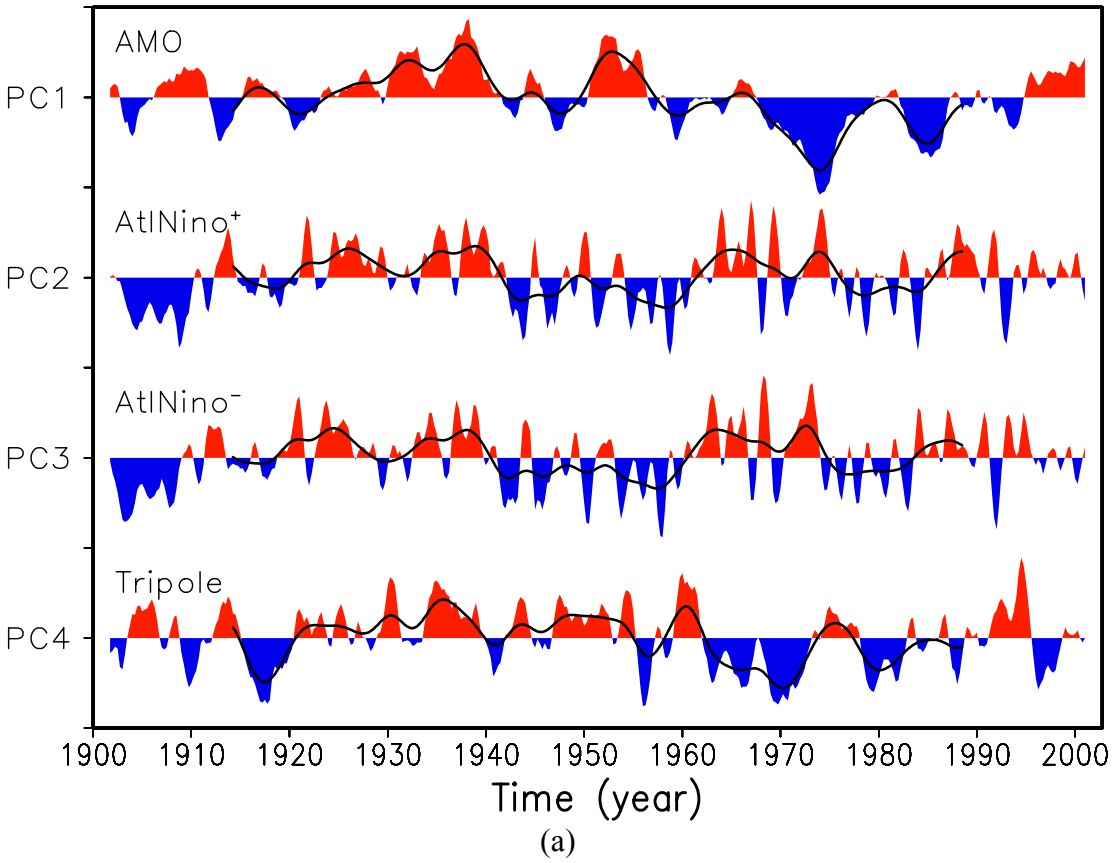

(a)

Fig. 3.10. (a) Principal components (PCs) of residual Atlantic SST variability in the twentieth century (1901–2001). Residual SSTs are obtained by linearly removing from the total SSTs the leading seven Pacific modes as extracted from the standard Pacific basin analysis (described in Chapter 2). Tick marks on the vertical axis are drawn every three units. The original PCs are shaded, while heavily-smoothed versions (from 50 applications of a 1-2-1 smoother) are shown using solid black lines. (b)–(m) Time evolution of the leading four modes of residual Atlantic SST variability. (b)–(d) AMO. (e)–(g) Decaying phase of Atlantic Niño. (h)–(j) Growing phase of Atlantic Niño. (k)–(m) Tripole. Note that the AMO evolution is displayed at four-season interval, the Atlantic Niño modes at two-season interval, while the tripole mode at three-season interval. Maps are obtained by regressing lead/lagged residual SST anomalies onto the PCs shown in (a), with the label *t* denoting simultaneous regressions. Contour interval is 0.1 K.

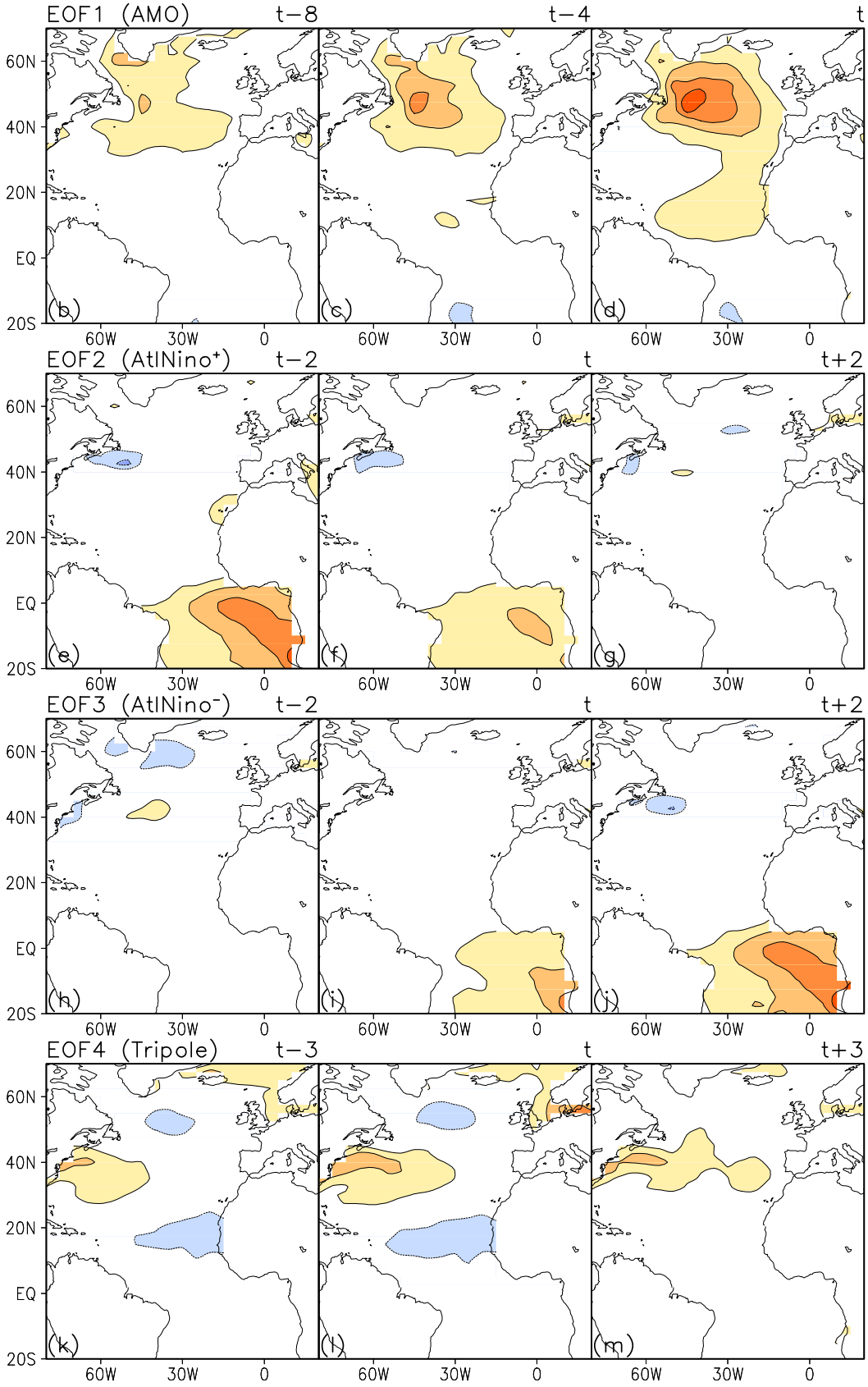

Fig. 3.10. (*cont'd*) (b)–(m)

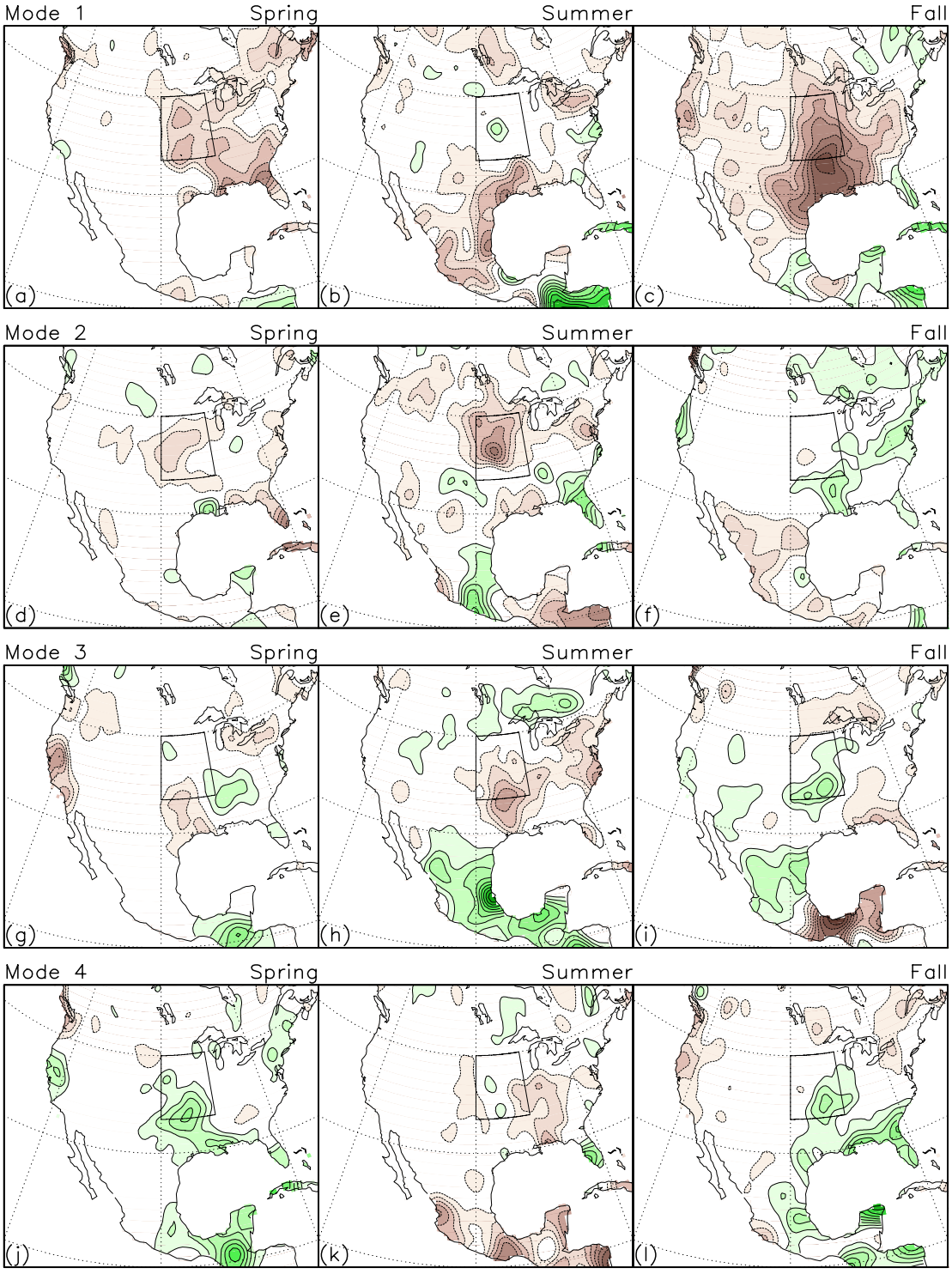

Fig. 3.11. Seasonal evolution of the SST-drought linkages: as Fig. 3.8 but for the four residual Atlantic modes. Contour interval is 0.05 mm day^{-1}.

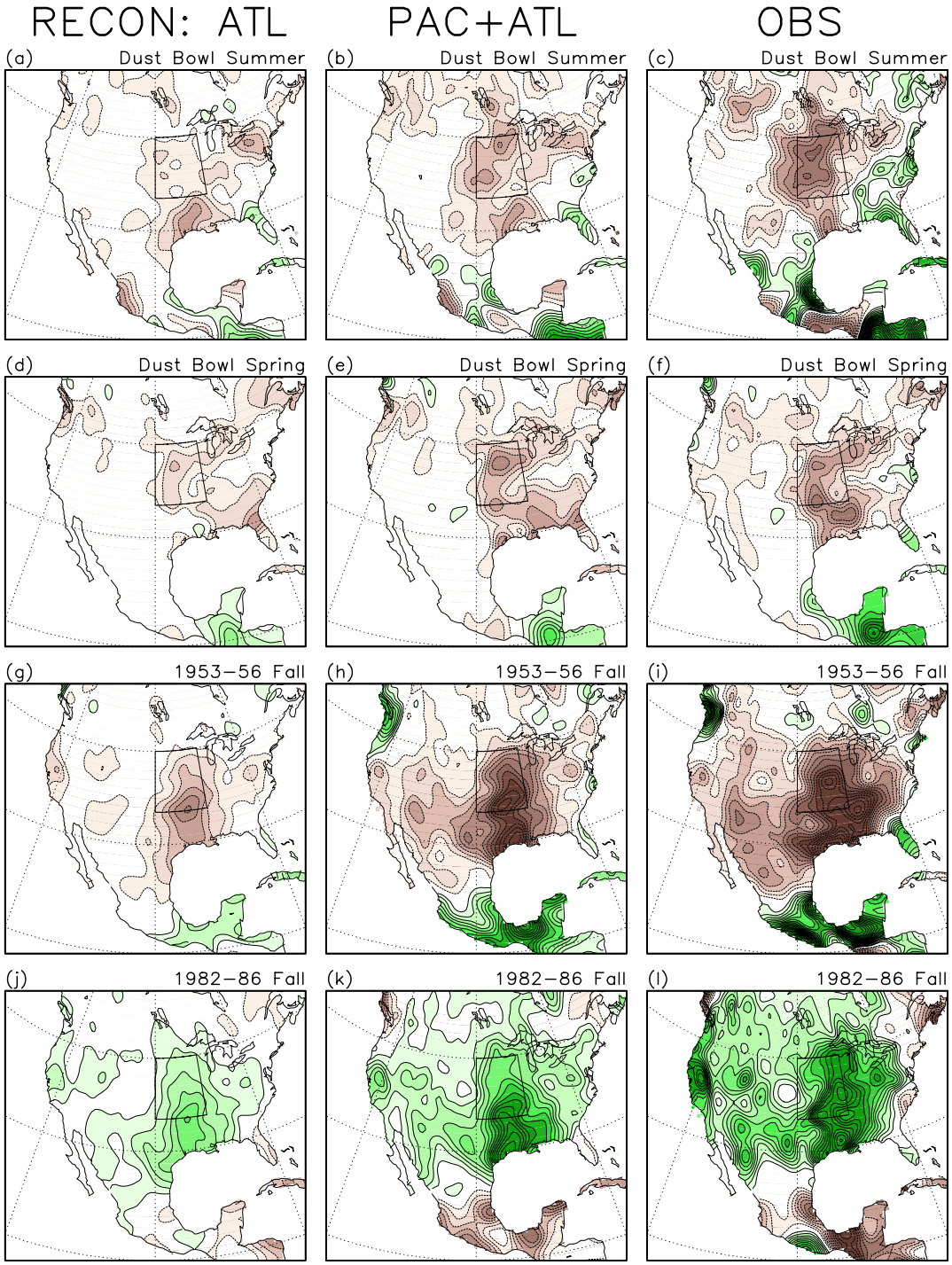

Fig. 3.12. (left and central) Reconstructed and (right) observed precipitation anomalies for (top) the Dust Bowl (1931–1939) summer, (second from top) the Dust Bowl spring, (second from bottom) the 1950s (1953–1956) fall drought and (bottom) the 1980s (1982–1986) fall wet period. Reconstructions are based on the four residual Atlantic modes in the left column, while contributions from the seven Pacific modes are added in the central column. Contour interval is 0.1 mm day^{-1}.

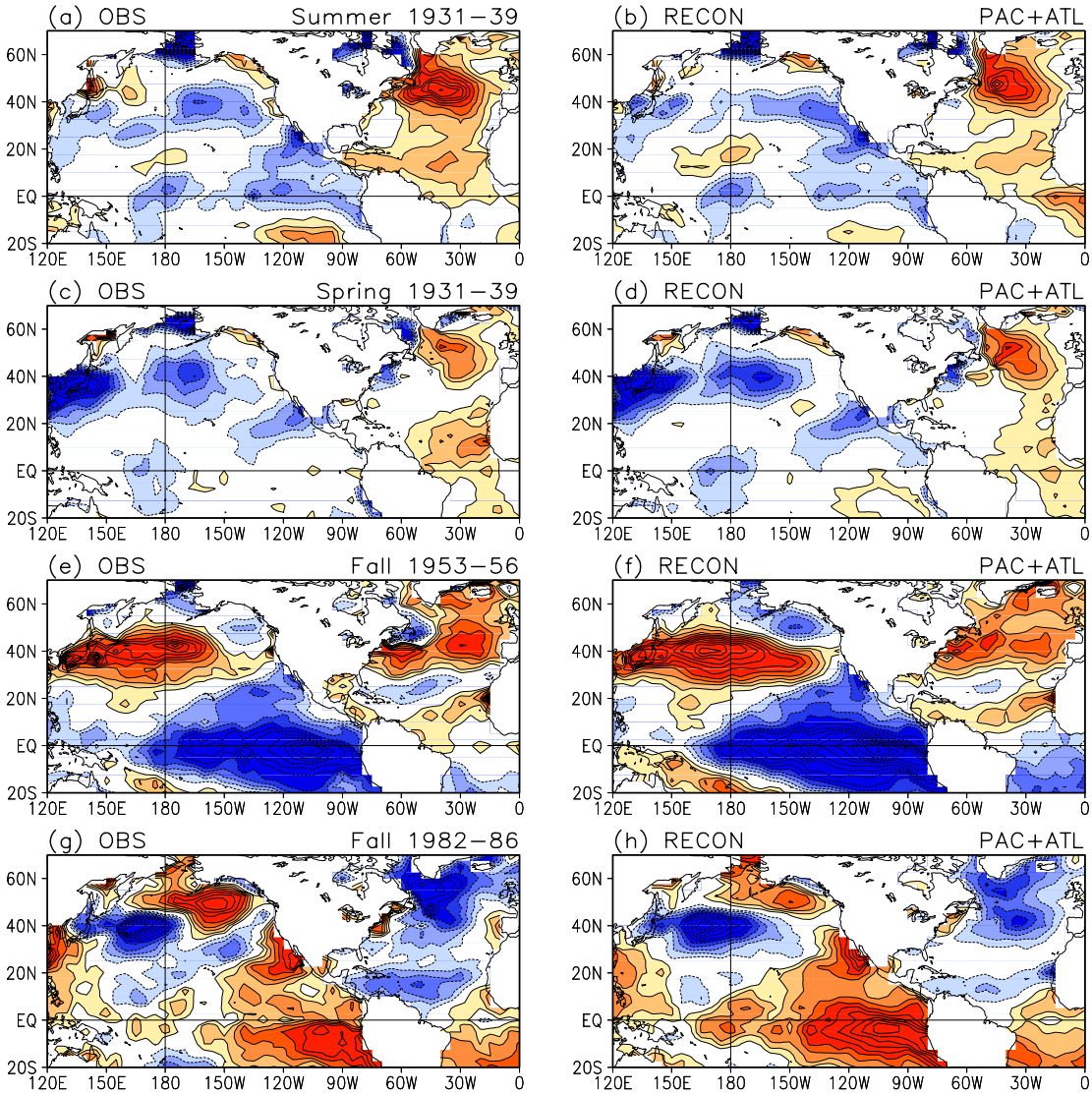

Fig. 3.13. (left) Observed and (right) reconstructed SST anomalies: as Fig. 3.9 except that the reconstructions are based on the seven Pacific modes plus the four residual Atlantic modes. Contour interval is 0.1 K.

Chapter 4 Summary and Discussion

4.1 Summary

In this dissertation, Pacific SST variability in the twentieth century, and its linkage to long-term hydroclimate variability over the Great Plains, is investigated. The work is motivated by the need to improve characterization of Pacific decadal variability (PDV), but the scope has been broader: the nature of the primary SST analysis enables a spatiotemporal characterization of *all* non-seasonal modes, including the secular trend, of the Pacific Ocean in a mutually consistent (and potentially improved) way. Based on that analysis, the dissertation investigates the connections between Pacific (and residual Atlantic) SSTs and long-term hydroclimate variations over the Great Plains. The focus has been on the reconstruction of major dry/wet episodes in the twentieth century, with the aim to clarify the relative importance of different ocean basins as external forcing.

In Chapter 2, the twentieth century Pacific SST variability is characterized by seven modes. The evolution-centric analysis effectively discriminates between biennial, ENSO, and decadal variabilities, and between these natural variability modes and secular trend. All modes are extracted in a single step, without recourse to pre-filtering and detrending. It is found that

- ENSO variability and changes are tracked by four modes. Canonical ENSO evolution is encapsulated in two modes that depict the growth (east-to-west along the equator) and decay (near-simultaneous amplitude loss across the basin) phases. Non-canonical ENSO, shown linked to the west-to-east SST development

seen in post–climate shift ENSOs, is represented by an interannual mode of comparatively lower frequency that has been energetic in recent decades. The biennial variability is described by a fourth mode;

- PDV is manifested in two spatially distinct modes: the Pan-Pacific mode has a horse-shoe shaped structure with the closed end skirting the North American coast; and a quiescent central/eastern equatorial Pacific. The North Pacific mode has a zonal band of SST anomalies extending eastward from Japan as its principal feature. The latter mode captures the 1976/77 climate shift and exhibits some correspondence to Mantua's Pacific Decadal Oscillation. None of the two PDV modes are "ENSO-like";
- a nonstationary SST-trend, including mid-century cooling, is characterized by the trend mode. Geographically, a sliver of cooling in the central equatorial Pacific is seen in the midst of widespread but nonuniform warming.

Based on the above analysis, Chapter 3 investigates the relative importance of SST variations in different ocean basins in forcing long-term hydroclimate variations over the Great Plains. Contributions of Pacific and residual Atlantic SSTs to three major dry/wet episodes in the twentieth century are analyzed on a mode-by-mode basis. The Pacific and the Atlantic Oceans are shown to have contributed comparable amounts to the observed precipitation anomalies during these periods. Specifically,

- low precipitation during the Dust Bowl summers is shown linked to three Pacific modes (non-canonical ENSO, trend, and PDV North Pacific) associated with cold SSTs in both tropical and extratropical Pacific, and two residual Atlantic modes (pre- and post-mature "Atlantic Niño") associated with growth and decay of warm

SSTs in the eastern tropical Atlantic. They together contribute ~61% to the observed precipitation anomalies over the Great Plains. In spring, on the other hand, extratropical SSTs in the two ocean basins (cold in North Pacific, associated with the trend mode; and warm in North Atlantic, associated with the "AMO"—the leading residual Atlantic mode) dominate, which together contributed ~90% to the observed precipitation anomalies;

- the 1950s fall drought is shown linked to warm extratropical SST anomalies in the two ocean basins (associated with PDV North Pacific and the "AMO"), as well as cold SSTs in the tropical eastern Pacific although less contributing. The 1980s wet episode structurally mirrors the 1950s drought in a broad sense; so does the SST forcing. In either case, the associated North Pacific and North Atlantic modes together contributed around 60% to the observed precipitation anomaly;
- connection patterns are seasonally dependent between Great Plains droughts and Pacific/Atlantic SSTs. Spring drought is most favored by midlatitude SST anomalies with opposing signs in the two ocean basins: cold in North Pacific associated with the trend mode[17], and warm in North Atlantic associated with the "AMO" mode. Both tropical and extratropical SSTs can be involved in a summer drought, with the most important contributions coming from the central tropical Pacific (cold SSTs associated with non-canonical ENSO) and eastern tropical Atlantic (warm SSTs associated with the "Atlantic Niño"). Fall droughts are most relatable to PDV North Pacific and the "AMO" mode, when warm SSTs are found in extratropical North Pacific/Atlantic.

[17] With a warming trend, this means spring is becoming less susceptible to droughts.

4.2 Discussion

The central contribution of this dissertation is the refined PDV characterization in the context of other natural variabilities and the non-stationary warming trend. Insights are much needed for the processes underlying the two PDV modes, including their impacts on local and global climate. Preliminary results show that the two PDV modes discussed here may involve quite different oceanic/atmospheric processes not inconsistent with existing theories.

Meanwhile, there are concerns that the PDV may simply result from integration, via the thermal inertia of the ocean, of the internal atmospheric variability. Since the latter is essentially white noise from decadal perspective, the PDV in this case can be best described as a red noise process. This has been found in simple and GCM modeling studies (Pierce 2001; Schneider et al. 2002), and supported by time series analysis (Pierce 2001; Rudnick and Davis 2003; Hsieh et al. 2005).

On the other hand, that the PDV could be explained as a red noise process shall not preclude the possibility that other processes are in play. For example, Rodionov (2006) showed that the PDO index still contains detectable regime shifts after removing the red noise component as fitted by a first-order autoregressive model. Also, it is of interest to note that the time series showed by Hsieh et al. (2005) to be stochastic also include the southern oscillation index, which is associated with known coupled ocean-atmosphere dynamics. The fundamental issue here is that the observed data record is so far insufficient to unambiguously determine the validity of the various hypotheses. While red noise is an appropriate null hypothesis, other

mechanisms, either primary or not, need to be explored since any predictability—beyond persistence—of the PDV shall lie in these other mechanisms.

The current work contains a new attempt to clarify the remote forcing of long-term Great Plains droughts, in view of recent modeling interests in the 1930s Dust Bowl. The observationally-based analysis suggests potentially underestimated importance of the extratropical ocean basins in drought forcing. Also, contributions from the Pacific and Atlantic oceans are shown comparable. Interestingly, GCM experiments (e.g., Schubert et al. 2004; Seager et al. 2005) have suggested that long-term droughts over the Great Plains are primarily tropically forced, by the Pacific Ocean. Why then are there comparatively strong North Pacific/Atlantic connections in nature during the 1950s drought (and the 1980s wet period)? Does midlatitude North Pacific/Atlantic have low-frequency variability sources independent of the Tropics that are not properly represented in these models? Or the model responses of midlatitude SST variations are unrealistically weak? A better understanding of North Pacific/Atlantic decadal variabilities, including their origins and mechanisms, is much needed to address these questions.

4.3 Future work

The results presented here provide a basis for a broader scope investigation of climate variability/change in the Pacific–North American region. Several topics are of interest. First, the physical processes underlying the two PDV modes need to be understood. Analysis of PDV-covarying ocean heat content and atmospheric circulation will be an immediate follow-up. Second, decadal connectivity between the Pacific and Atlantic Oceans has surfaced to some extent in the SST analysis, which

seems to be in effect during long-term drought development. GCM experiments need to be conducted to understand how PDV is linked to decadal North Atlantic variability and how this covariability between the two ocean basins might affect long-term hydroclimate variations over North America. Analysis of PDV's link to North Atlantic decadal climate variability (specifically, the NAO) in nature is underway, based on the clarified PDV structure. Another question concerns drought simulation (and prediction): previous modeling studies have argued for the driving role of tropical La Niña-like SSTs in long-term U.S. droughts. The current analysis suggests that midlatitude SSTs in both North Pacific and North Atlantic could be at least as well important. A question, however, remains to be answered as how these midlatitude SSTs are generated and maintained on decadal time scales. It is clear that a better understanding of the mechanisms of PDV and other variability modes in the adjoining ocean basins is needed for improved simulation and prediction of long-term U.S. droughts.

Appendix

A Rotated Extended EOF

A.1 Construction of the data matrix

First, seasonal anomalies are formed and appropriately weighted, denoted by

$$A(t) = \begin{bmatrix} a_{1,1} & a_{1,2} & \dots & a_{1,M} \\ a_{2,1} & a_{2,2} & \dots & a_{2,M} \\ \vdots & \vdots & \ddots & \vdots \\ a_{N,1} & a_{N,2} & \dots & a_{N,M} \end{bmatrix} \tag{A.1}$$

where N is the number of seasons, and M the number of grid cells. For extended EOF analysis with a $(2L+1)\Delta t$ temporal sampling window, an extended anomaly matrix, A_E, is constructed as

$$A_E = \begin{bmatrix} A(t - L\Delta t) & A(t - (L-1)\Delta t) & \dots & A(t + L\Delta t) \end{bmatrix} \tag{A.2}$$

A.2 SVD-based EOF

Singular value decomposition (SVD) of A_E is given by $A_E = USV^T$, with $U^T U = I$ and $V^T V = I$, and S a diagonal matrix containing the singular values. The covariance matrix C is then $C \equiv A_E^T A_E / N = V(S^T S / N)V^T$. Post-multiplying by V gives $CV = V(S^T S / N)$, which is the eigenvalue problem conventionally solved in EOF analysis. Here, the eigenvectors V and eigenvalues $S^T S/N$ are obtained from SVD of A_E, thus bypassing the need to form the covariance matrix. The modal decomposition is given by $A_E = TX_E^T$, where $T = U$ and $X_E = \left(SV^T\right)^T$.

The units (if any) of A_E will be carried by the spatial patterns (EOFs) X_E, while the time series (principal components or PCs) T are dimensionless.[18] The matrix X_E can be divided into $2L+1$ submatrices

$$X_E = \begin{bmatrix} X(t-L\Delta t) \\ X(t-(L-1)\Delta t) \\ \vdots \\ X(t) \\ \vdots \\ X(t+(L-1)\Delta t) \\ X(t+L\Delta t) \end{bmatrix} \tag{A.3}$$

which give the evolution of X over a period of $(2L+1)\Delta t$. SVD-based EOF is desirable due to the computational efficiency. In MATLAB, it is achieved by the *svd* function.

A.3 Rotation

The VARIMAX technique is used. Let R denote the rotation matrix, which satisfies $R^T R = I$. The rotated EOFs and corresponding PCs are nothing but $X_R = XR$ and $T_R = TR$. Here we have $T_R X_R^T = TR(XR)^T = TRR^T X^T = TX^T = A_E$, which means the matrix A_E can be fully recovered from the rotated EOFs.[19] Further, orthogonality of the PCs is maintained since $T_R^T T_R = (TR)^T TR = (UR)^T UR = R^T U^T UR = I$. Orthogonality of the EOFs is, however, relaxed after rotation since $X_R^T X_R = (XR)^T XR = (VS^T R)^T VS^T R = R^T SV^T VS^T R = R^T SS^T R$ is not diagonal.

[18] X_E and T are often rescaled such that the PCs have variance one.
[19] Practically, only a leading subset of the EOFs will be rotated. Therefore, A_E can only be partially recovered. The total variance explained by the subset of EOFs remains the same after rotation.

A.4 Lead/lag regressions

Using Eq. A.3, the modal decomposition $A_E = TX_E^T$ can be rewritten as

$$A_E = T\begin{bmatrix} X(t-L\Delta t) \\ X(t-(L-1)\Delta t) \\ \vdots \\ X(t) \\ \vdots \\ X(t+(L-1)\Delta t) \\ X(t+L\Delta t) \end{bmatrix}^T \tag{A.4}$$

which, by comparison to Eq. A.2, gives

$$A(t+l\Delta t) = TX^T(t+l\Delta t) \qquad (-L \le l \le L) \tag{A.5}$$

Let $\mathbf{t}_k$ denote the k^{th} column of T, $\mathbf{x}_k(t+l\Delta t)$ denote the k^{th} column of $X(t+l\Delta t)$, Eq. A.5 can be rewritten as

$$A(t+l\Delta t) = \mathbf{t}_1\mathbf{x}_1^T(t+l\Delta t) + \mathbf{t}_2\mathbf{x}_2^T(t+l\Delta t) + \cdots + \mathbf{t}_K\mathbf{x}_K^T(t+l\Delta t) \tag{A.6}$$

where K is the number of EOFs. Using Eq. A.6 and noting the orthogonality of T, the regression of $A(t+l\Delta t)$ on $\mathbf{t}_k$ can be obtained as

$$\begin{aligned} \frac{\mathrm{COV}(A(t+l\Delta t), \mathbf{t}_k)}{\mathrm{VAR}(\mathbf{t}_k)} &= \frac{A^T(t+l\Delta t)\mathbf{t}_k / N}{1/N} \\ &= (\mathbf{x}_1(t+l\Delta t)\mathbf{t}_1^T + \mathbf{x}_2(t+l\Delta t)\mathbf{t}_2^T + \cdots + \mathbf{x}_K(t+l\Delta t)\mathbf{t}_K^T)\mathbf{t}_k \\ &= \mathbf{x}_k(t+l\Delta t) \end{aligned} \tag{A.7}$$

This shows that in extended EOF, lead/lag regressions of the data on the PCs are identical to the corresponding EOFs at the same time lead/lag. This also applies when the EOFs are rotated.

Abbreviations and Notations

AMO	Atlantic Multidecadal Oscillation
AtlNino^{-}	Growing phase of Atlantic Niño
AtlNino^{+}	Decaying phase of Atlantic Niño
CPC	Climate Prediction Center
CRU	Climatic Research Unit
CTI	Cold-Tongue Index
ECCO	Estimating the Circulation and Climate of the Ocean
ECMWF	European Centre for Medium-Range Weather Forecasts
EEOF	Extended EOF
ENSO	El Niño–Southern Oscillation
ENSO^{-}	Growing phase of ENSO
ENSO^{+}	Decaying phase of ENSO
ENSO^{NC}	Non-canonical ENSO
EOF	Empirical Orthogonal Function
ERA-40	ECMWF 40 Year Re-analysis
GCM	General Circulation Model
GHCN	Global Historical Climatology Network
GISS	Goddard Institute for Space Studies
HadISST	Hadley Centre sea Ice and Sea Surface Temperature dataset
NAO	North Atlantic Oscillation
NASA	National Aeronautics and Space Administration
NCAR	National Center for Atmospheric Research
NCEP	National Centers for Environmental Prediction
NOAA	National Oceanic and Atmospheric Administration
PC	Principal Component
PDO	Pacific Decadal Oscillation
PDSI	Palmer Drought Severity Index
PDV	Pacific Decadal Variability
PDV^{NP}	PDV North Pacific
PDV^{PP}	PDV Pan-Pacific
r	Correlation coefficient
SST	Sea Surface Temperature
SVD	Singular Value Decomposition
UKMO	United Kingdom Met Office

Bibliography

Barlow, M., S. Nigam, and E. H. Berbery, 2001: ENSO, Pacific decadal variability, and U.S. summertime precipitation, drought, and stream flow. *J. Climate*, **14**, 2105–2127.

Barnett, T. P., 1991: The interaction of multiple timescales in the tropical climate system. *J. Climate*, **4**, 269–285.

Cane, M. A., A. C. Clement, A. Kaplan, Y. Kushnir, D. Pozdnyakov, R. Seager, S. E. Zebiak, and R. Murtugudde, 1997: Twentieth-century sea surface temperature trends. *Science*, **275**, 957–960.

Carton, J. A., and B. Huang, 1994: Warm events in the tropical Atlantic. *J. Phys. Oceanogr.*, **24**, 888–903.

Cattell, R. B., 1966: The scree test for the number of factors. *J. Multiv. Behav. Res.*, **1**, 245–276.

Chavez, F. P., J. Ryan, S. E. Lluch-Cota, and M. Ñiquen C., 2003: From anchovies to sardines and back: multidecadal change in the Pacific Ocean. *Science*, **299**, 217–221.

Chiang, J. C. H., and D. J. Vimont, 2004: Analogous Pacific and Atlantic meridional modes of tropical atmosphere-ocean variability. *J. Climate*, **17**, 4143–4158.

Chung, C., and S. Nigam, 1999: Weighting of geophysical data in principal component analysis. *J. Geophys. Res.*, **104**, 16925–16928.

Chung, C. E., and V. Ramanathan, 2006: Weakening of North Indian SST gradients and the monsoon rainfall in India and the Sahel. *J. Climate*, **19**, 2036–2045.

Czaja, A., and C. Frankignoul, 2002: Observed impact of Atlantic SST anomalies on the North Atlantic Oscillation. *J. Climate*, **15**, 606–623.

Dai, A., K. E. Trenberth, and T. Qian, 2004: A global dataset of Palmer drought severity index for 1870–2002: Relationship with soil moisture and effects of surface warming. *J. Hydrometeor.*, **5**, 1117–1130.

Deser, C., and A. S. Phillips, 2006: Simulation of the 1976/77 climate transition over the North Pacific: Sensitivity to tropical forcing. *J. Climate*, **19**, 6170–6180.

Deser, C., and J. M. Wallace, 1990: Large-scale atmospheric circulation features of warm and cold episodes in the tropical Pacific. *J. Climate*, **3**, 1254–1281.

Deser, C., and M. L. Blackmon, 1995: On the relationship between tropical and North Pacific sea surface temperature variations. *J. Climate*, **8**, 1677–1680.

Ebbesmeyer, C. C., Cayan, D. R., McLain, D. R., Nichols, F. H., Peterson, D. H., and Redmond, K. T., 1991: 1976 step in the Pacific climate: forty environmental changes between 1968–1975 and 1977–1984. In *Proceedings of the Seventh Annual Climate (PACLIM) Workshop, April 1990* (J. L. Betancourt, and V. L. Tharp (eds.)), 115–126 pp. California Department of Water Resources. Interagency Ecological Studies Program Technical Report 26.

Enfield, D. B., A. M. Mestas-Nuñez, and P. J. Trimble, 2001: The Atlantic multidecadal oscillation and its relation to rainfall and river flows in the continental U.S. *Geophys. Res.Lett.*, **28**, 2077–2080.

Graham, N. E., 1994: Decadal-scale climate variability in the tropical and North Pacific during the 1970s and 1980s: observations and model results. *Climate Dyn.*, **10**, 135–162.

Gu, D., and S. G. H. Philander, 1994: Secular changes of annual and interannual variability in the Tropics during the past century. *J. Climate*, **8**, 864–876.

Guan, B., and S. Nigam, 2008: Pacific sea surface temperatures in the twentieth century: An evolution-centric analysis of variability and trend. *J. Climate*, **21**, 2790–2809.

Guan, B., and S. Nigam: Analysis of Atlantic SST variability factoring inter-basin links and the secular trend: Clarified structure of the Atlantic Multidecadal Oscillation. To be submitted to *J. Climate*.

Guan, B., S. Nigam, and A. Ruiz-Barradas: Long-term hydroclimate variations over the Great Plains: Reconstruction of the Dust Bowl and other episodes during the twentieth century. In preparation for *J. Climate*.

Hansen, J., M. Sato, R. Ruedy, K. Lo, D. W. Lea, and M. Medina-Elizade, 2006: Global temperature change. *Proc. Natl. Acad. Sci.*, **103**, 14288–14293.

Hare, S. R., and N. J. Mantua, 2000: Empirical evidence for North Pacific regime shifts in 1977 and 1989. *Prog. Oceanogr.*, **47**, 103–145.

Hegerl, G. C., F. W., Zwiers, P., Braconnot, N. P., Gillett, Y., Luo, J. A. M., Orsini, N., Nicholls, J. E., Penner, and P. A., Stott, 2007: Understanding and attributing climate change. In *Climate Change 2007: The Physical Science Basis. Contribution of Working Group I to the Fourth Assessment Report of the Intergovernmental Panel on Climate Change* (S. Solomon, D. Qin, M. Manning, Z. Chen, M. Marquis, K. B. Averyt, M. Tignor, and H. L. Miller (eds.)), Cambridge University Press.

Hoerling, M. P., J. W. Hurrell, T. Xu, G. T. Bates, and A. S. Phillips, 2004: Twentieth century North Atlantic climate change. Part II: Understanding the effect of Indian Ocean warming. *Climate Dyn.*, **23**, 391–405.

Horel, J. D., 1981: A rotated principal component analysis of the interannual variability of the Northern Hemisphere 500 mb height field. *Mon. Wea. Rev.*, **109**, 2080–2092.

Huang, J., H. M. van den Dool, and K. P. Georgakakos, 1996: Analysis of model-calculated soil moisture over the United States (1931–1993) and applications to long-range temperature forecasts. *J. Climate*, **9**, 1350–1362.

Kalnay, E., M. Kanamitsu, R. Kistler, W. Collins, D. Deaven, L. Gandin, M. Iredell, S. Saha, G. White, J. Woollen, Y. Zhu, A. Leetmaa, R. Reynolds, M. Chelliah, W. Ebisuzaki, W. Higgins, J. Janowiak, K. Mo, C. Ropelewski, J. Wang, R. Jenne, and D. Joseph, 1996: The NCEP/NCAR 40-year reanalysis project. *Bull. Amer. Meteor. Soc.*, **77**, 437–471.

Kaplan, A., M. A. Cane, Y. Kushnir, A. C. Clement, M. B. Blumenthal, and B. Rajagopalan, 1998: Analysis of global sea surface temperatures 1856–1991. *J. Geophys. Res.*, **103**, 18567–18589.

Kaplan, A., Y. Kushnir, and M. A. Cane, 2000: Reduced space optimal interpolation of historical marine sea level pressure: 1854–1992. *J. Climate*, **13**, 2987–3002.

Kawamura, R, 1994: A rotated EOF analysis of global sea surface temperature variability with interannual and interdecadal scales. *J. Phys. Oceanogr.*, **24**, 707–715.

Koehl, A., D. Dommenget, K. Ueyoshi, D. Stammer, 2006: The Global ECCO 1952 to 2001. Ocean Synthesis Rep. 40, 43 pp.

Koster, R. D., M. J. Suarez, and M. Heiser, 2000: Variance and predictability of precipitation at seasonal-to-interannual timescales. *J. Hydrometeor.*, **1**, 26–46.

Lau, K. M., S. S. P. Shen, K.-M. Kim, and H. Wang, 2006: A multimodel study of the twentieth-century simulations of Sahel drought from the 1970s to 1990s. *J. Geophys. Res.*, **111**, D07111, doi:10.1029/2005JD006281.

Levitus, S., J. Antonov, and T. Boyer, 2005: Warming of the world ocean, 1955–2003, *Geophys. Res. Lett.*, **32**, L02604, doi:10.1029/2004GL021592.

Mantua, N. J., and co-authors, 1997: A Pacific interdecadal climate oscillation with impacts on salmon production. *Bull. Amer. Meteor. Soc.*, **78**, 1069–1079.

McCabe, G. J., M. A. Palecki, and J. L. Betancourt, 2004: Pacific and Atlantic Ocean influences on multidecadal drought frequency in the United States. *Proc. Natl. Acad. Sci.*, **101**, 4136–4141.

Mestas-Nuñez, A. M., and D. B. Enfield, 1999: Rotated global modes of non-ENSO sea surface temperature variability. *J. Climate*, **12**, 2734–2746.

Mestas-Nuñez, A. M., and D. B. Enfield, 2001: Eastern equatorial Pacific SST variability: ENSO and non-ENSO components and their climatic associations. *J. Climate*, **14**, 391–402.

Miller, A. J., Cayan, D. R., Barnett, T. P., Graham, N. E., and Oberhuber, J. M., 1994: The 1976–77 climate shift of the Pacific Ocean. *Oceanogr.*, **7**, 21–26.

Miller, A. J., M. A. Alexander, G. J. Boer, F. Chai, K. Denman, D. J. Erickson, R. Frouin, A. J. Gabric, E. A. Laws, M. R. Lewis, Z. Liu, R. Murtugudde, S.

Nakamoto, D. J. Neilson, J. R. Norris, J. C. Ohlmann, R. I. Perry, N. Schneider, K. M. Shell, and A. Timmermann, 2003: Potential feedbacks between Pacific Ocean ecosystems and interdecadal climate variations. *Bull. Amer. Meteor. Soc.*, **84**, 617–633.

Minobe, S., 1997: A 50–70 year climatic oscillation over the North Pacific and North America. *Geophys. Res. Lett.*, **24**, 683–686.

Mitchell, T. D., and P. D. Jones, 2005: An improved method of constructing a database of monthly climate observations and associated high-resolution grids. *Int. J. Climatol.*, **25**, 693–712.

Monahan, 2001: Nonlinear principal component analysis: Tropical Indo-Pacific sea surface temperature and sea level pressure. *J. Climate*, **14**, 219–233.

Nakamura, H., G. Lin, and T. Yamagata, 1997: Decadal climate variability in the North Pacific during the recent decades. *Bull. Amer. Meteor. Soc.*, **78**, 2215–2225.

Nigam, S., and H.-S. Shen, 1993: Structure of oceanic and atmospheric low-frequency variability over the tropical Pacific and Indian Oceans. Part I: COADS observations. *J. Climate*, **6**, 657–676.

Nigam, S., M. Barlow, and E. H. Berbery, 1999: Analysis links Pacific decadal variability to drought and streamflow in United States. *EOS, Transactions, American Geophysical Union*, **80**, 621–625.

Nitta, T., and S. Yamada, 1989: Recent warming of tropical sea surface temperature and its relationship to the Northern Hemisphere circulation. *J. Meteor. Soc. Japan*, **67**, 375–383.

Overland, J. E., and R. W. Priesendorfer, 1982: A significance test for principal components applied to a cyclone climatology. *Mon. Wea. Rev*., **110**, 1–4

Palmer, W. C., 1965: Meteorological drought. U.S. Weather Bureau Tech. Paper 45, 58 pp. Available from NOAA/National Weather Service, 1325 East-West Highway, Silver Spring, MD 20910.

Peterson T. C., R. Vose, R. Schmoyer, V. Razuvaev, 1998: Global Historical Climatology Network (GHCN) quality control of monthly temperature data. *Int'l J. Climatol.*, **18**, 1169–1179.

Rasmusson, E. M., and T. H. Carpenter, 1982: Variations in tropical sea surface temperature and surface wind fields associated with the Southern Oscillation/El Niño. *Mon. Wea. Rev.*, **110**, 354–384.

Rasmusson, E. M., X. Liang, and C. F. Ropelewski, 1990: The biennial component of ENSO variability. *J. Mar. Sys.*, **1**, 71–96.

Rayner, N. A., and co-authors, 2003: Global analyses of sea surface temperature, sea ice, and night marine air temperature since the late nineteenth century. *J. Geophys. Res.*, **108**, No. D14, 4407, doi:10.1029/2002JD002670.

Richman, M. B., 1986: Rotation of principal components. *Int'l J. Climatol.*, **6**, 293–335.

Ruiz-Barradas, A., J. A. Carton, and S. Nigam, 2000: Structure of interannual-to-decadal climate variability in the tropical Atlantic sector. *J. Climate*, **13**, 3285–3297.

Ruiz-Barradas, A., and S. Nigam, 2005: Warm season rainfall variability over the U.S. Great Plains in observations, NCEP and ERA-40 reanalyses, and NCAR and NASA atmospheric model simulations. *J. Climate*, **18**, 1808–1830.

Seager, R., Y. Kushnir, C. Herweijer, N. Naik, and J. Velez, 2005: Modeling of tropical forcing of persistent droughts and pluvials over western North America: 1856–2000. *J. Climate*, **18**, 4065–4088.

Schneider, N., and B. D. Cornuelle, 2005: The forcing of the Pacific Decadal Oscillation. *J. Climate*, **18**, 4355–4373.

Schubert, S. D., M. J. Suarez, P. J. Pegion, R. D. Koster and J. T. Bacmeister, 2004: On the cause of the 1930s Dust Bowl. *Science*, **303**, 1855–1859.

Ting M., and H. Wang, 1997: Summertime U.S. precipitation variability and its relation to Pacific sea surface temperature. *J. Climate*, **10**, 1853–1873.

Trenberth, K. E., 1990: Recent observed interdecadal climate changes in the Northern Hemisphere. *Bull. Amer. Meteor. Soc.*, 71, 988–993.

Trenberth, K. E., and D. P. Stepaniak, 2001: Indices of El Niño evolution. *J. Climate*, **14**, 1697–1701.

Uppala, S. M., and Coauthors, 2005: The ERA-40 Re-Analysis. *Quart. J. Roy. Meteor. Soc.*, **131**, 2961–3012.

van den Dool, H., J. Huang, and Y. Fan, 2003: Performance and analysis of the constructed analogue method applied to U.S. soil moisture over 1981–2001. *J. Geophys. Res. Letts.*, **108**, No. D16, 8617, doi:10.1029/2002JD003114.

Visbeck, M. H., J. W. Hurrell, L. Polvani and H. M. Cullen, 2001: The North Atlantic Oscillation: Past, present, and future. *Proc. Natl. Acad. Sci.*, **98**, 12876–12877.

von Storch, H., and F.W. Zwiers, 1999: Statistical Analysis in Climate Research, Cambridge University Press, ISBN 0 521 45071 3, 494 pp.

Wang, B., 1995: Interdecadal changes in El Niño onset in the last four decades. *J. Climate*, **8**, 267–285.

Weare, B. C., and J. S. Nasstrom, 1982: Examples of extended empirical orthogonal function analyses. *Mon. Wea. Rev.*, **110**, 481–485.

Wu, L., Z. Liu, R. Gallimore, R. Jacob, D. Lee, and Y. Zhong, 2003: Pacific decadal variability: The tropical Pacific mode and the North Pacific mode. *J. Climate*, **16**, 1101–1120.

Xie, S.-P., T. Kunitani, A. Kubokawa, M. Nonaka, and S. Hosoda, 2000: Interdecadal thermocline variability in the North Pacific for 1958–1997: A GCM simulation. *J. Phys. Oceanogr.*, **30**, 2798–2813.

Zhang, R.-H., and A. J. Busalacchi, 2005: Interdecadal change in properties of El Niño-Southern Oscillation in an intermediate coupled model. *J. Climate*, **18**, 1369–1380.

Zhang, Y., J. M. Wallace, and D. S. Battisti, 1997: ENSO-like interdecadal variability: 1900–93. *J. Climate*, **10**, 1004–1020.

Zhang, Y., J. M. Wallace, and N. Iwasaka, 1996: Is climate variability over the North Pacific a linear response to ENSO? *J. Climate*, **9**, 1468–1478.